Cranfield

CoA Report No. 8913

September, 1989

Euler Calculations with Emphasis on the Nonoverlapped Composite Grid and Hypersonic Flows

by

Hong-Chia Lin

Aerodynamics
College of Aeronautics
Cranfield Institute of Technology
Cranfield, Beds, U.K.

Cranfield

CoA Report No. 8913

September, 1989

Euler Calculations with Emphasis on the Nonoverlapped Composite Grid and Hypersonic Flows

by

Hong-Chia Lin

Aerodynamics

College of Aeronautics

Cranfield Institute of Technology

Cranfield, Beds, U.K.

SUMMARY

This report concerns mainly the computation of inviscid steady hypersonic flow on the nonoverlapped composite grid with implicit schemes.

Chapter 1 is about the post-shock oscillations of slow moving shocks in one dimension. The objective is to reduce the oscillations and increase the convergence speed for later work in two dimension; however, We find that other problems are more influential in term of reaching steady state in two dimension. Nevertherless the result is still useful for unsteady calculations.

Chapter 2 studies the interaction of the shock and grid size change in one dimensional unsteady and two dimensional steady flows by the explicit scheme. Some interesting results are presented.

Chapter 3 discusses the implicit scheme for two dimensional steady state solutions. Various solvers are tried and special problems associated with hypersonic calculations are emphasised.

Chapter 4 concerns the main theme of our research on implicit zonal method. A simple treatment on the zonal boundary conditions is presented with results from different implicit solvers.

Since each chapter is quite independent the concluding remarks are given at the end of each chapters.

CONTENT

CHAPTER 4. The implicit zonal method

CHAPTER 1 : NUMERICAL EXPERIMENTS OF RIEMANN SOLVERS ON SLOWLY MOVING SHOCKS

1.1 Introduction : Post-Shock Oscillation Problem

It has been observed for some time that when a shock is moving slowly some upwind schemes may produce wiggles at the higher density (post-shock) region, even when those schemes satisfy TVD conditions in the scalar case.

This problem only can happen in coupled systems, it does not occur in the scalar equation or in systems of equations that can be decouplable.

The non-monotone behavoour is certainly unwanted in unsteady flow calculations. Also it may cause convergence difficulty when one is using an unsteady approach to find the steady state solution.

Later in this chapter, we first review some previous works. In section 1.3 some results of extensive tests on Roe's scheme, which is known to have post-shock oscillations, are presented. In section 1.4 we give a brief review of schemes. We investiget the P variant of Osher's and introduce Bell's method in section 1.5. In section 1.6 we show some results from Roe's scheme with dissipation. Section 1.7 shows how to reduce the post-shock oscillations of second order schemes. Concluding remarks are given in section 1.8.

1.2 Previous Works

The first detailed account of this problem is by Colella and Woodward [1] in their paper about PPM method. They observe that low amplitude post-shock oscillations occur when the characteristic speed associated with a strong shock, measured relatived to the grid, vanished. And the dissipation introduced by Godunov's method vanishes as the shock speed goes to zero and therefore dissipation present in a slowly moving shock using Godunov's method is not sufficient to guarantee correct entropy production across the shock.

They show an example for an extremely strong shock moving slowly from right to left (see Fig. 1). There are substantial oscillations on both entropy and $u-2a/(\gamma-1)$, but the quantity $u+2a/(\gamma-1)$ the Riemann invariant transported along the (u+a) characteristic is well behaved. Their explanation is that in (u+a) wave any errors generated in that variable are immediately driven back to the shock transition layer while in the u and u+a waves the errors are carried away from the shock (see Fig. 2), therefore post-shock oscillations only appear in nonlinear system of equations. They propose to add some dissipations to decrease the oscillations.

Roberts [2] compares Godunov's [3], Roe's [4,5], and Osher's [6] schemes on a Mach 3 shock which takes 50 steps to cross a cell for Courant number 0.95. He shows Osher's scheme behaves quite well while Godunov's and Roe's schemes exhibit obvious post-shock oscillations not only for extremely strong shocks but even for weak shocks. He also shows that the results from Roe's scheme with minmod limiter are worse than those from

the first order Roe's scheme. The reason is because 2nd order scheme is less dissipative to suppress the oscillations. One more interesting result obtained from Osher's scheme with natural ordering of wave paths shows that it is not as good as the original scheme which uses reversed ordering of wave paths. He also shows the oscillations will occur for schemes with flux functions that give "exact" shock resolution such as Godunov's and Roe's schemes.

1.3 Numerical Experiments and Results on Roe's Scheme

Our purposes in doing the numerical experiments are first to reproduce Roberts' results and then test the schemes more systematically to find the parameters associated with the post-shock phenomena.

The initial data for thess tests are obtained by superimposing a velocity on a zero velocity shock, this velocity can be either positive or negative (see Fig. 3). The shock condition is labeled by 'Mach Number X'. Here the "Mach number X" shock means the shock data, such as pressure jump, are obtained from the steady normal shock relations for Mach number X and ratio of specific heats 1.4. The grid is uniform. The results shown later in some graphs are for the denstiy, $u-2a/(\gamma-1)$, entropy, and $u+2a/(\gamma-1)$. The last three quantities are the Riemann invariants of u-a, u, and u+a waves, and they will be denoted as R1, R2,and R3 thereon. It should be noted that the scales change from graph to graph.

There are three main conclusions from this experiment.

Firstly, we stress again that the post-shock oscillstions occur even when the shock strength is very weak. Fig. 4 and 5 are for Roe's and Osher's schemes with Mach no. 1.2. The oscillations in density, R2, R3 are obvious while R2 behaves quite well. Because of the graph scale the oscillations seem quite large, actually they are very small. We can also observe from the pictures that Osher's scheme performs better than Roe's. Fig. 6 and 7 are for Roe's and Osher's schemes with Mach no. 20 for SR 0.035 (SR to be defined later). The pictures speak for themselves for results from Osher's scheme, therefore we will concentrate on Roe's scheme.

Secondly, the Courant number is not important. In other words how many time steps the shock takes to cross a cell is not important. We have even tried with Courant no. 0.05.

Thirdly, the relative shock speed is important. If the shock moves slowly or fast enough then the oscillations are very small. The amplitude of oscillations first increases then decreases when the shock speed is increasing or decreasing from zero. The maximum amplitude of density oscillations for shocks moving from low density to high density region is bigger than for shocks moving in another direction, but for entropy oscillations the situation reverses. To nondimensionalise the shock velocity the shock speed is divided by the (u+a) of the right side state. The nondimensionalised shock speed is called SR. The reason to use (u+a) of right state instead of the associated characteristic speed is to avoid the SR value becoming too small. Fig. 8 gives the maximum amplitude of density oscillation versus SR. The SR value which produces maximum oscillation is around +0.035. SR -0.035 with Courant number 0.95 is very close to Roberts' test.

1.4 Brief Review of Schemes

Here we only point out some important differences betweens various schemes. The reader is assumed to be familar with them. For more complete comparisons we recommend the papre by Van Leer [7] for the scalar equation and the lecture notes by Pandolfi [8] for nonlinear systems.

We first start with the scalar equation

$$W_t + [f(W)]_x = 0$$

The 1st order conservative scheme can be written as

$$W^{n+1} - W^n + \frac{\Delta t}{\Delta x}\left[H_{i+1/2}(W_i, W_{i+1}) - H_{i-1/2}(W_{i-1}, W_i)\right] = 0$$

For the Godunov's scheme $H^G(W_L, W_R)$ is equal to the exact flux value of the Riemann problem at $x=0.5(x_L+x_R)$ and $T=\Delta t$ with W_L and W_R as left and right states. For Roe's we have

$$H^R(W_L, W_R) = \frac{1}{2}(f_R+f_L) - \frac{1}{2}\left|\frac{f(W_R)-f(W_L)}{W_R-W_L}\right|(W_R-W_L)$$

For Enquist-Osher's [9] we have

$$H^{EO}(W_L, W_R) = \frac{1}{2}(f_R+f_L) - \frac{1}{2}\int_{W_L}^{W_R}\left|\frac{df}{dW}\right| dW$$

For (W_L, W_R) does not contains the sonic point, these three fluxes are the same. However for the interval contains the sonic point (now we only consider the sonic point in the compression wave) we have $H^G = H^R \neq H^{EO}$. Analytically H^{EO} is smooth but not H^G or H^R.

For the one dimension Euler equation

$$W_t + F(W)_x = 0$$

The 1st order conservative scheme is

$$W^{n+1} - W^n + \frac{\Delta t}{\Delta x}\left[H_{i+1/2}(W_i, W_{i+1}) - H_{i-1/2}(W_{i-1}, W_i)\right] = 0$$

Godunov's scheme uses exact Riemann solution for $H_{i+1/2}$. In the approximate Riemann solver of Roe three linearlised waves replace two nonlinear waves and one linear wave, therefore the expansion wave is replace by a single wave. For Osher's three simple waves replace the real wave system, therefore shock wave is replaced by compression wave. On each simple wave the E-O method is applied. In the original Osher's paper (O variant) the left to right state is connected by u+a, u, and u-a waves in a physically reversed order. This can be considered as a solution of backward Riemann problem. Another possibility is to use P (physical) variant. The only difference to O variant is that the left to right state is connected by u-a, u, u+a simple waves in physically correct order. This has been used by Hemker [10] for transonic calculation.

Fig. 9 gives a graphical picture of these Riemann solvers.

1.5 Results of P Variant and Bell's

Although Roberts have pointed out that Osher's P variant do not produce as good results as O variant. We still try to look it again. From our experiment we confirm Roberts' results. We also observe one strange behaviour that when the Mach number is high and SR is more negative P variant tends to produce a very large overshoot, see Fig. 10. It will cause porgram to stop. The result seems to tell the E-O flux formulation is not the main or the only recipe for success.

We try further to implement E-O flux in Roe's Scheme. Bell et al [11] propose an approximate Riemann solver to general systems of hyperbolic conservation laws. Their higher order scheme is basically a PPM approach. It is also extended to problems that are not strictly hyperbolic and exhibit local linear degeneracies in the wave fields. However no result for Euler

equations is given.

Here we give an outline of their first order scheme.

Their scheme can be thought as a simplification of Osher's scheme or an enhancement of Roe's scheme. In stead of evaluating the intermediate points $W_{i+1/3}$ and $W_{i+2/3}$, which separate different waves, and possible sonic points W_{S1} and W_{S2}, see Fig. 11, by equations of Riemann invariants in Osher's scheme, they are evaluated by eigenvector decomposition and interpolation, and natual ordering of wave paths is assumed. Or to start with Roe's linear wave decompostion, the u-a or u+a waves are not considered as a single wave each and then Engquist-Osher flux formula is used in stead of Roe flux formula.

Assume we have a subroutine of Osher's solver. That is, the flux $H_{i+1/2}$ will be computed from intermediate states $W_{i+1/3}$, $W_{i+2/3}$, and any sonic states that are met with. We only need to change few lines to become a subroutine of Bell's solver. First we replace the equations for $W_{i+1/3}$, and $W_{i+2/3}$ by

$$W_{i+1/3} = W_i + \alpha^1 e^1$$

$$W_{i+2/3} = W_{i+1/3} + \alpha^2 e^2$$

which involve no expansive exponent calculations. α^k and e^k are simply in term of $0.5(W_i + W_{i+1})$. Roe's averaging is not required. Since natural ordering of wave paths is used, the eigenvalue or wave speed associated with wave path 1 must be change back to u-a and u+a for wave path 3. Finally to replace the equations for sonic points, W_{S1} and W_{S2}, at wave path 1 and 3, the wave speeds λ^1 and λ^3 are assumed to vary linearly from W_i to $W_{i+1/3}$ and $W_{i+2/3}$ to W_{i+1}. For example, to find W_{S1}, we solve equations

$$C_1\lambda_i^1+C_2 = W_i$$

$$C_1\lambda_{i+1/3}^1+C_2 = W_{i+1/3}$$

to obtain C_2. And at sonic point λ^1 is zero, so $W_{S1} = C_2$. Again in evaluating the sonic points no exponent calculation is needed. Note that in [11] Hermite cubic interpolation is used.

In general the post shock oscillations are reduced but it does have another problem. For large Mach no. and negative SR it produces a very big overshoot simliar to that by Osher's P variant, although it is not as large as Osher's P variant.

The results simply tell that E-O flux fomulation is not the sole reason of the success of Osher's O variant.

1.6 Roe's Scheme with Harten's Dissipation

From the above results it is obvious that Osher's scheme is better than Roe's for solving slowly moving shocks. However Osher's is quite expensive to compute and difficult to use on more complicated problems, such as real , reacting gas , etc because of the evaluation of the flux integral.

In contrast Roe's is much cheaper to run and easier to use on complicated problems. Therefore we are trying to modify Roe's to cure its post-shock oscillations. Follow Colella and Woodward's approach we add some dissipations in Roe's scheme explicitly.

In Roe's approach, the interface flux is

$$H^R(W_L,W_R) = \frac{1}{2}(F_R+F_L) - \frac{1}{2}\sum_{k=1}^{3}|\lambda_k|\alpha_k e_k$$

In order to break the unphysical solution from this formula, Harten [12,13] uses

$$H^H(W_L,W_R)=\frac{1}{2}(F_R+F_L)-\frac{1}{2}\sum_{k=1}^{3}Q_k\alpha_k e_k\frac{\Delta x}{\Delta t}$$

where

$$Q_k = \begin{cases} |\nu_k| & \text{if } |\nu_k| > \delta \\ \frac{1}{2}\left(\frac{\nu_k^2+\delta^2}{\delta}\right) & \text{if } |\nu_k| \le \delta \end{cases}, \quad \nu_k = \lambda_k\frac{\Delta t}{\Delta x}$$

at the expense of some deterioration in resolution, especially at the shock.

The post-shock oscillations can be suppressed by this dissipation with well-tuned δ and the solution can match that from Osher's.

One main disadvantage is that δ needs to adjusted for each case and it is CFL number dependent. We modified this formula by consider Q_k as function of ν_k, $\Delta\nu_k$ and Δt^{max}, where $\Delta\nu_k$ is the difference of Courant number in the same type of wave and Δt^{max} is the local maximum allowed time steps, see Fig. 12. The modified Q_k is given by

$$Q_k=\frac{1}{2}\left(\frac{\nu_k^2+\delta_k^2}{\delta_k}\right), \quad \delta_k=\frac{\Delta t}{\Delta t^{max}}\Delta\nu_k\delta_1, \quad \Delta\nu_k=\left|(\nu_k)_R-(\nu_k)_L\right|$$

where δ_1 is taken as 0.5 from numerical experiments. This is only implemented in the interval which contains the shock point.

Fig. 13 shows side by side comparison of several schemes on the Mach 3 shock.

1.7 Second Order Schemes

Second order scheme is less dissipative than the first order scheme. One can expect it will produce larger oscillations. Roberts givess a demonstration of 2nd order result with Roe's Riemann solver and minmod limiter. Here we attempt to decrease the oscillations from the second order or higher order schemes.

Lax-wendroff scheme with TVD limiter is used, see Roe and Pike [14]. To use Lax-wendroff scheme we need to have the average wave speed for each wave family. Roe's scheme provides average speeds but not Osher's. We can take the average wave speed as the average of the wave speed at the start and end of each simple wave for Osher's. This approach is verified by checking the shock tube solution. The oscillations for the slow moving shock are now visible for second order schemes using Osher's.

The cure we propose is to check if the interval between left and right states contains any sonic point then we switch off limiter. Therefore it reduces to first order scheme in the shock layer. This proves to work well. The global solution is not degraded and the postshock oscillations are decreased significantly. The method is very easy to implement into Osher's solver.

Note that sonic points include not only the sonic point in the compression wave but also the sonic point in the exapnsion wave. It is well known that the numerical sonic flux for the expansion wave is not appropriate to simulate the physical expansion. Using limiter for the sonic flux will produce worse results. Therefore it is reasonable to switch off limiter when evaluating the sonic flux. For the 2nd scheme using Roe's same technique can be applied plus dissipation. The result is much improved. Fig. 14 give comparisons of results from 2nd order schemes.

1.8 Conclcuding Remarks

We do not have real success in the quest of why Osher's O variant has the best performance on slow moving shocks. The dissipation approach for Roe's scheme is not a very good solution. Nevertherless some porgresses are made to understand this problem. To switch off limiter inside the shock layer will reduce the noises generation. This should be quite useful for the unsteady calculations; however, as we find out later, this approach is not suitable for implicit schemes on the steady state calculations because it introduces unsmothness.

CHAPTER 2 : EFFECTS OF MESH SIZE CHANGE ON SHOCKS

2.1 Introduction

For the multiblock method, it allows local grid refinement to obtain better local flow resolution. Here we investigate two possible problems due to the mesh size change.

Firstly, we apply 1st order flux difference splitting schemes (Roe's and Osher's) for the moving shock problem on nonuniform grid in one dimension. For simplicity, the grid consists of two nonoverlapped uniform zones with different mesh sizes.

The main purpose is to investigate how the mesh size change influences the solutions when shocks passing the zone boundary and hopefully to gain some insight for explaning similar problems on two dimensions.

Pike [15] shows that 1st order schemes will degrade to zero order schemes and 2nd order schemes will become 1st order accurate on irregular grids. First and 2nd order schemes on irregular grids are developed, however no extension to multidimension is proposed in [15]. In this work, we only consider the original first order schemes.

Osher's scheme is used for most tests because it has least post-shock oscillations. If Roe scheme is used we might have difficulty to separate the post-shock oscillations and noises generated at zone boundary. We will also show that with additional dissipations in Roe's scheme it will produce same results as Osher's.

The other problem we investigate here is the case that the steady shock lies on two different uniform grids in two dimension. The motivation of this work is from Berger and Colella's paper [16]. They report considerable degradation at interfaces where the shocks are not aligned with the mesh. Again first order scheme is used. To save the CPU time mainly Roe's scheme is used instead of Osher's since in the oblique shock case two schemes perform quite similarly due to the shock smearing.

In section 2.2 we discuss the test cases for the moving shock in one dimension. The results are discussed in section 2.3. Section 2.4 is for oblique shock results. Concluding remarks are given in Section 2.5.

2.2 Test Cases for the Moving Shock in One Dimension

By exchanging the mesh sizes of left and right zones and letting the shock move in either positive or negative directions four tests, A, B, C and D, can be done for a certain Mach number and shock speed (see Fig. 15).

In the graph for each test case, six shock positions, P1, P2, P3 ,P4 ,P5 and P6, are monitored, see Fig. 16. Because the initial data, which has no intermediate shock point, does not satisfy the numerical scheme, starting error appears immediately after one time step. P1 is where the shock just travels across one cell. The starting error is clearly present. P2 is where the shock postion is just one or two cells from the zone boundary. It is for checking if the starting error has nearly vanished. In most graphs, P3 is approximately where the noises generated by shock crossing zone boundary reaches its maximun and P4 is just little away from P3. P3 and P4 are for observing the mesh size change effect. P5 is where the shock position is a little away

from the zone boundary and P6 is further away from the zone boundary. From P5 and P6 we can see how the noises are dissipated and propagated.

2.3 Results and Discussion of the Moving Shock

Fig. 17 to 20 are for Mach no. 20 shock and mesh ratio 5:1 with SR ± 0.035, and Fig. 21 to 24 are for SR=± 0.28, for all four cases. We can observe that in cases A and D for which shocks move from coarse to fine zone bumps in density are created, and in case B and C for which shocks move from fine to coarse zone depressions in density are generated, especially for SR 0.28. It is also obvious that these noise magnitudes increase when SR increases. Some tests on intermediate SR values support this observation.

As conceivable the noises increase when the mesh size difference and Mach number increase.

Fig. 25 is for case A, Mach no. 20, SR 0.035 and mesh ratio 5:1 for Roe's scheme. The post-shock oscillation effect is mixed with the effect of noises induced by mesh size change. Fig. 26 is also for Roe's scheme but with Harten's dissipation. It is nearly as good as Fig. 17 since the post-shock oscillation is supressed once the dissipation is added appropriately. Fig. 27 is for Roe's scheme with SR 0.28. The result is quite the same as Fig. 21 from Osher's scheme because the post-shock oscillation is nearly removed at such SR.

Now we present a explanation for some computed results. It is simply based on the shock resolution characteristics of 1st order FDS scheme.

The number of mesh points needed by FDS schemes to resolve shocks depends mainly on the shock speed. Therefore if the shock is resolved on coarse grid by N points it will also be resolved by N points on fine grid. But the shock transition lengths are different.

For shock move from zone 1 with mesh spacing DX1 to zone 2 with mesh spacing DX2, the shock transition length change is equal to N(DX1-DX2). The length change increases when DX1-DX2 or N increase. In other words, it increases when mesh ratio or shock speed increases (because 1st order FDS scheme is quite dissipative the N value increases with shock speed). This explain the results that relative noise magnitude increases when mesh ratio and shock speed increase.

Second order schmes will be less sensitive to shock speed change since they are less dissipative, but they will still suffer from mesh size change.

The bump or depression feature is not easy to explain. It is perhaps because in the case for shock move from coarse to fine grid part of the shock profile is suddenly forced to steepen and in the case for shock move from fine to coarse grid it is suddenly flattened.

2.4 Test Cases and Finite Volume Scheme for the Steady Oblique Shock

The test case is a two dimensional steady oblique shock. One can imagine it is the flow past a wedge and the computational domain is rotated with respect to the free stream flow direction. Therefore we can have arbitrary shock to grid angle but keep the shock strength unchanged, see Fig. 28.

First order finite vloume upwind scheme (not operator splitting) is used. The initial condition can be either the free stream or postshock condition. The initial shock will appear at the bottom/left boundary if the initial condition is the freestream/postshock condition then it will move to its steady state position. We choose the flow conditions and computational domain such that we have always supersonic flow boundaries. At inflow boundaries the exact boundaries are prescribed and at the outflow boundaries zero order extraploation is used.

Fig. 29 is for a Mach number 20 oblique shock in single uniform grid. The flow properties are slightly below the right values at post-shock position. The computed shock is slightly curved. These problems are due to boundary conditions and narrow computation domain.

By changing the grid spacing we can do some tests on two zones by using the programme for one zone. Fig. 30 to 31 are for the shock to grid angle 70 degree. Because the shock has more inclination towards the Y direction mesh refinement in Y direction has nearly no effect on the solution. Mesh refinement in X direction improves the shock resolution but induces overshoot.

For the more general grid boundary, a simple treatment on the interface fluxes is adopted. For example, see Fig. 32, the interface flux at 1-2 is $H_{12}(W_c, W_a)$ and at 2-3 is $H_{23}(W_c, W_b)$. To update the coarse cell we need H_{13}, H_{13} is simply taken as the sum of H_{12} and H_{23}.

Coarse zone and fine zone perform one iteration each to count for one iteration for whole domain.

If the fine zone is on the top, we can observe big overshoot at post shock position; however, if the coarse zone is on the top there is no overshoot , see Fig. 33 and 34. The explanation for this is that the coarse zone on the bottom provides a bad boundary condition for the fine zone on the top. One can see quite clearly from the cross section density plot in Fig. 34 the shock transition in the first row of fine zone is staircaselike. On the contrary if the fine zone is on the bottom the transition is smooth.

We try futher two types of interface flux evalution based on one dimensional interpolation, see Fig. 35. For method 3 we can obtain smooth transition at the first row; however, the overshoot is still produced, see Fig. 36.

While the above results are from girds with integer spacing. For grid with noninterger spacing it does not seem to produce extra problem. Fig. 37 is for same grid ratio but discontinuous grid lines and Fig. 38 for different grid ratio. The results are very similar to the interger spacing cases.

The process of shock evolution is quite smooth for freestream as initial condition, but much harder for post shock condition as initial condition and for local time stepping. We can see from the Fig. 39 and 40 that very big noises are generated during the evolution process. Fortunately they porpogate out the computational domain very quickly.

2.5 Concluding Remarks

We now understand that for shock moving across two different grids, large disturbances can be generated. Fortunately this phomemona does not hamper the convergence if they propogate out of

the boundary quickly. We do not know what will happen if the noises is trap in a computational domain. It might take time to dissipate.

From the oblique shock results we suggest that where shocks is likely to be present large mesh ratio should be avoided even for steady state calculation.

CHAPTER 3. THE IMPLICIT SCHEME

3.1 Introduction

The explicit scheme, especilly the TVD scheme, needs thousands of iterations to reach convergence due to the CFL rule restriction. Implicit schemes escape the CFL rule in theory. Although most implicit schemes cannot converge as fast as theory suggests, they still converge faster than explicit schemes in terms of iteration number and CPU time.

To prepare for the next chapter on the implicit zonal method, we investigate the implicit scheme here with emphasis on inviscid hypersonic flow.

Section 3.2 introduces the explicit operator and blunt nose instability problem. The implicit operator is discussed in section 3.3. Several methods for solving the matrix equation generated by the implicit scheme are briefly described in section 3.4. Explicit and implicit boundary conditions are explained in section 3.5. Section 3.6 presents the results from various solvers. The experience on linear and nolinear GMRES is describes in section 3.7. Finally concluding remarks are given in section 3.8.

3.2 The Explicit Operator

The scheme we use is a 2nd order accurate finite volume scheme with TVD flux limiter and Roe's Riemann solver is adopted. There are several reasons behind this choice.

The finite volume approach is most naturally in preserving the conservation in the nonoverlapped composite grid. As we will demonstrate in next chapter that it is easier to implement than

the finite difference approach.

The order of accuracy is another issue. First order is not accurate enough. The so called 3rd order schemes are only true in one dimension; besides, in the zonal calculation we need to store more data of the neighbourhood of the interface due to the wider stencils of 3rd order schemes. Thus the 2nd order schemes are preferred. In the 2nd order scheme category we can have at least three choices, fully upwind, Lax-Wendroff and central difference. However fully upwind and Lax-wendroff are not 2nd order accurate in two/three dimensions without resorting to operator splitting or predictor-corrector method. The only choice left is the central difference scheme with TVD limiter.

Th explicit operator is first proposed by Osher and Chakravarthy [17] and later uses by Rai [18]; however, its property was not well understood. Roe [19] gave a clearer insight of this operator with emphasis on Navier-Stoke equations. We will only give a brief description here.

The Euler equations in two dimension is given by

$$\frac{\partial W}{\partial t}+\frac{\partial F}{\partial x}+\frac{\partial G}{\partial y}=0$$

where

$$W=\begin{vmatrix}\rho\\ \rho u\\ \rho v\\ e\end{vmatrix},\quad F=\begin{vmatrix}\rho u\\ \rho uu+p\\ \rho uv\\ u(e+p)\end{vmatrix},\quad G=\begin{vmatrix}\rho v\\ \rho vu\\ \rho vv+p\\ v(e+p)\end{vmatrix}$$

The semidiscrete finite volume form for a quadrilateral cell i,j is, see Fig. 41,

$$A_{i,j}\frac{\partial W_{i,j}}{\partial t}+H_{i+1/2,j}-H_{i-1/2,j}+H_{i,j+1/2}-H_{i,j-1/2}=0$$

where A is the cell area and H is the interface flux. For the later use we define

$$R(W_{i,j})=(H_{i+1/2,j}-H_{i-1/2,j}+H_{i,j+1/2}-H_{i,j-1/2})$$

For first order scheme we have, for example,

$$H_{i+1/2,j} = 0.5\,(F_{i+1,j} + F_{i,j})\,s^x_{i+1/2,j} + 0.5\,(G_{i+1,j} + G_{i,j})\,s^y_{i+1/2,j}$$
$$- 0.5 \sum_{k=1}^{4} |\lambda_k|\,\alpha_k\,e_k\,s_{i+1/2,j} \quad = h_{i+1/2,j}$$

where λ_k, α_k, e_k are obtained from one dimensional wave decomposition along the normal of the segment ab. The normal is given by

$$\vec{s}_{i+1/2,j} = s^x_{i+1/2,j}\vec{i} + s^y_{i+1/2,j}\vec{j}$$
$$s^x_{i+1/2,j} = y_a - y_b$$
$$s^y_{i+1/2,j} = x_b - x_a$$

We further define the interface flux Jacobian as

$$J_{i+1/2,j}(W_{i+1,j} - W_{i,j}) = (F_{i+1,j} - F_{i,j})\,s^x_{i+1/2,j} + (G_{i+1,j} - G_{i,j})\,s^y_{i+1/2,j}$$

$$J_{i+1/2,j} = (RDL)_{i+1/2,j}$$

J, R, D and L are 4x4 matrices. R is the matrix of right eigenvector e_k. D is a diagonal matrix with λ_k, wave speed, as diagonal entry. L is the matrix of left eigenvector ℓ_k. The formula for R,D,L and be found in [20] for 2D case and [21] for 3D case. The wave strength α_k is given by

$$\alpha_k = \ell_k (W_{i+1,j} - W_{i,j})$$

Therefore we have

$$\sum_{k=1}^{4} \lambda_k\,\alpha_k\,e_k\,s_{i+1/2,j} = (F_{i+1,j} - F_{i,j})\,s^x_{i+1/2,j} + (G_{i+1,j} - G_{i,j})\,s^y_{i+1/2,j}$$

For second order scheme the interface flux is

$$H_{i+1/2,j} = h_{i+1/2,j} + 0.5 \sum_{k=1,4}^{k+} \phi(r^{k+}_{i+1/2,j})\,\Delta f^{k+}_{i+1/2,j} - 0.5 \sum_{k=1,4}^{k-} \phi(r^{k-}_{i+1/2,j})\,\Delta f^{k-}_{i+1/2,j}$$

where

$$\Delta f^{k+}_{i+1/2,j} = \lambda_k\,\alpha_k\,e_k\,s_{i+1/2,j} \quad \text{for } \lambda_k \geq 0$$

$$\Delta f^{k-}_{i+1/2,j} = \lambda_k\,\alpha_k\,e_k\,s_{i+1/2,j} \quad \text{for } \lambda_k < 0$$

$$r^{k+}_{i+1/2,j} = \frac{\Delta f^{k+}_{i-1/2,j}}{\Delta f^{k+}_{i+1/2,j}} \qquad r^{k-}_{i+1/2,j} = \frac{\Delta f^{k-}_{i+3/2,j}}{\Delta f^{k-}_{i+1/2,j}}$$

ϕ is the limiter function. In our work minmod and van Albada's

limiter are used. For more detail about the flux-limiter see Sweby [22]. The mimmod and van Albada limiter is given by

$$\text{minmod}: \ \phi(r)=\begin{matrix} 0 & \text{if } r<0 \\ r & \text{if } 0\le r\le 1 \\ 1 & \text{if } r>1 \end{matrix}, \quad \text{van Albada}: \ \phi(r)=\frac{r+r^2}{1+r^2}$$

One can see immediately that if the flow is smooth ϕ is about 1 then this scheme becomes central difference.

The semidiscrete form can be approximated to high order accuracy in time by Runge-Kutta scheme. To preserve the TVD property in time nót all classes of Runge-Kutta scheme can be used, see Shu [23] for more details.

The above scheme does not satisfied entropy condition. In [24] Yee proposes a modification from Harten's dissipation of Roe's Riemann solver for breaking nonphysical expansion shocks. Here Yee's formula is adpoted. The $Q(\lambda_k)$, which replaces λ_k, is given by

$$Q(\lambda_k)=\begin{cases} \lambda_k & \text{if } |\lambda_k|>\delta_k \\ \frac{1}{2}\left(\text{sign}(\lambda_k)\,\frac{\lambda_k^2+\delta_k^2}{2\delta_k}+\lambda_k\right) & \text{if } |\lambda_k|\le\delta_k \end{cases}$$

where

$$\delta_k=\tilde{\delta}_k(|V_n|+|V_t|+c)$$

V_n is the normal velocity and V_t the tangential velocity with respect to the interface boundary and **c** the interface sound speed.

The dissipation is not necessary for u waves for breaking expansion shocks; however, in the hypersonic blunt body calcuation we do need it for the u waves. It has been observed by some people (but not seen in any literature) that Roe's and Osher's Riemann solvers produce instability when they are used to compute supersonic flow over blunt bodies, see Fig 42. The cause is not clear. For the 2nd order scheme, we have to set the dissipation coefficient for u waves to a quite large value to overcome the

blunt nose instability. The convergence rate is quite dependent on the maginitude of the dissipation. With Van Leer's flux vector splitting, we find that no extra dissipation is required. As it is known flux vector splitting is very dissipative for the u waves, this explains why it works. We need larger number for $\tilde{\delta}_2$ and $\tilde{\delta}_3$ then that for the symmetric TVD used by Yee. The symmetric TVD is also quite dissipative in the u waves.

The other problem associated with hypersonic calculations is the evaluation of r. The equation we mentioned previously is appropriate for transonic calculation. To have monotone shock transition in hypersonic cases we have to scale it by square of sound speed, as suggested by Yee [24]. Thus it becomes

$$r^{k+}_{i+1/2,j} = \frac{\Delta f^{k+}_{i-1/2,j}\, c^2_{i-1/2,j}}{\Delta f^{k+}_{i+1/2,j}\, c^2_{i+1/2,j}} \qquad r^{k-}_{i+1/2,j} = \frac{\Delta f^{k-}_{i+3/2,j}\, c^2_{i+3/2,j}}{\Delta f^{k-}_{i+1/2,j}\, c^2_{i+1/2,j}}$$

3.3 The Implicit Operator

Since we are only interested in steady state calculations we only consider first order Euler implicit equation,

$$W^{n+1}_{i,j} - W^{n}_{i,j} + \mu_{i,j} R(W^{n+1}_{i,j}) = 0 \qquad \text{where} \quad \mu_{i,j} = \frac{\Delta T_{i,j}}{A_{i,j}}$$

After lineraisation it becomes

$$(I + \mu \frac{\partial R(W)}{\partial W})\, \delta W_{i,j} = -\mu_{i,j} R(W_{i,j}) \qquad \text{where} \quad \delta W_{i,j} = W^{n+1}_{i,j} - W^{n}_{i,j}$$

Follow Yee's work [24], two approximations for $\partial R/\partial W$ can be made, nonconservative and conservative forms. The "conservation" here is for the time conservation which is not important for steady state calculation.

The nonconservative form is

$$-\mu_{i,j} J^{+}_{i-1/2,j} \delta W_{i-1,j} - \mu_{i,j} J^{+}_{i,j-1/2} \delta W_{i,j-1} + \mu_{i,j} J^{-}_{i+1/2,j} \delta W_{i+1,j} + \mu_{i,j} J^{-}_{i,j+1/2} \delta W_{i,j+1}$$
$$+ [\, I + \mu_{i,j} (J^{+}_{i-1/2,j} - J^{-}_{i+1/2,j} + J^{+}_{i,j-1/2} - J^{-}_{i,j+1/2})\, \delta W_{i,j} = -\mu_{i,j} R(W_{i,j})$$

where $J^{+}_{i+1/2,j} = (RD^{+}L)_{i+1/2,j}$ $\qquad$ $J^{-}_{i+1/2,j} = (RD^{-}L)_{i+1/2,j}$

D^{+} contain the positive entry of D while D^{-} the negative entry.

The conservative form is

$$-0.5\mu_{i,j}(J^{E}_{i-1,j}+|J_{i-1/2,j}|)\,\delta W_{i-1,j} - 0.5\mu_{i,j}(J^{S}_{i,j-1}+|J_{i,j-1/2}|)\,\delta W_{i,j-1}$$
$$+0.5\mu_{i,j}(J^{W}_{i+1,j}-|J_{i+1/2,j}|)\,\delta W_{i+1,j} + 0.5\mu_{i,j}(J^{N}_{i,j+1}-|J_{i,j+1/2}|)\,\delta W_{i,j+1}$$
$$+[I+0.5\mu_{i,j}(|J_{i-1/2,j}|+|J_{i+1/2,j}|+|J_{i,j-1/2}|+|J_{i,j+1/2}|)\,\delta W_{i,j} = -\mu_{i,j}R(W_{i,j})$$

where $J^{E}_{i,j} = J_f S^{x}_{i+1/2,j} + J_g S^{y}_{i+1/2,j}$, $J^{W}_{i,j} = J_f S^{x}_{i-1/2,j} + J_g S^{y}_{i-1/2,j}$, $|J| = R(D^{+}-D^{-})L$

$J^{N}_{i,j} = J_f S^{x}_{i,j+1/2} + J_g S^{y}_{i,j+1/2}$, $J^{S}_{i,j} = J_f S^{x}_{i,j-1/2} + J_g S^{y}_{i,j-1/2}$, $J_f = \frac{\partial F}{\partial W}$, $J_g = \frac{\partial G}{\partial W}$

Initially our experience was on the nonconservative form, later we switch to conservative form. The convergence speed, as stated by Yee, is much improved especially in the high Mach number case.

Both forms can be casted as

$$M_{i-1,j}\,\delta W_{i-1,j} + M_{i,j-1}\,\delta W_{i,j-1} + M_{i+1,j}\,\delta W_{i+1,j} + M_{i,j+1}\,\delta W_{i,j+1} + D_{i,j}\,\delta W_{i,j} = -\mu_{i,j}R(W_{i,j})$$

Using this form we solve the matrix equation once then update the solutions. With small modifications one can choose to do several suiterations inside every time step to obtain time accuracy. Since we only want steady state solutions, we do not consider the subiteration approach here.

The pentadiagonal matrix eqs is too expensive to solve directly. One have some options to solve it approximately. Several methods are tested.

3.4 Different Solvers

The backward and forward line Gauss-Siedel line relaxation can be expressed as

Backward sweep :

$$M_{i,j-1}\,\delta W^{*}_{i,j-1} + D_{i,j}\,\delta W^{*}_{i,j} + M_{i,j+1}\,\delta W^{*}_{i,j+1} = -\mu_{i,j}R(W_{i,j}) - M_{i+1,j}\,\delta W^{*}_{i+1,j}$$

Forward sweep :

$$M_{i,j-1}\,\delta W_{i,j-1} + D_{i,j}\,\delta W_{i,j} + M_{i,j+1}\,\delta W_{i,j+1} = -\mu_{i,j} R(W_{i,j}) - M_{i+1,j}\,\delta W^{*}_{i+1,j} - M_{i-1,j}\,\delta W_{i-1,j}$$

LU scheme is a symmentric Gauss-Siedel relaxation. It can be expressed as

$$D_{i,j}\,\delta W^{*}_{i,j} = -\mu_{i,j} R(W_{i,j}) - M_{i-1,j}\,\delta W^{*}_{i-1,j} - M_{i,j-1}\,\delta W^{*}_{i,j-1}$$

$$D_{i,j}\,\delta W_{i,j} = -\mu_{i,j} R(W_{i,j}) - M_{i-1,j}\,\delta W^{*}_{i-1,j} - M_{i,j-1}\,\delta W^{*}_{i,j-1} - M_{i+1,j}\,\delta W_{i+1,j} - M_{i,j+1}\,\delta W_{i,j+1}$$

The sweep is along I+J=constant.

The most widely used is perhaps the approximate factorisation scheme (AF) or ADI scheme:

I sweep :

$$M_{i-1,j}\,\delta W^{*}_{i-1,j} + D^{I}_{i,j}\,\delta W^{*}_{i,j} + M_{i+1,j}\,\delta W^{*}_{i+1,j} = -\mu_{i,j} R(W_{i,j})$$

J sweep :

$$M_{i,j-1}\,\delta W_{i,j-1} + D^{J}_{i,j}\,\delta W_{i,j} + M_{i,j+1}\,\delta W_{i,j+1} = \delta W^{*}_{i,j}$$

where D^{I}/D^{J} contains only the M in the I/J direction.

The other AF scheme by Lombard [25] called DDADI (diagonal dominant ADI) is:

I sweep :

$$M_{i-1,j}\,\delta W^{*}_{i-1,j} + D_{i,j}\,\delta W^{*}_{i,j} + M_{i+1,j}\,\delta W^{*}_{i+1,j} = -\mu_{i,j} R(W_{i,j})$$

J sweep :

$$M_{i,j-1}\,\delta W_{i,j-1} + D_{i,j}\,\delta W_{i,j} + M_{i,j+1}\,\delta W_{i,j+1} = D\,\delta W^{*}$$

Unlike AF there is no three dimension extension of DDADI.

The last scheme we will explain immediately later does not belong to the approximate solver category. It is essentially quite different from the above four methods.

For the all the above schemes the values of W are not updated until the sweeps complete. We can also choose to update the W immediately, One of these approach by Bardina and Lombard [26] and Chakravarthy [21] is

back/forward marching:

$$M_{i-1,j}\,\delta W_{i-1,j} + D_{i,j}\,\delta W_{i,j} + M_{i+1,j}\,\delta W_{i+1,j} = -\mu_{i,j} R(W_{i,j})$$

for/backward marching:

$$M_{i-1,j}\,\delta W_{i-1,j} + D_{i,j}\,\delta W_{i,j} + M_{i+1,j}\,\delta W_{i+1,j} = -\mu_{i,j} R(W_{i,j})$$

The marching direction is usually chosen as the streamwise direction. Here we call one single sweep as one iteration. The matrix equation is only tridiagonal, which can be solved exactly. This method is usually used with AF or DDADI in three dimension calculation. AF and DDADI are used on the cross plane and this method is used on the streamwise direction. The advantage is that one can work with three/five planes at one time for 1st/2nd scheme. The core memory is easier to manage, see Bardina and Lombard [26] and Chakravarthy [21] for more details. We will call it as method 5 for later reference.

3.5 Boundary Conditions

For the supersonic inflow we put halo cells in the inflow. The values of halo cells are fixed for explicit part, therefore the change δW for the implicit part is zero. For the supersonic outflow we set the flow values in the halo cell equal to the values upstream, thus the Jacobian M is zero. $M\delta W$ is therefore zero. For subsonic inflow and outflow farfield we can set the values of halo cells to the free stream, since the interface fluxes obtain from upwind scheme are automatically characteristics based. Because we fix the halo cell the change δW is zero.

For the solid wall we use simple reflected boundary condition, the halo cell is assigned to have same but negative normal momentum to the boundary cell. The change δW in the halo cell is

$$\begin{vmatrix} \delta\rho \\ -\delta\rho V_n \\ \delta\rho V_t \\ \delta e \end{vmatrix}_{halo} = \begin{vmatrix} \delta\rho \\ \delta\rho V_n \\ \delta\rho V_t \\ \delta e \end{vmatrix}_{inside}$$

From the above relation we can work out $\delta\rho u$ and $\delta\rho v$. This is only first order accurate which is consistent with the implicit operator. Without this boundary condition the implicit scheme converges much slower. For the explicit part we need a better interface flux, we simply extrapolate the pressure from the interior to the boundary. This can be further refined.

3.6 Results from Different Solvers

Te residual is defined as

$$\text{Residual} = [\sum_{i=1}^{imax}\sum_{j=1}^{jmax} |R(\rho_{i,j})| / A_{i,j}\,]/(\text{imax jmax})$$

This is better than

$$\text{Residual} = [\sum_{i=1}^{imax}\sum_{j=1}^{jmax} |\delta\rho_{i,j}| / \Delta T_{i,j}\,]/(\text{imax jmax})$$

The residual defined by the second equation could be misleading if large CFL number is used. Although we advance sloution by a certain time, the flow does not evolve so fast due to the errors from linearisation and approximate solver. The residual evaluated from the first equation is normally smaller than that from the second equation. The residual from the frist equation reflects the state of the flow and it is independent with the time step size.

Throught out this work local time step is used for convergence acceleration. The optimun CFL number is about 10-20, which is quite modest. The initial conditions are always the free stream conditions.

For 1st order scheme all solvers works reasonable well, we will not discuss the 1st order result here.

For the GAMM bump, the line Gauss-Siedel and LU schemes have difficulty to drive residual down for the second order scheme. For blunt body it is worse. We will not disscuss these scheme anymore.

In general method 5 and DDADI perform quite well, but for AF we have problem at high Mach number flow.

The CPU time required for Method 5 depends on the grid size and marching direction. If the grid has more cells in I direction than in J direction then marching in I direction implies solving the matrix equation in J direction. In this case CPU time required is smaller than DDADI. If it marchs in J direction then the CPU time required will be much longer. Our codes are not optimised, especially for the method 5, therefore no exact comparison of CPU time will be given. The data management method mentioned in section 3.4 is not used since we can afford to store all data in small calculations.

DDADI is able to converge with nonconservative implicit operator but not with conservative implicit operator. To be able to converge with conservative operator the sweep directions need to be changed alternatively. More precisely for odd iterations we use I sweep then J sweep and for even iterations we use J sweep then I sweep.

At low Mach number AF works quite well. But for higher Mach number the performance of AF begins to degrade. It needs extra dissipation to push residual down. In contrast to the excellent results of AF by Yee [24] our AF is not successful for high Mach number. We suspect the difference might come from boundary conditions.

Van Albada's limiter gives slightly better convergence rate than minmod. All the results shown later are from using van Albada's limiter.

Fig. 43, 44, and 45 show results of Mach 2, 5, and 20 flows from various solvers.

3.7 Experience with GMRES Solver

The GMRES solver by Saad and Schultz [27] is a conjugate gradient-like mehtod for solving linear systems of equations. Since we only solve the matrix equation approximately and the factorisation error is not small, we could possibly solve it with same or more accuracy by GMRES with only few iterations. From the numerical experiments few subiterations inside GMRES for each iteration is required initially, however when residual reduces by the order of two or three the subiterations required increase very quickly. We conclude that to use linear GMRES as approximate solver is not competetive. If we solve the matrix equation very accurately at the expanse of long CPU time only few hundred iterations is able to drive the residual to machine zero. This indicates our boundary conditions are sufficient good at least for DDADI.

The nonlinear GMRES by Brown and Saad [28] is a clever combination of inexact Newton method and linera GMRES for solving the nonlinear systems of equations. According to Wighton [29], with any solvers such as AF as preconditioner, the nonlinerar GMRES will help convergence in the difficult case and help to stabilise scheme. In our experience we are not able to have any gain. We decide not to use it.

3.8 Concluding Remarks

We have produced basic implicit codes by DDADI and method 5 for hypersonic calculations. Although we are not successful with AF we believe our implicit codes provide a reasonable start for investigating zonal method.

The biggest difficulty we have during this investigation is the blunt nose instability. Further research on this problem is required.

CHAPTER 4. THE IMPLICIT ZONAL METHOD

4.1 Introduction

To ease the grid generation in three dimension and to improve the grid quality the most flexible approach is to use overlapped grid. The biggest obstacle to use the overlapped grid is to maintain the flux conservation. As pointed out by Berger [30] it is extremely difficult to achieve exact conservation. An good example of bad result from nonconservative interpolation algorithm is given by Benek et al [31].

Nevertherless it is perhaps not necessary to have EXACT flux conservation, if the flux conservation is met to certain degree of accuracy. The approach suggested by Thomas et al [32] seems to meet this condition. They conserve the conserved variable A•W instead of interface flux. Their results on nonoverlapped composite grid are quite encourging. Moon and Liou [33] make significant refinement on this technique and apply it to overlapped and overlaid grid in two dimension showing very promising result. One inherent problem of this approach is that the complexity of programming and computing overhead is larger than nonoverlapped approach especially in three dimension.

Here we only persue the nonoverlapped grid approach, that is grids with common boundaries.

We first categorise the zonal boundaries, see Fig. 46. Type B1 has continuous grid lines, it can be either continuous or discontinuous in slopes. Type B2 has integer grid spacing, while type B3 has noninteger grid spacing.

The composite grid can be classified as two types. Type G1 is globally structured, the zonal boundaries can only be the B1 type. Type G2 is golbally unstructured which is the case in practices, the zonal boundaries consists of all three types. One important advantage of G2 type grid is that it allows local grid refinement. For the flow solvers, we can have either explicit (S1) or implicit (S2) solver. The explicit solver uses only local grid data to march in time, while the implicit scheme needs all data in the computational domain to march in time. This difference has important implication on the zonal method.

For data management we assume the data stores in both the primary and secondary menory, which is the situation for realistic 3D calculaton. Type M1 uses the data in the primary and secondary menory at the same time, see Fig. 47. The time spent on the data access is in general too long. Type M2 uses only the data in the main memory, the data in the main menory and secondary menory exachanges periodically. Type M2 is the usual case.

Combine the grid, slover, and data management we have several options.

M1/M2+S1+G1 is simply the case for single zone grid. M1+S1+G2 is easy in the finite volume formulation. M2+S1+G2 adds some problems on the data exchange. M1+S2+G1 is trivially the case for single zone. M1+S2+G2 can be done but the matrix becomes unstructured, for which no efficient solver is available. The most challeging combination are M2+S2+G1/G2. The matrix is structured for using G1 grid for which efficient approximate solver can be used; however, the order of the matrix equation is very large. One do not wish to solve it as a whole. The situation for G2 grid is even difficult. One will prefer to from

the matrix equation and solve it zone by zone. But with this approach the implicit scheme now can not receive all the data. This will the the centre issue of our research.

4.2 Selected Literature Review

There are so many papers about the zonal method that an complete review is impossible. Here we only concentrate on some works. The reader is encourging to read the references cited.

Rai [18] uses AF finite difference scheme on G2 type grid. We consider his treatment on the conservation is more complicated due to the finite difference setting. The implicit zonal boundary condition he use is not stable for one subiteration. In [34] by relaxation method one subiteration is stable. The implicit boundary condition he choose is simply to set the δW in the other zone to zero. Mach 2 is the maximun tested Mach no.

Belk and Whitefield [35] use LU finite volume scheme on G1 type grid. The implicit zonal boundary condition is either to set the $\delta W=0$ in the other zone or take the $\delta W = \delta W_{old}$, where the δW_{old} is the δW from previous iteration . With the M2 case one can choose to use the old data or to use the newest data available from the other updated zone. They name synchronisation (SYN) as using only the old data and unsynchronisation (UNSYN) as using the newest available data. The test problem is transonic flow passing wing. The main conclusion from their work is that the convergence speed in order is UNSYN+ $\delta W=0$ first, SYN+ $\delta W=0$ second, and UNSYN+ $\delta W_{old}=0$ last. The SYN+ $\delta W_{old}=0$ approach is not stable.

Morice [36] uses a noncentred finite volume scheme on G1 grid. The test case is M=0.85 GAMM bump. His implicit characteristic boundary condition is perhaps the most reasonable in our opinion. However it is still not genuinely implicit because of intrinstic restriction of the M2 case. He shows the same convergence rate as for single grid case can be achieved.

Kathong [37] first applies Ramshaw's algorithm [38] to find the overlapped areas in the 3D block boundary. This point will be addressed later.

Eriksson and Rai [39] give the first numerical stability analysis of the Jameson type scheme and upwind scheme. They conclude the upwind scheme is superior in stability for all B1, B2, B3 type zonal boundaries. Usually for nonupwind schemes extra dissipation is required for using B2 and B3 type boundaries.

4.3 The Explicit zonal boundary condition

As we stated earlier the explicit part calculation only needs local data. There is basically no difficult. With the finite volume and the flux limiter approach one can assume the flow is locally uniform inside the computational cell. With reference to Fig. 48 one can work out the 1st order flux across ab by simply solving the Riemann problem with W1 and W2 as the left and right states. For the 2nd order flux, we need to compare Δf^{k-} at mn with Δf^{k-} at ab to obtain r^{k-}. When $r^{k\pm}_{ab}$ is evaluated we scale the $\Delta f^{k\pm}$. The r for limiter function is therefore

$$r^{k+}_{ab} = \frac{\Delta f^{k+}_{de} c^2_{de} |S_{ab}|}{\Delta f^{k+}_{ab} c^2_{ab} |S_{de}|} \qquad r^{k-}_{ab} = \frac{\Delta f^{k-}_{mn} c^2_{mn} |S_{ab}|}{\Delta f^{k-}_{ab} c^2_{ab} |S_{mn}|}$$

After all interface fluxes are found the R(W) for cell 1 is equal to $H_{ab}+H_{bc}-H_{de}+H_{ad}-H_{ce}$.

In the above approach we assume there is a common boundary running through different zones. One needs a table of the data at the neighbourhood of zone boundary. The table is most convenient to produce during the grid generation stage. In the grid generator one first establishes all the boundaries, such as solid boundaries, far field boundaries, and zonal boundaries etc. These boundaries are usually represented in parametric from. In two dimension one parameter is enough. By comparing the number of the parameter one can establish the table quickly. Three dimension case will be discussed in section 4.6.

Because the assumption of common boundary the cells at the boundaries are not quadrilateral in general. In our calculation, for example, the area of the cell abcde is assumed to have the same area of abcd. Note that we still keep flux conservation. The error will be insignificant if the zonal boundary is quite straight with respect to each cell. If one decide to have to exact area it is most conveniently supplied from the grid generator.

4.4 The Implicit Zonal Boundary Condition

With the M2 data management and the basic implicit scheme we use in chapter 3 there will be no real implicit zonal boundary condition if one do not want to solve the complete matrix equation. With this understanding we believe the success of implicit zonal schemes comes from the coupling of explicit part. In general the implicit schemes still need hundreds of iterations to reach convergence in single grid calculation. During the iterations the explicit part couples different zone effictively.

Therefore we adopt the $\delta W=0$ approach. The diagonal term D has to treated properly especially when the G2 grid is used.

Use similar approach as in the explicit part we can work out the interface Jacobian. Take the conservative form for example the diagonal term for cell abcde, see Fig. 49, is

$$D=I+0.5\mu\,(|J_{ab}|+|J_{bc}|+|J_{de}|+|J_{ad}|+|J_{ce}|)$$

A try which does not include the Jacobian in the zonal interface turns out to be unstable.

4.5 Results and Discussion

In general the schemes which can converge in single grid have no stability porblem in two zone cases with $\delta W=0$ and the SYN or UNSYN updating approach except when a strong shock lies on the zone boundary. This conclusion also applies to AF, which is unstable according to Rai [18].

If one takes the single grid and bisects it to two zones. One can compare the convergence rate of two-zone calculations with single grid calculations. In general the convergence rate for two-zone calculations is only slightly slower.

The UNSYN approach converges faster than the SYN approach in general because in the UNSYN approach the number of explicit coupling DOUBLES.

Before the results are presented we have to explain how to look our contour plottings. Since we use finite volume formulation the flow data is cell-centred. We plot the contours zone by zone and inside each zone we do not try to extrapolate the contour lines. Therefore at the zonal boundary the contour lines are not connected. Nevertheless it is easy to use imagination to

connect the lines.

Fig. 50 is for GAMM bump computed by SYN approach with nonconservative from with DDADI solver. The zonal boundary lies exactly inside the shock. The convergence rate is only slighted degraded. Fig. 51 is for the integer grid spacing case with UNSYN approach.

All the following results are from the conservative form. Fig. 52 shows the results for Mach 2 flow past cylinder. In this case the UNSYN and SYN approaches have nearly the same convergence rate.

Fig. 53 to 58 are for Mach 5 flow past reentry body. Fig. 54 and 55 have zonal boundary inside the shock. The zonal boundary of Fig. 55 is one more cell away from the body then that of Fig. 54. In this case SYN approach is UNSTABLE for CFL no. equal 10. Lower CFL no. has to be used. Fig. 56 has small shock to zonal boundary angle. Fig. 57 has zonal boundary in the supersonic region. Fig. 57 is produced by method 5 with marching in the radial direction to the body. Of these results shock positions do not seem to produce problems with UNSYN approach. Fig. 58 is for the integer grid spacing case.

Fig. 59, 60 , and 61 are examples for Mach 20 flow past cylinder with various zonal boundaries.

4.6 Generalisation to Three Dimension

The method we use can be generalised to 3D in principle.

To keep the conservation we need the overlapped area on the zonal plane. If the zone boundary is a straight plane Ramshaw's conservative re-zoning algorithms can be implemented efficiently,

e.g. Kathong [37]. However the zone boundary is generally a curved plane no efficient method exists to the auther's knowledge. One possible solution is to apply Ramshaw's technique on (s,t) parameter plane after the curved boundary is parameterised, see Fig. 62, and this should be integrated to grid generation procedure.

To compute the volume of multiface cell abutting on the zonal boundary extra effort is required. If the boundary is quite straight, one can again calculate the cell volume as if it is a texahedrons. Some of the cell surfaces intersecting the zonal boundaries might have more than four edge. The area vector of these surfaces is required for the finite volume scheme. Again if the zonal boundary is quite straight we can calculate it as a four-edge surface.

These geometry problems is not too difficult to overcome and not costly to compute.

Another problem associated in a 3D patched-grid is addressed in Thomas et al [40]. Near a solid wall the grid could be unable to match especially for highly stretched mesh for thin-layer N-S calculation. For further details see Thomas et al [40]. We will prefer to avoid this situation.

4.7 Concluding Remarks

The W=0 approach seems to work well for the finite volume scheme. This is partly because the optimun CFL number for the basic implicit scheme is quite modest and the matrix formed from upwind scheme is diagonal dominance.

Although our explicit operator is a central-difference operator with TVD limiter, we believe other explicit operators can be used if the 1st order implicit operator is treated as before.

Although promising result is obtained in 2D three dimensional test still has to be done.

ACKNOWLEDGEMENT

This work is supported by Dassault (AMD-BA). The author wishes to thank Dr. J.Periaux and Dr. Q.V.Dinh for their warm hospitality during his stay in Paris and especially Dr. Dinh for the help on implementing GMRES. Finally the author would like to express his appreciation to Professor P.L.Roe, for his supervision and encouragement during the course of this work.

REFERENCE

1. Colella, P and P.R. Woodward, "The Piecewise Parabolic Metehod (PPM) for Gas Dynamical Simulation", J. Comput. Physics 54, 174-201, 1984.

2. Roberts, T.W., "The Behaviour of Flux Difference Splitting Schemes Near Slowly Moving Shock Waves", in "Numerical Methods for Fluid Dynamics III", eds by K.W. Morton and M.J. Baines, Oxford University Press, 1988.

3. Godunov, S.K., "Finite-Difference Method for Numerical Computation of Discontinuous Solution of the Equations of Fluid Dynamics", Math. Sbornik, 47 (1959), pp. 217-306.

4. Roe, P.L., "The Use of the Riemann Problem in Finite Difference Schemes", Lecture Notes in Physics, 141, Spring-Verlag, New York, 1981, pp. 354-559.

5. Roe, P.L., "Approximate Riemann Solvers, Parameter Vectors and Difference Schemes", J. Comput. Physics, 43, 1981, pp. 357-372.

6. Osher, S. and F. Solomon, "Upwind Difference Schemes for Hyperbolic Systems of Conservation Laws", Math. Comp., Vol. 18, no. 158, 1982, pp. 339-374.

7. Van Leer, B., "On the Relation between the Upwind-Difference Scheme of Godunov, Engquist-Osher and Roe", SIAM J. Sci. Stat. Comput., Vol. 5, No. 1, March 1984.

8. Pandolfi, M., "Upwind Formulations for the Euler Equations", Computational Fluid Dynamics, VKI lecture Series 1987-04.

9. Engquist, B. and S. Osher, "Stable and Entropy Satisfying Approximations for Transonic Flow Calculations", Math. Comp., 34,1980, pp.45-75.

10. Hemker, P.W. and S.P. Spekreijse, "Multiple Grid and Osher's Scheme for the Efficient Solution of the Steady State Euler Equations", Applied Num. Math. 2. ,00 475-493, 1986.

11. Bell, J., Colella, P., and Trangenstein, J., "Higher-Order Godunov Methods for General Systems of Hyperbolic Conservation Laws", J. Comput. Physics 82, 1989.

12. Harten, A., "Self Adjusting Grid Methods For One-Dimensional Hyperbolic Conservation Laws", J. Comput. Physics 50, 235-269, 1883.

13. Harten, A., "High Resolution Schemes for Hyperbolic Conservation Laws", J. Comput. Physics 49, 357-393, 1983.

14. Roe, P.L., "Efficient Construction and Utilisation of Approximate Riemann Solutions", in "Comput. Methods. Appl. Science Engrg, VI", North-Holland, 1984.

15. Pike, J., "Grid Adaptive Algorithms for the Solution of the Euler Equations on Irregular Grids", J. Comput. Physics 71, 194-223, 1987.

16. Berger, M.J. and Colella, P., "Local Adaptive Mesh Refinement for Shock Hydrodynamics", J. Comput. Physics 82, 64-84, 1989.

17. Osher, S. and S. Chakravarthy, "High Resolution Schemes and the Entropy Conditions", SIAM J. Numer. Anal. Vol.21 No.5 Oct 1984.

18. Rai, M.M., "An Implicit, Conservative, Zonal Boundary Scheme for Euler Equation Calculations', Computer and Fluids 14, no. 3, pp. 295-319, 1986.

19. Roe, P.L., "Finite-Volume Methods for the Compressible Navier-Stokes equations, 5th International Conf. on Numerical Methods on Laminar and Turbulent Flow", 1987.

20. Chakravarthy, S.R. and S. Osher, "A New Class of High Accuracy TVD Schemes for Hyperbolic Conservation Laws", AIAA-85-0363.

21. Chraravarthy, S.R. and K-Y Szema, "Euler Solvers for Three Dimensional Supersonic Flows With Subsonic Pockets", J. Aircraft, Vol 24, No. 2, Feb 1987.

22. Sweby, P.K., "High Resolution Schemes Using Flux Limiters For Hyperbolic Conservation Laws", SIAM J. NUMER. Anal., Vol 24, No. 5, Oct, 1984, P995.

23. Shu, Chi-Wang and S. Osher, "Efficient Implementation of Essentially Non-Oscillatory Shock-capturing Scheme", J. Comp. Physics, Vol.77, p439,1988.

24. Yee, H-C, "Upwind and Symmetric Shock-Capturing Scheme", NASA TM89464

25. Lombard, C.K., "Multi-Dimensional Formulation of CSCM - an Upwind Eigenvector Split Method for the Compressible Navier-Stokes Equations", AIAA-83-1985, 1983.

26. Bardina, J. and C.K. Lombard, "Three Dimensional CSCM Method for the Compressible Navier-Stokes Equations with Application to Multi-Nozzle Exhaust Flow Field", AIAA-85-1193, 1985.

27. Saad, Y and M.H. Schultz, "GMRES: A Generalized Minimal Residual Algorithm for Solving Nonsymmetric Linera Systems", SIAM J. Sci. Stat. Comput., Vol. 9, no. 3, 1986.

28. Brown, P.N. and Y.Saad, "Hybrid Krylov Method for Nonlinear Systems of Equations", preprint.

29. Wighton, L.B. et al, "GMRES Acceleration of Computational Fluid Dynamics Codes", AIAA-85-1495, 1985.

30. Berger, M.,"On Conservation at Grid Interfaces", SIAM J. Numer. Anal., Vol. 24, No. 5, Oct, 1987.

31. Benek, J.A. et al, "A Flexible Grid Embedding Technique with Application to the Euler Equations", AIAA-83-1944, 1983.

32. Thomas, J.L. et al,"Patched-grid Computations of High Speed Inlet Flows", in ASME Symposium: Advances and Applications in Comp. Fluid. Dyn. 1988, Vol. 66, pp11-12.

33. Moon, Y-J and M-S Liou, "Conservative Treatment of Boundary Interface for Overlaid Grids and Multi-level Grid Adaptions", AIAA-89-1980CP, 1989.

34. Rai, M.M.,"A Relaxation Approach to Patched-Grid Calculations with the Euler Equations", AIAA-85-0295.

35. Belk, D.M. and D.L. Whitfield, "Three-dimensional Euler Solutions on Blocked Grids Using an Implicit Two-pass Algorithm", AIAA-87-0450, 1987.

36. Morice, Ph, "Transonic Computations by Multidomain Techniques with Potential and Euler Solvers", ONERA T.P. no 1988-78.

37. Kathong, M. et al, "A Conservative Approach for Flow Field Calculations on Multiple Grids", AIAA-88-0224.

38. Ramshaw, J.D., "Conservative Rezoning Algorithm for Generalized Two-Dimensional Meshes", J. Comput. Physics 59, pp. 193-199, 1985.

39. Eriksson, L-E and M.M. Rai, "A Stability Analysis of Various Patched grid Interface Conditions for Hyperbolic equations", FFA report 144, 1988.

40. Thomas, J.L. et al, "A Patched-Grid Algorithm for Complex Configurations Directed Towards the F-18 Aircraft", AIAA-89-0121.

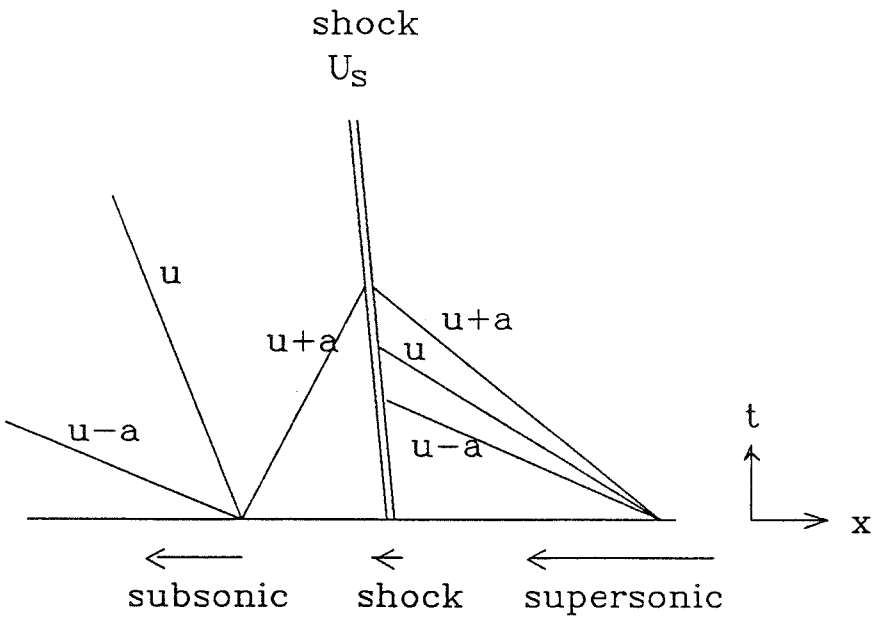

Fig. 1 wave diagram of Woodward and Colllela's test.

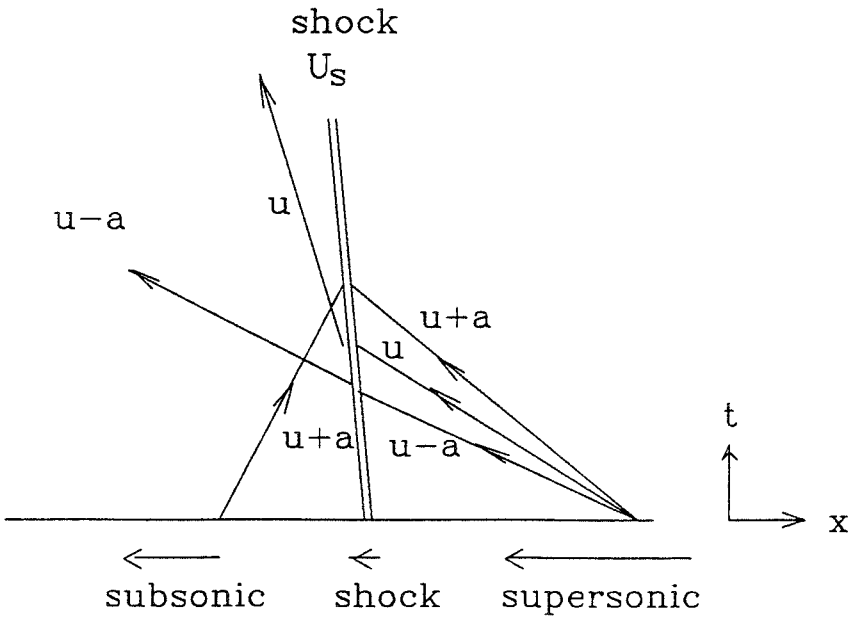

Fig. 2 wave diagram for explaning the post-shock behaviour.

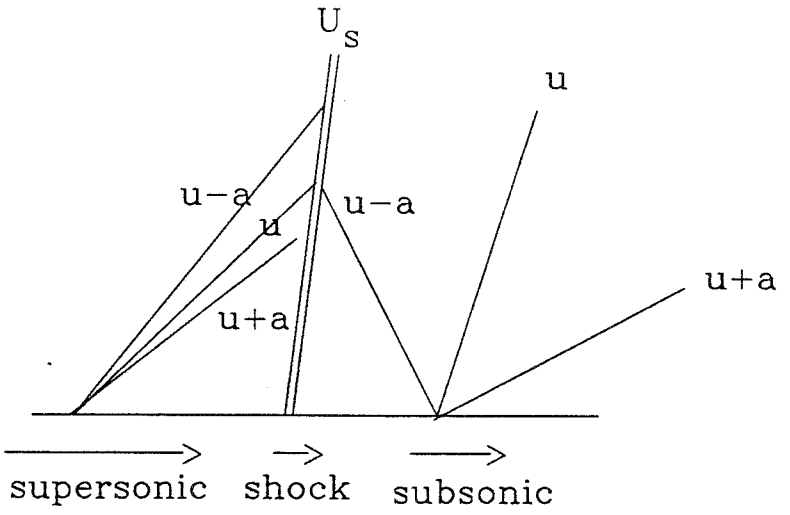

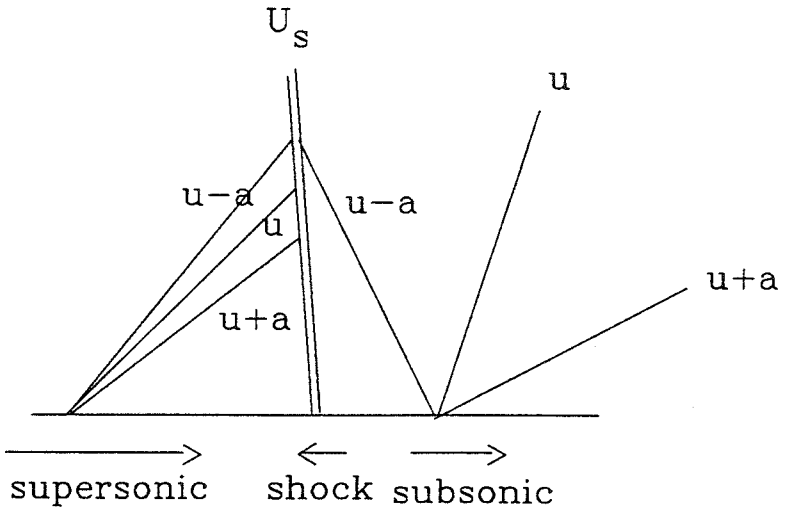

Fig. 3 test case wave diagrams

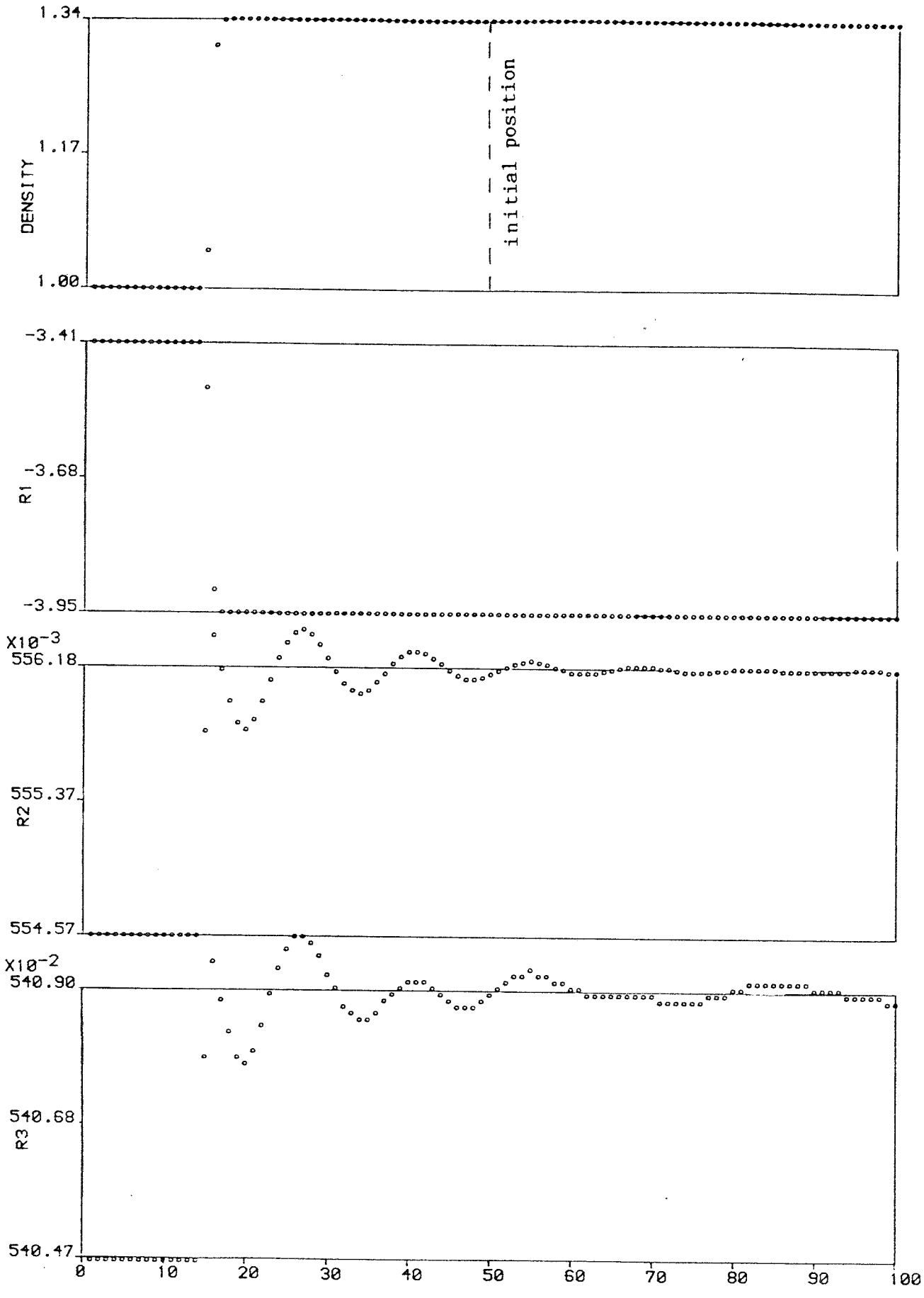

Fig. 4 : Roe's scheme M=1.2 SR=-0.035

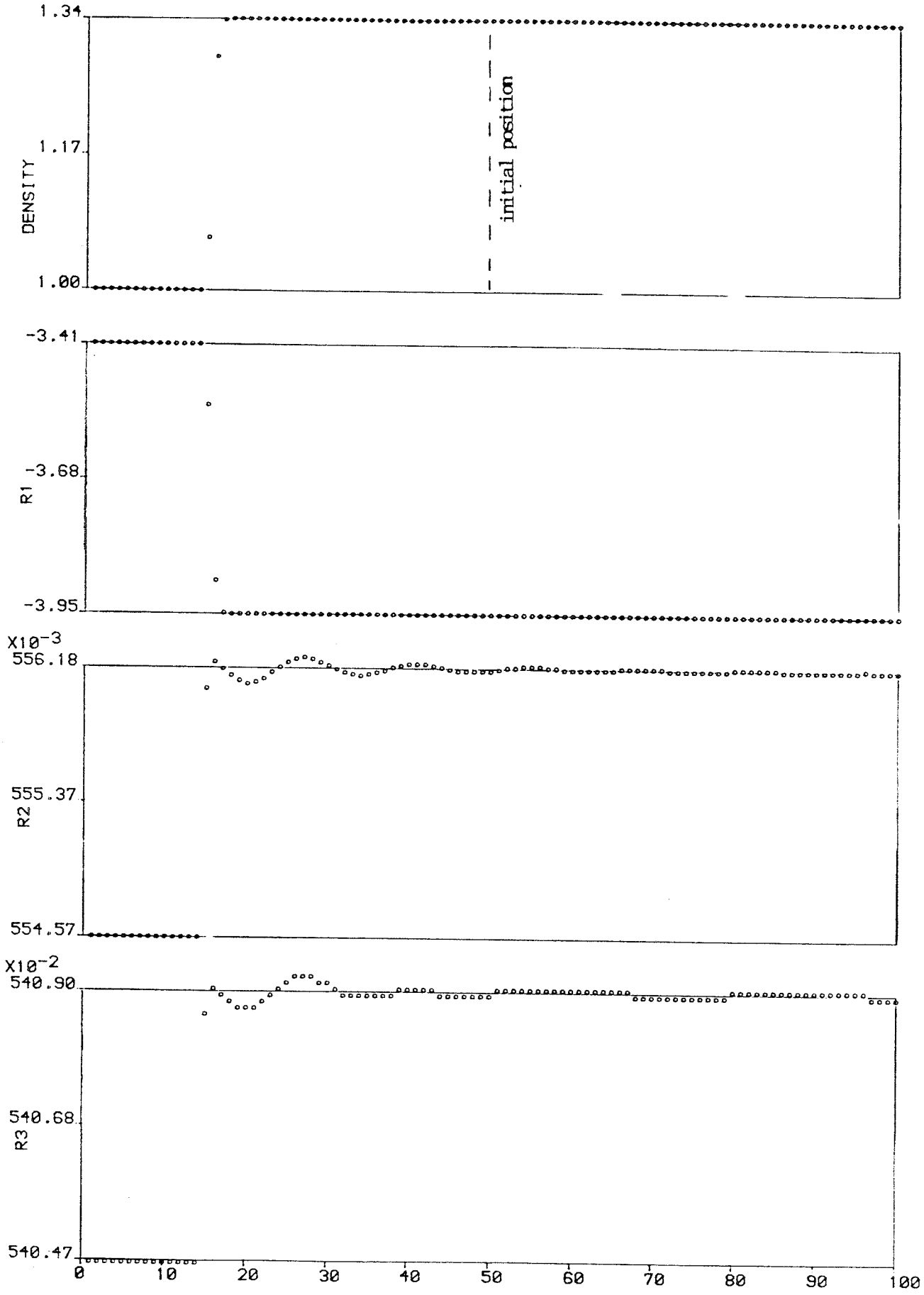

Fig. 5 : Osher's scheme M=1.2 SR=-0.035

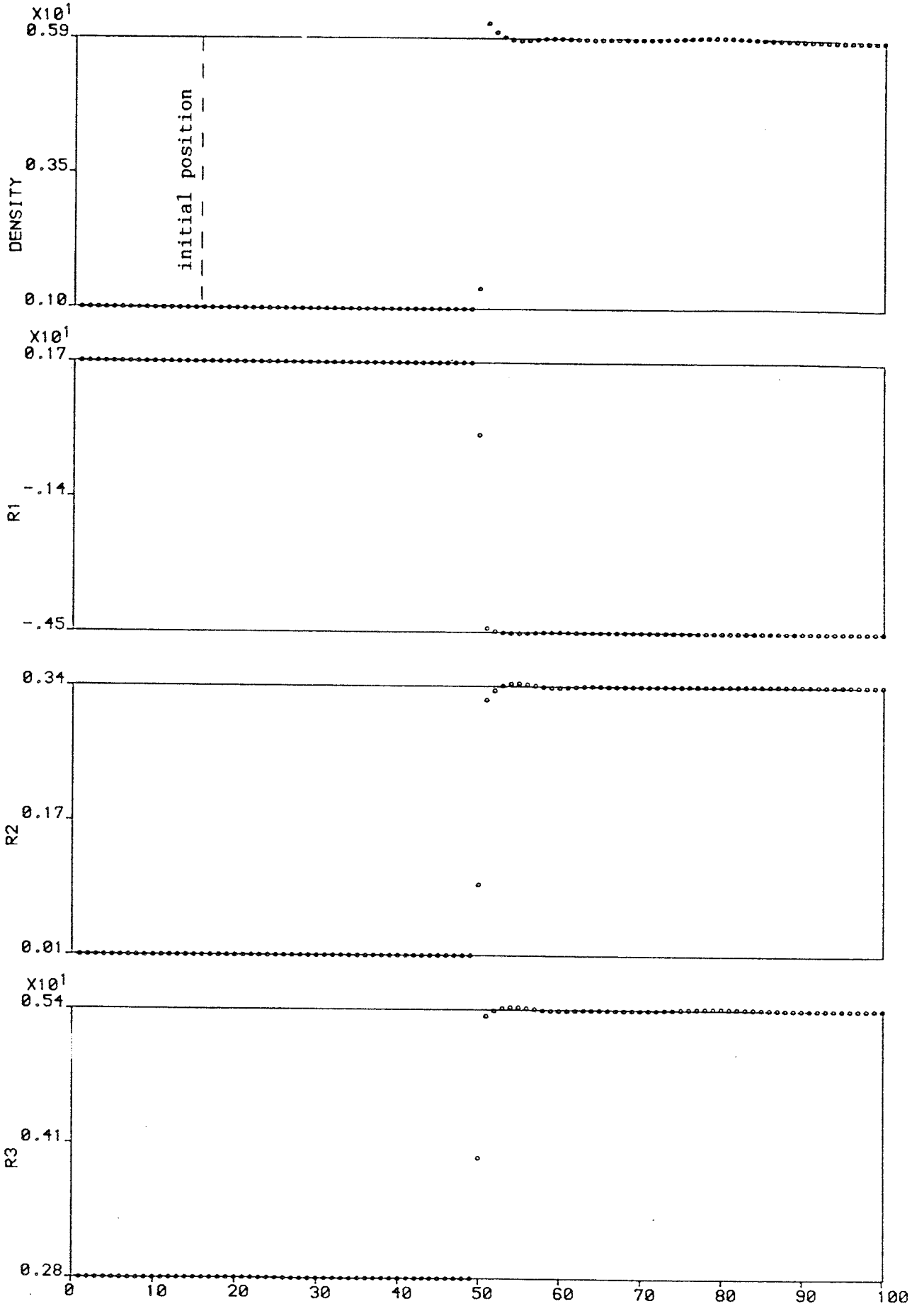

Fig. 6 : Roe's scheme M=20 SR=+0.035

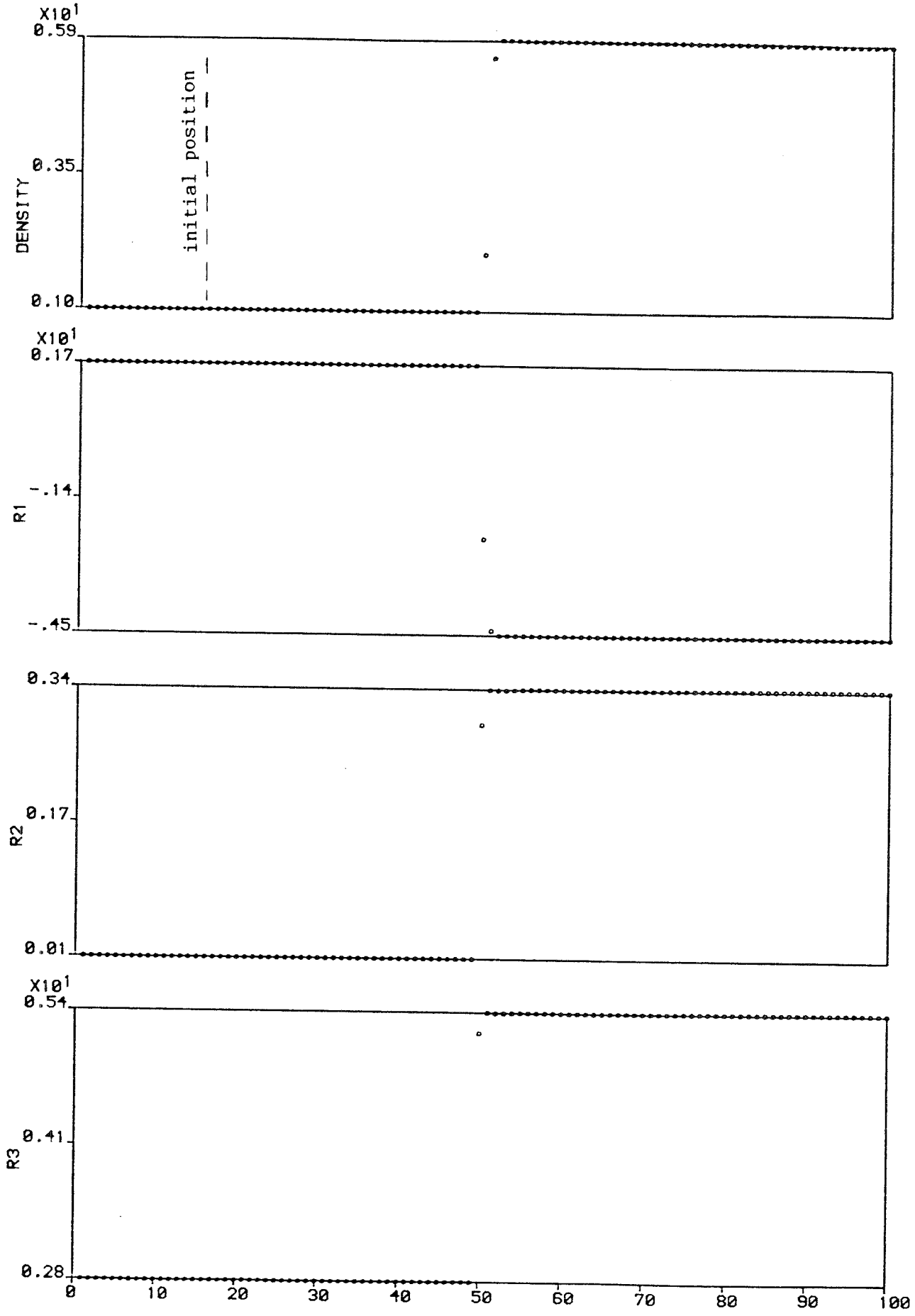

Fig. 7 : Osher's scheme M=20 SR=+0.035

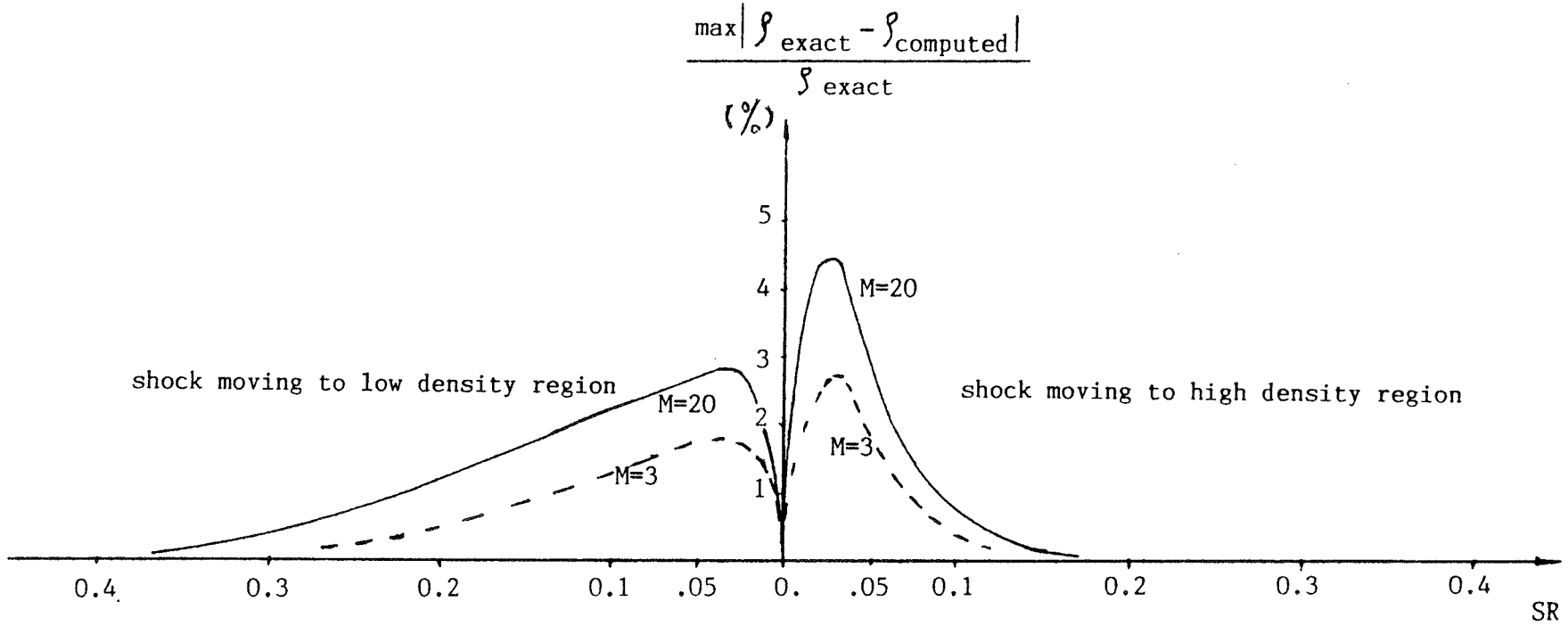

Fig. 8 : Density oscillation magnitude vs. SR for Roe's scheme

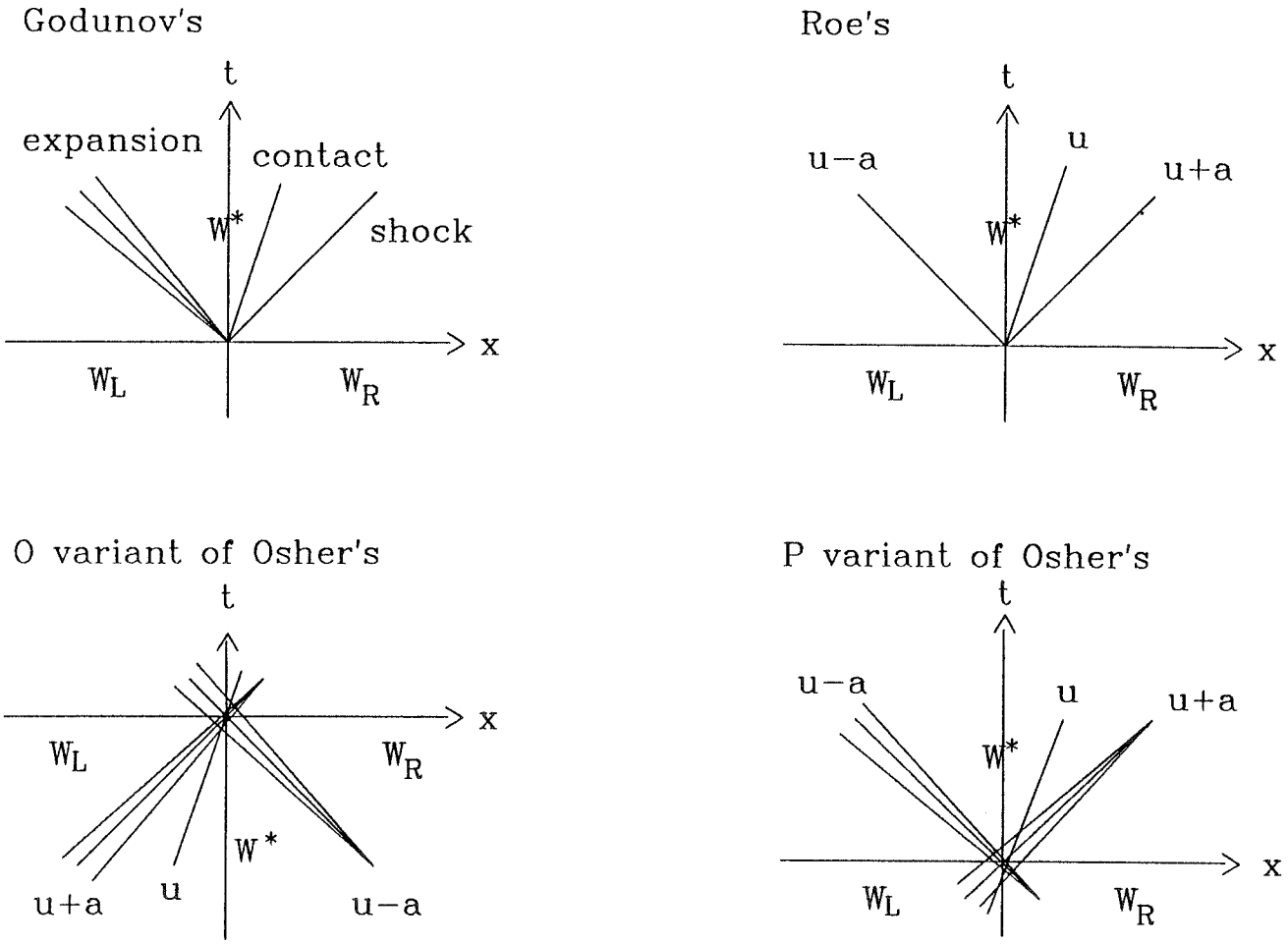

Fig. 9 wave diagrams for various Riemann solvers

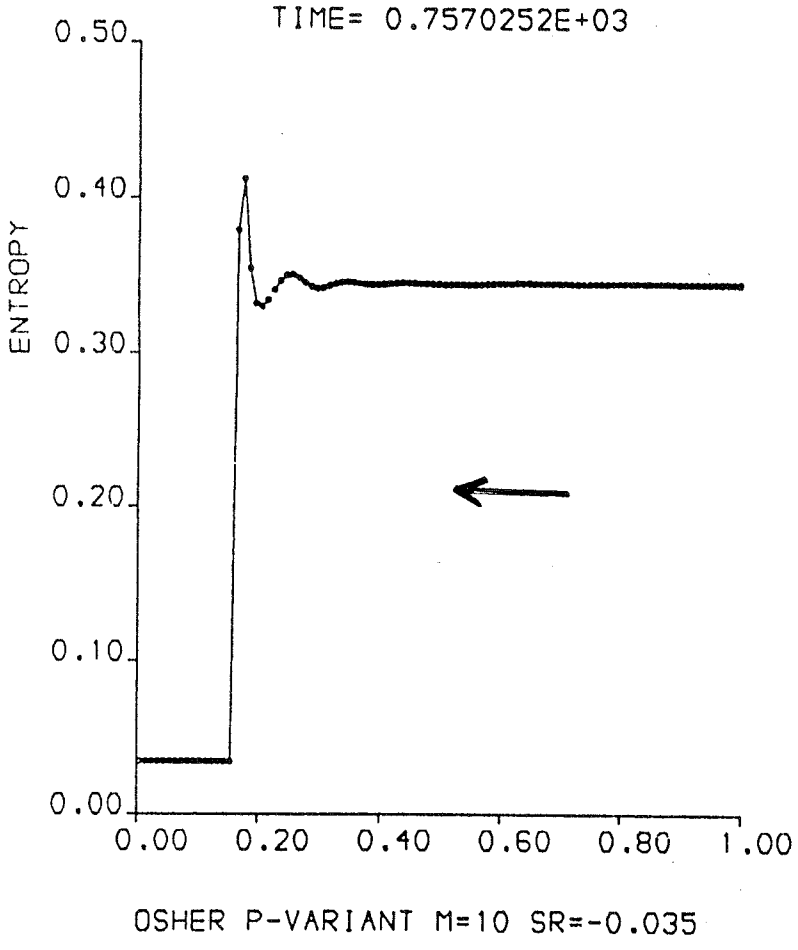

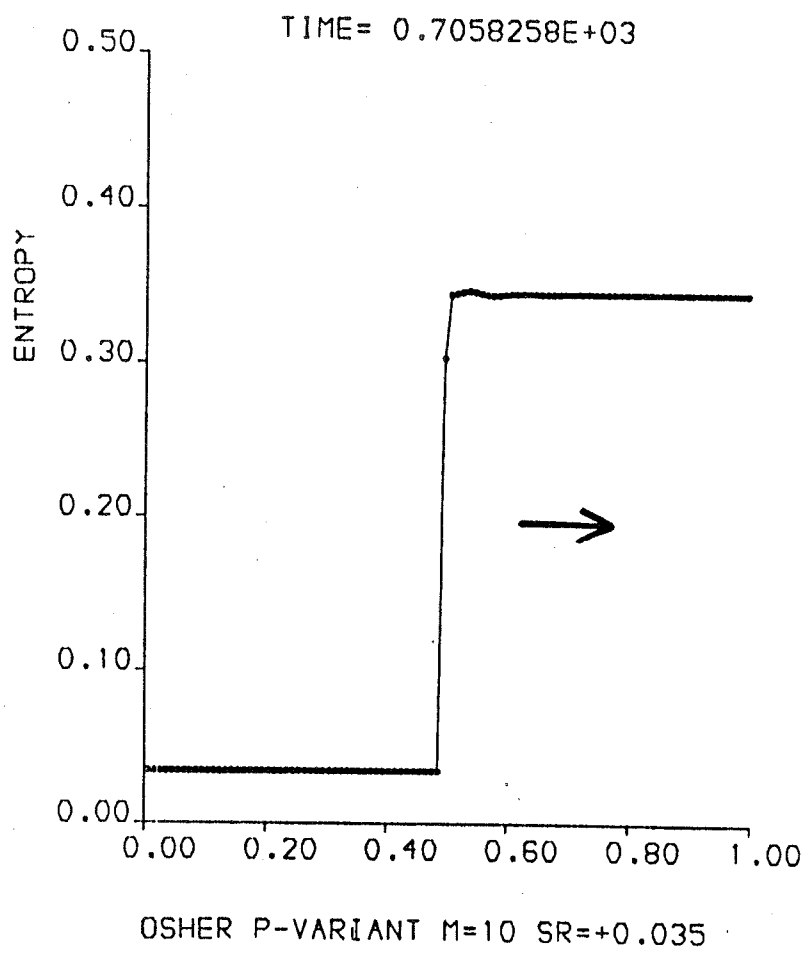

Fig. 10 moving shock results from P variant.

in phase space

——— Osher's scheme

..... Bell's scheme
with linera interpolation of λ

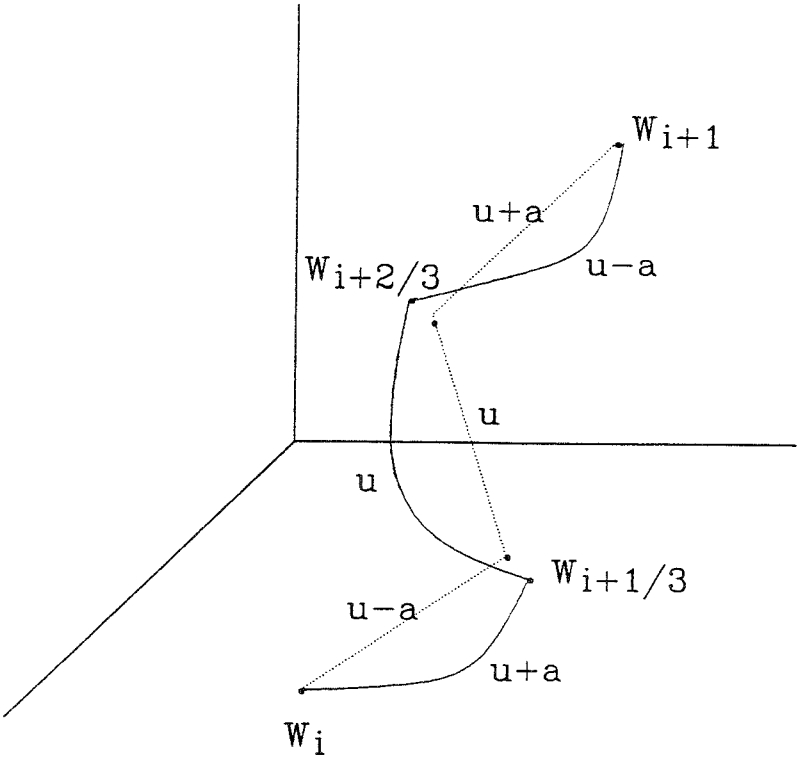

Fig. 11 wave paths of Osher's and Bell's schemes in the phase space

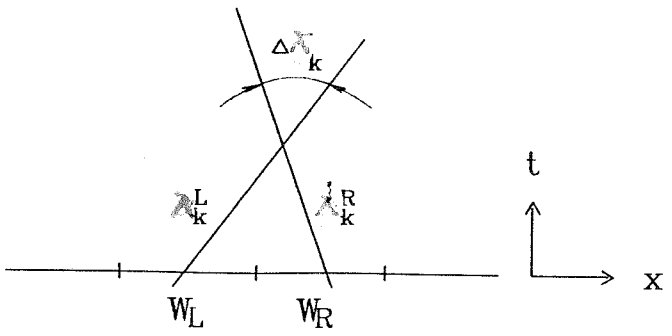

Fig. 12 wave diagram for dissipation

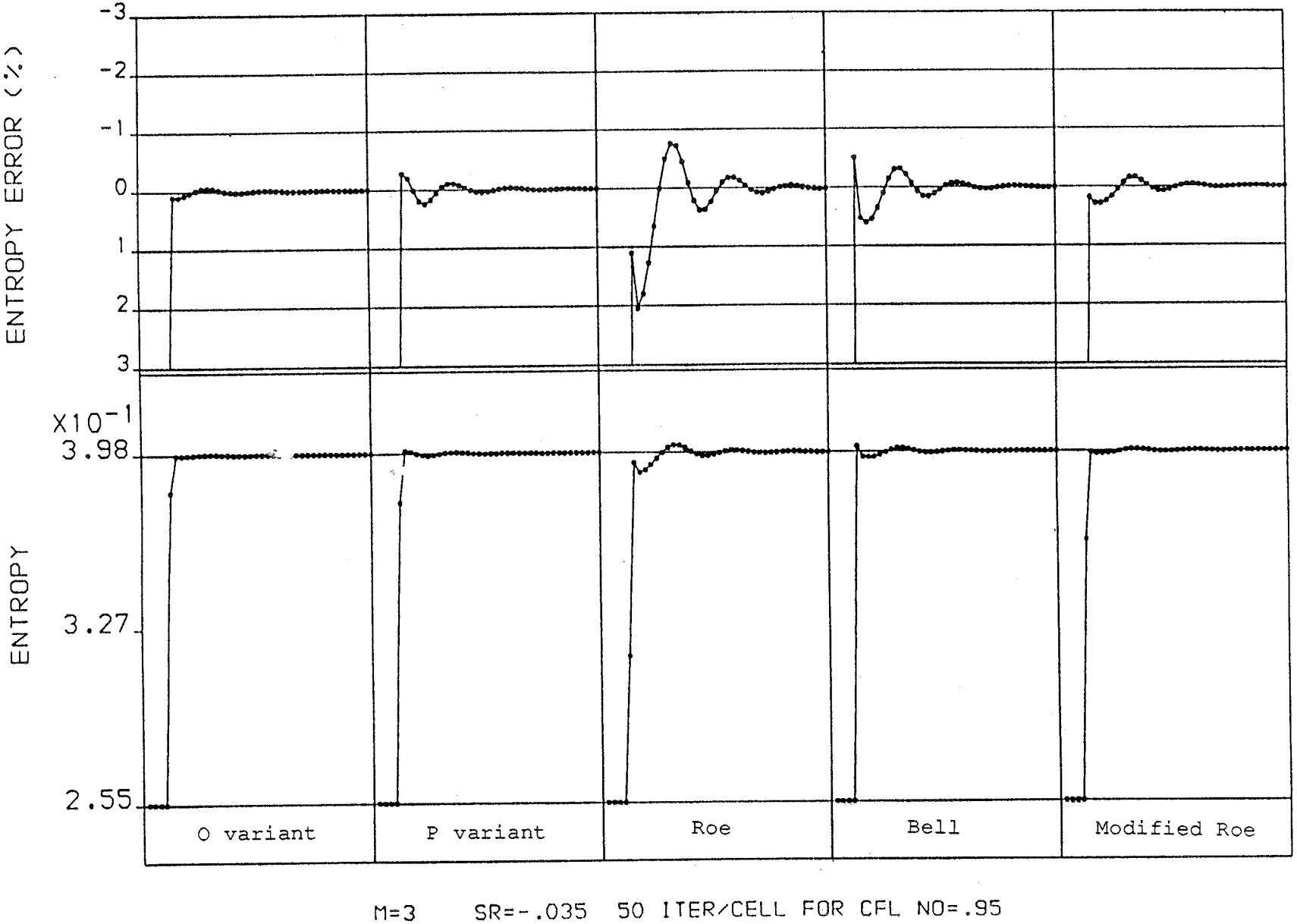

Fig. 13 Comparison of entropy oscillations for 1st order results

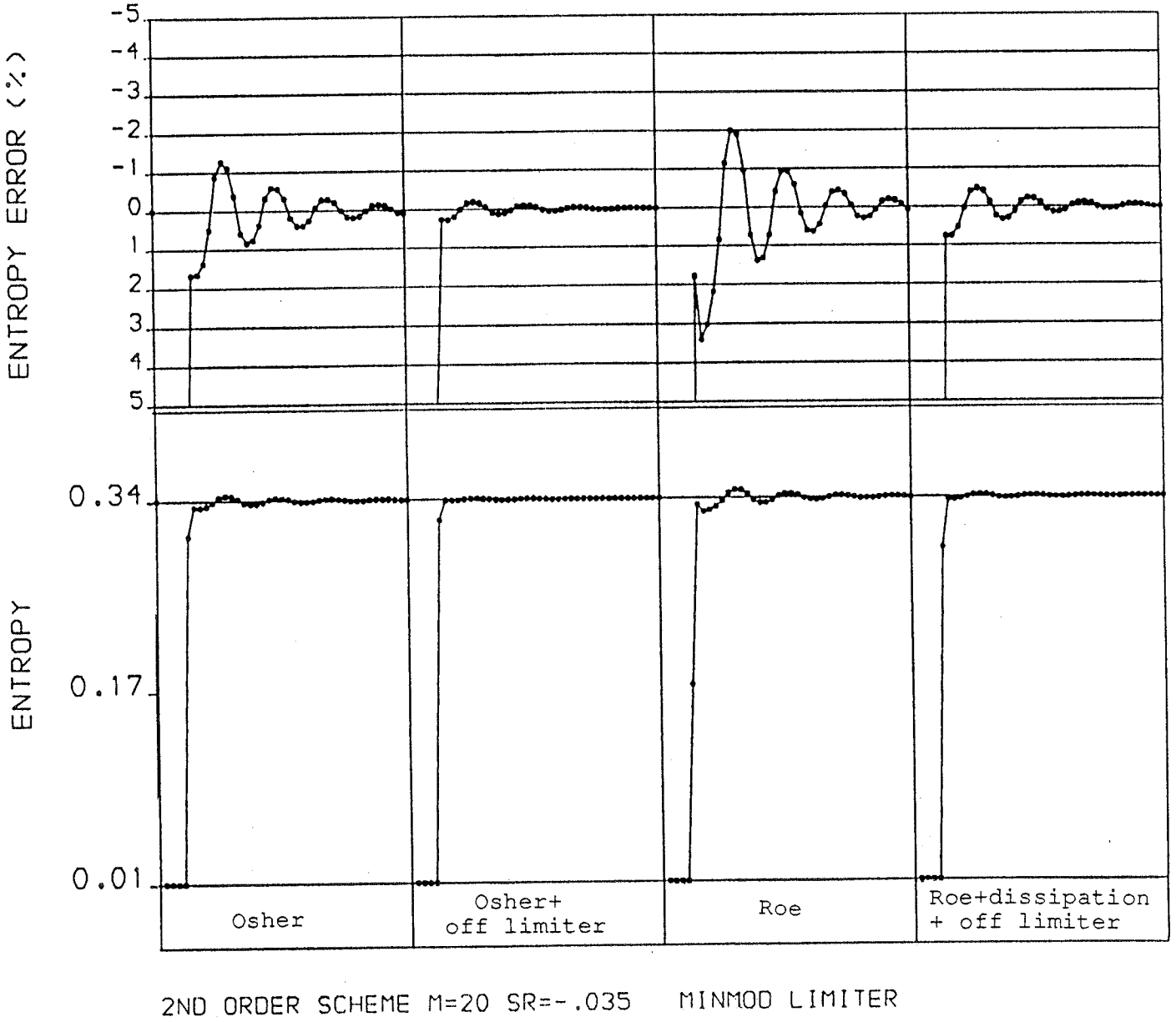

Fig. 14 Comparison of entropy oscillations for 2nd order results
(Lax-Wendroff scheme with minmod limiter)

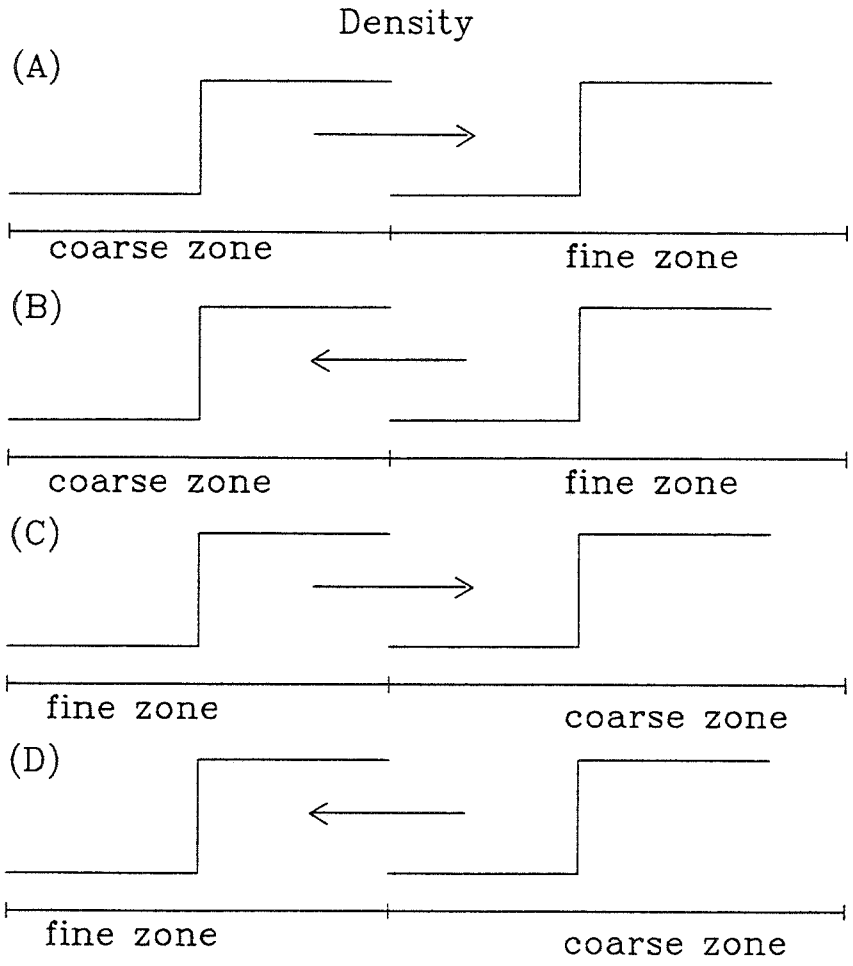

Fig. 15 moving shock test cases

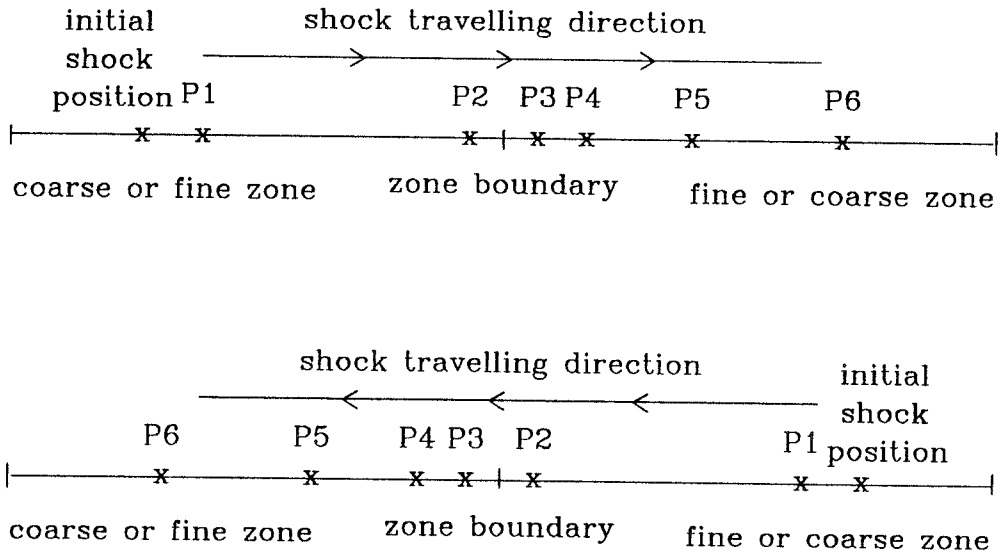

Fig. 16 monitored points for the moving shock test

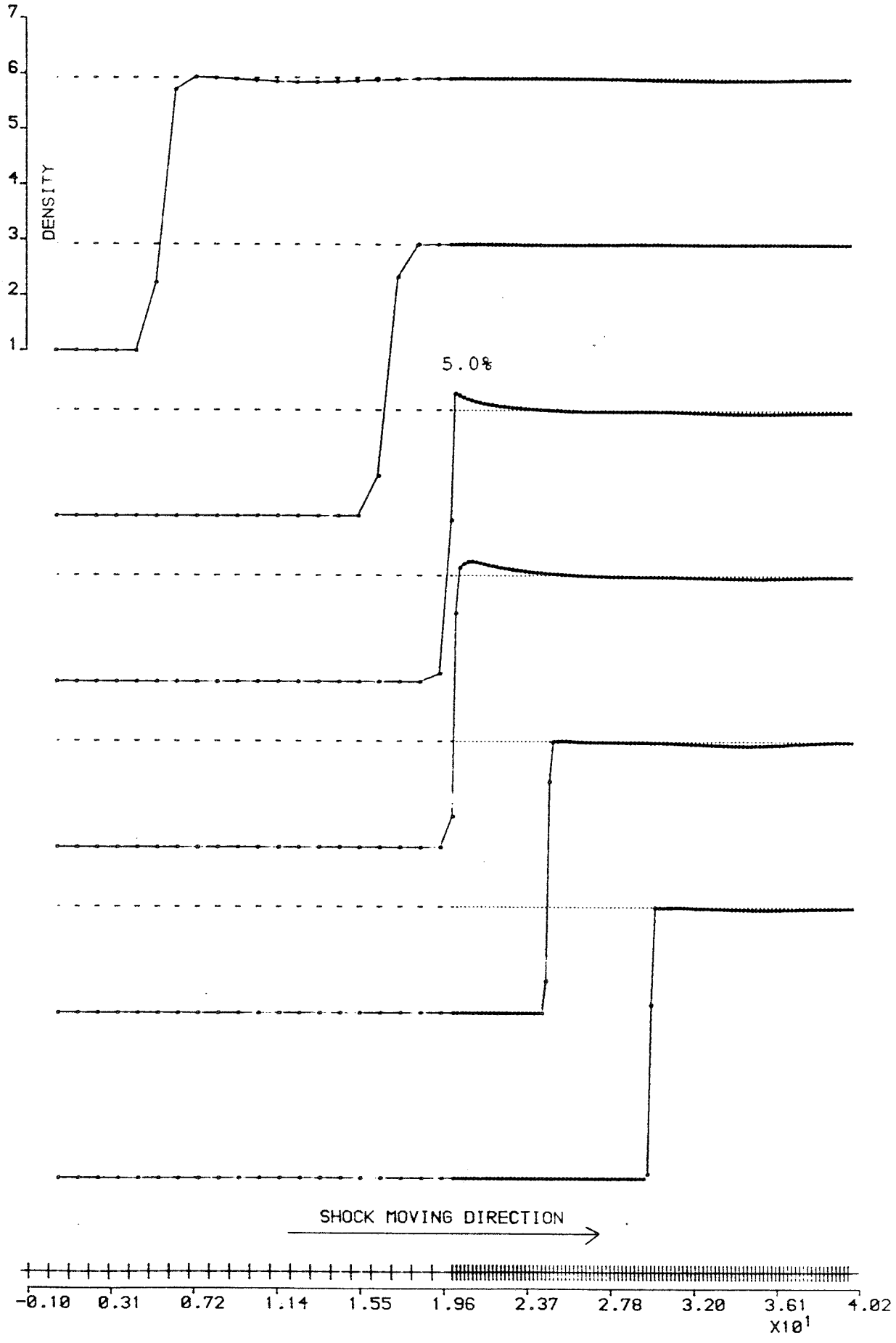

Fig. 17 : Osher's scheme M=20 SR=+0.035 Case A Mesh ratio 5:1

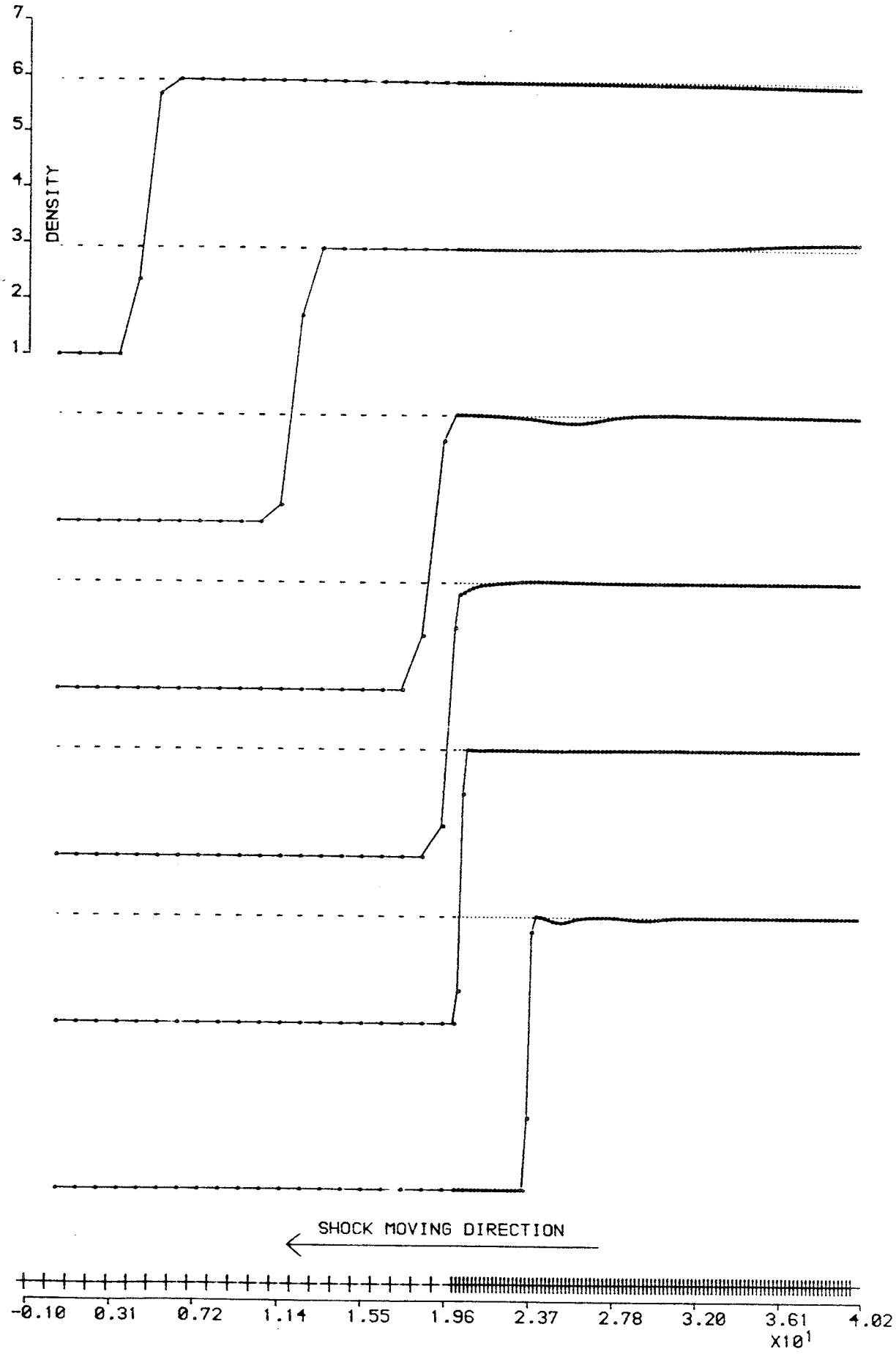

Fig. 18 : Osher's scheme M=20 SR=-0.035 Case B Mesh ratio 5:1

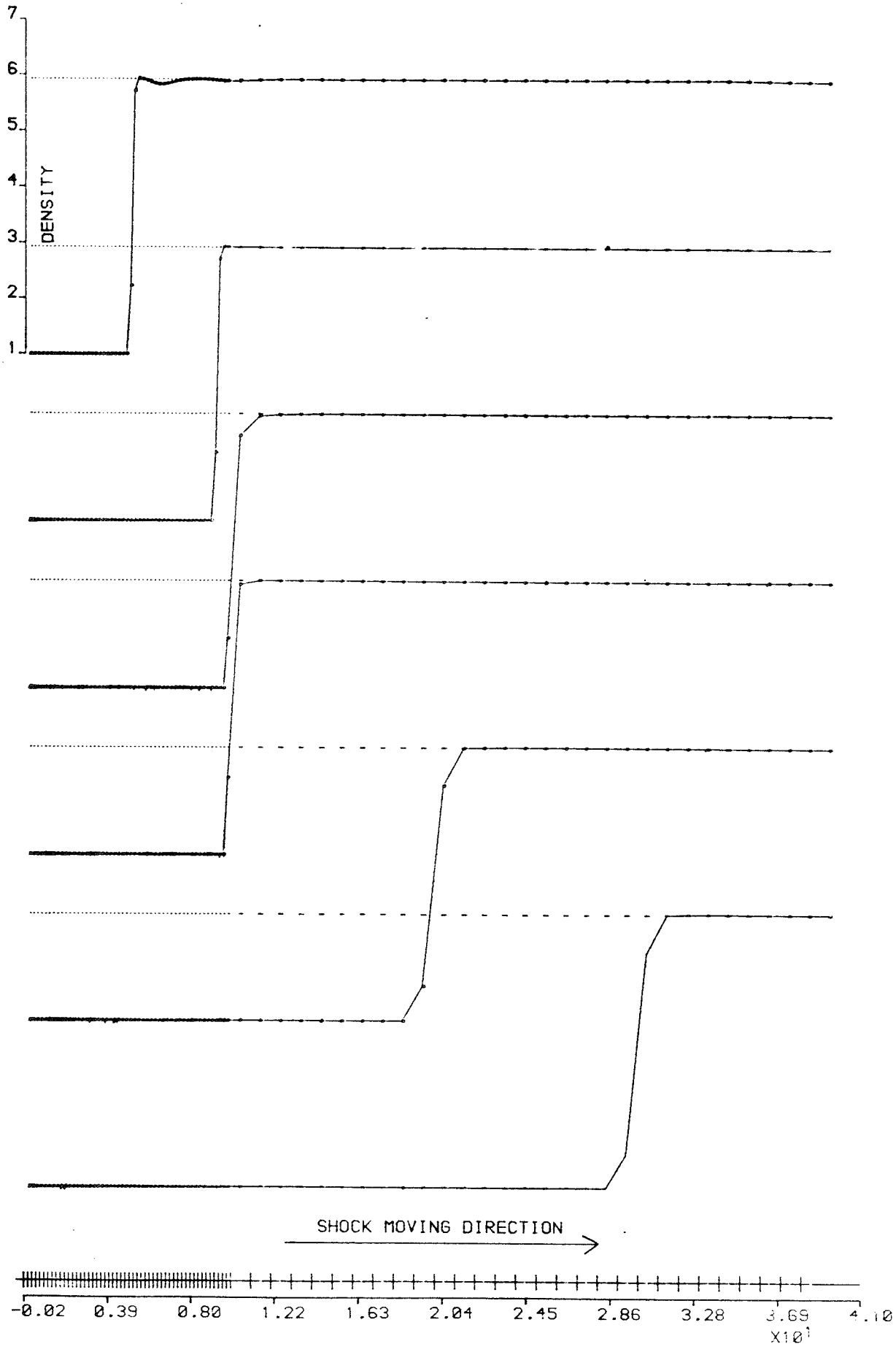

Fig. 19 : Osher's scheme M=20 SR=+0.035 Case C Mesh ratio 1:5

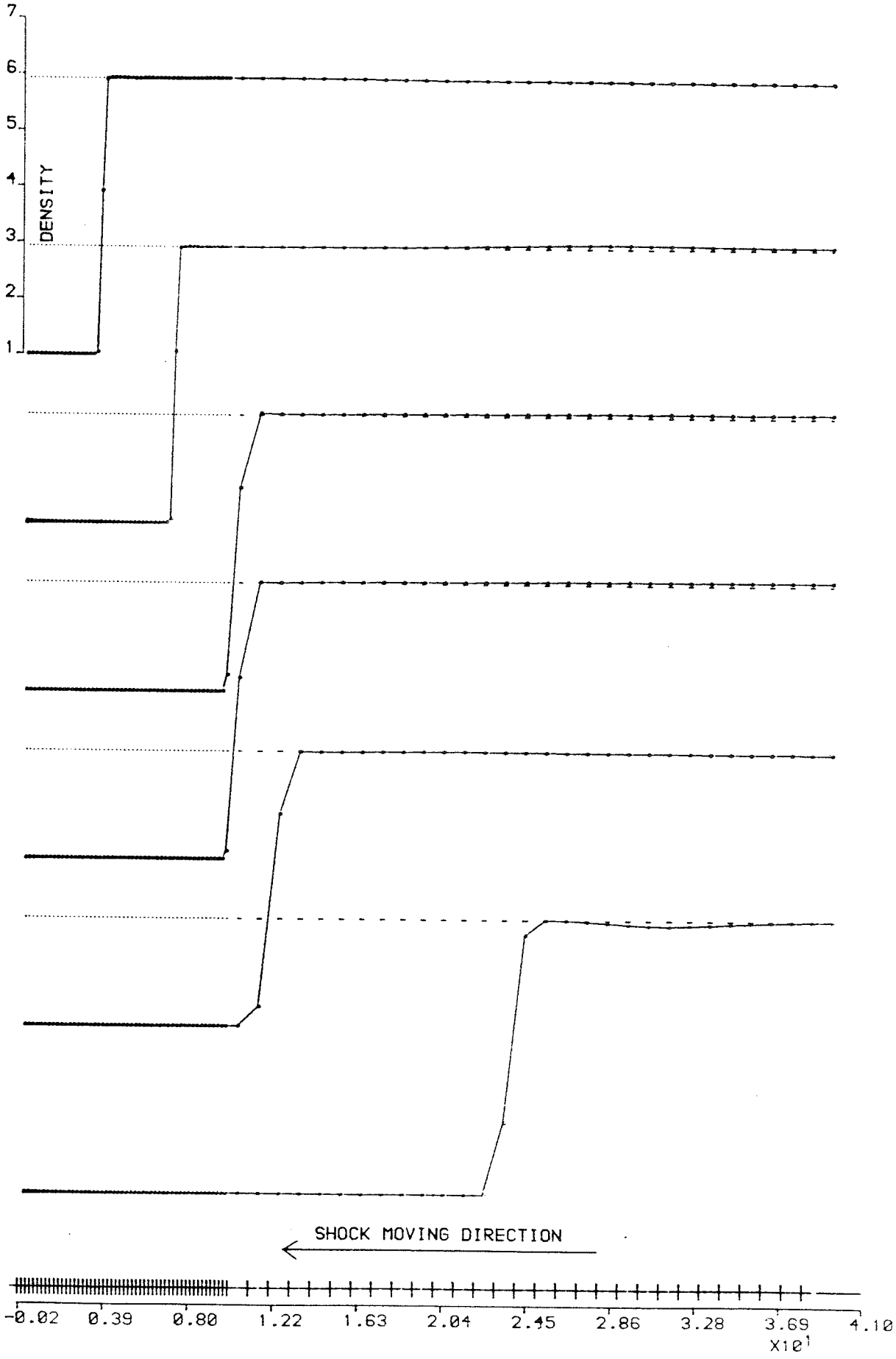

Fig. 20 : Osher's scheme M=20 SR=-0.035 Case D Mesh ratio 1:5

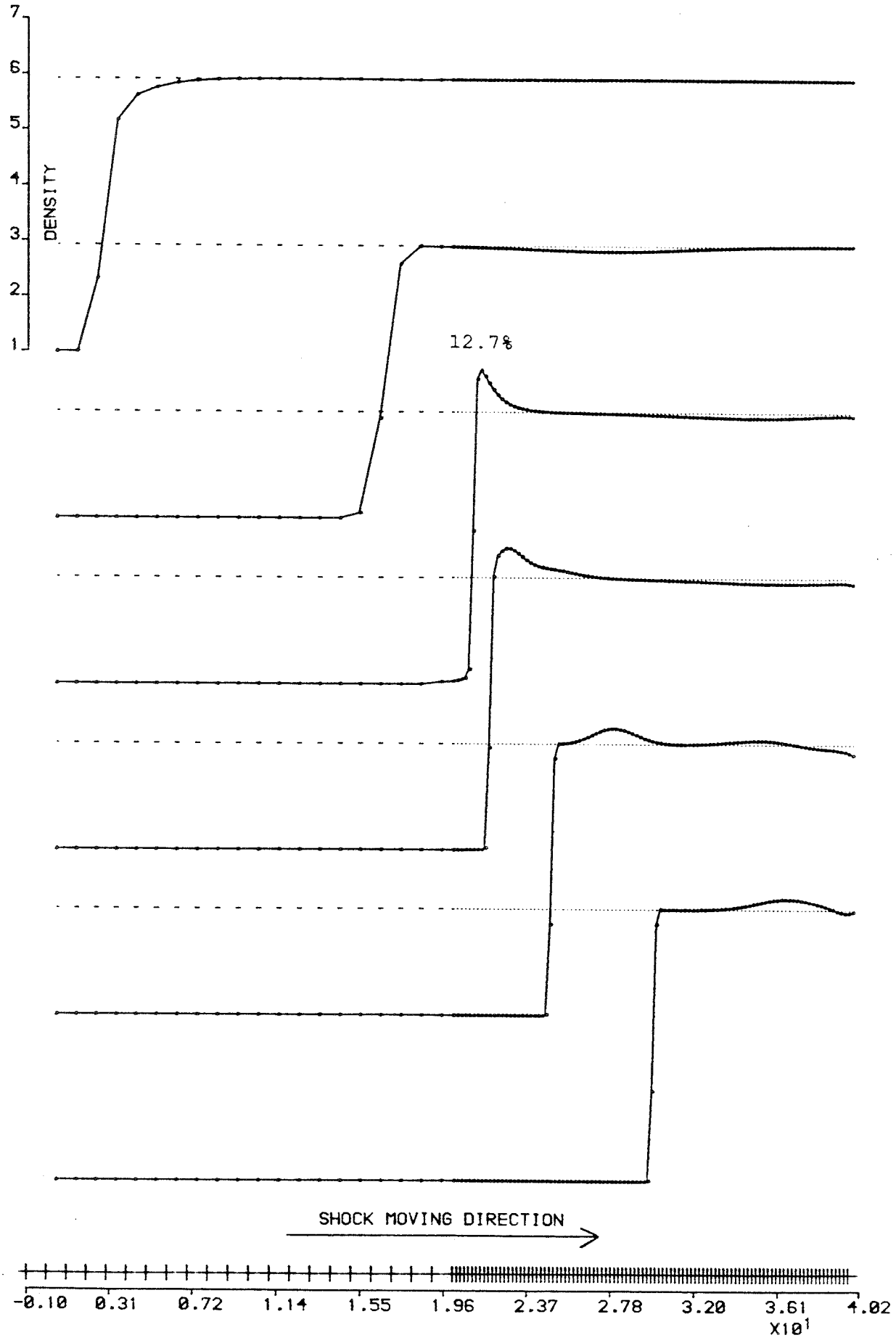

Fig. 21 : Osher's scheme M=20 SR=+0.28 Case A Mesh ratio 5:1

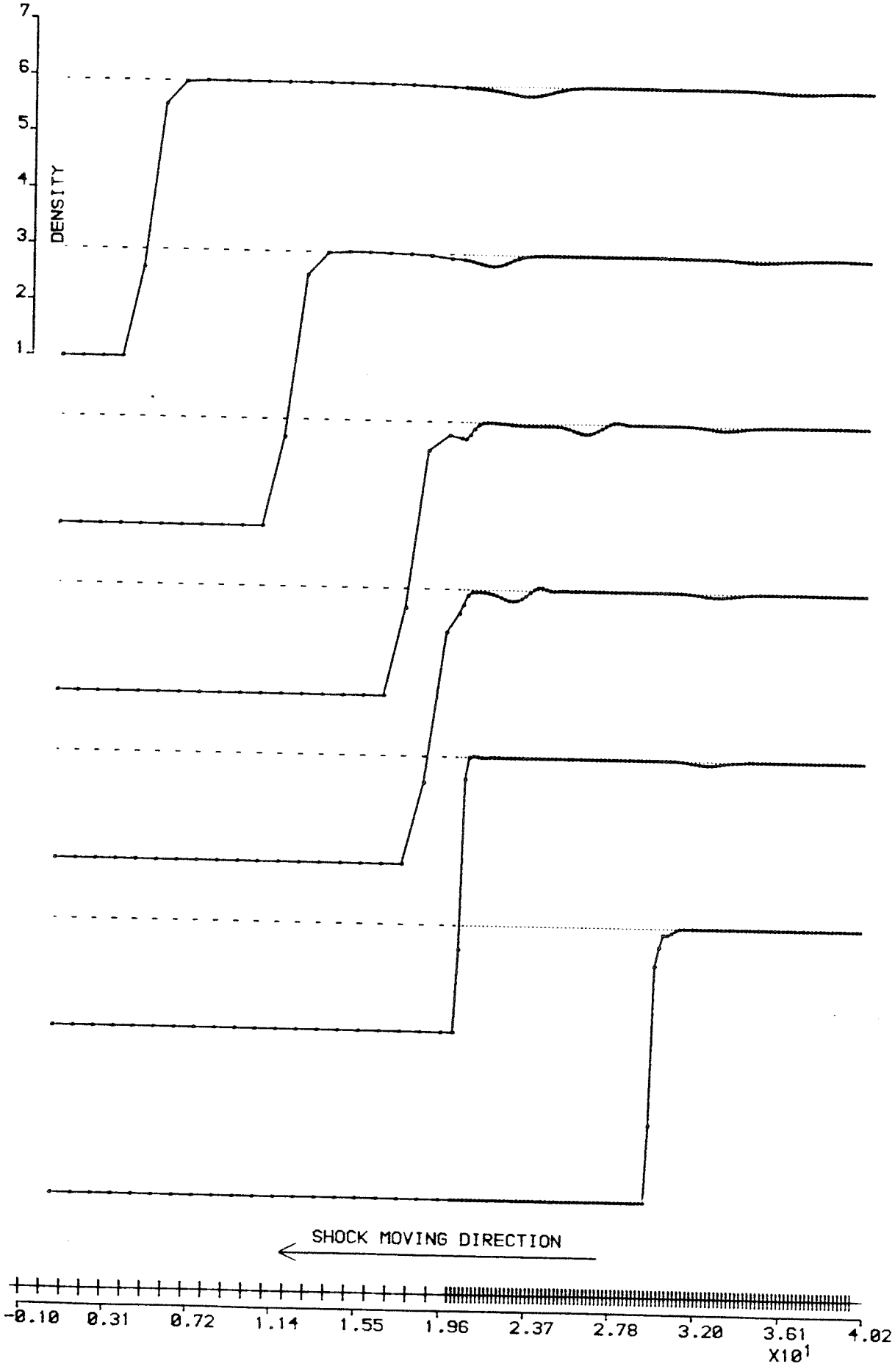

Fig. 22 : Osher's scheme M=20 SR=-0.28 Case B Mesh ratio 5:1

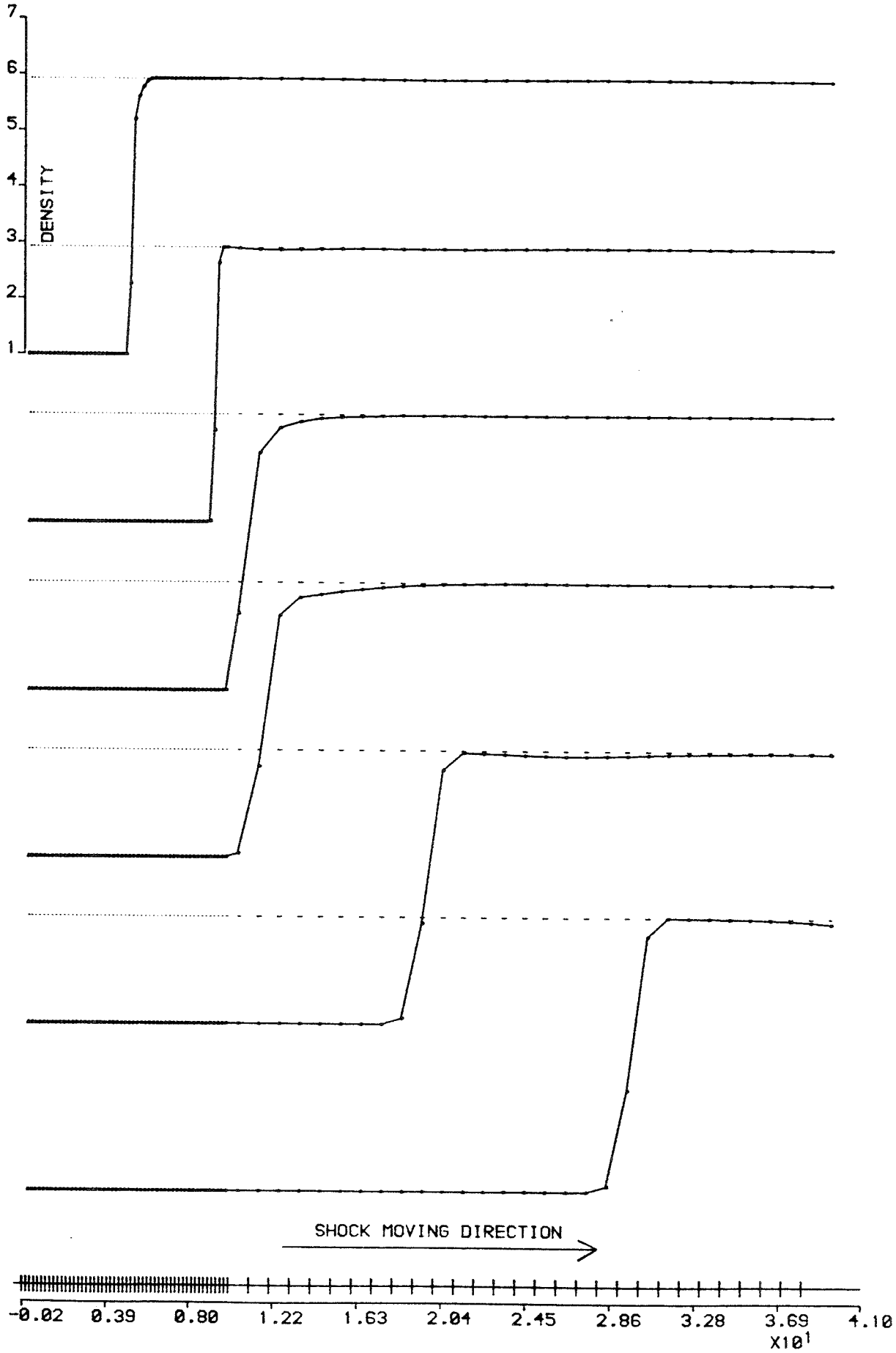

Fig. 23 : Osher's scheme M=20 SR=+0.28 Case C Mesh ratio 1:5

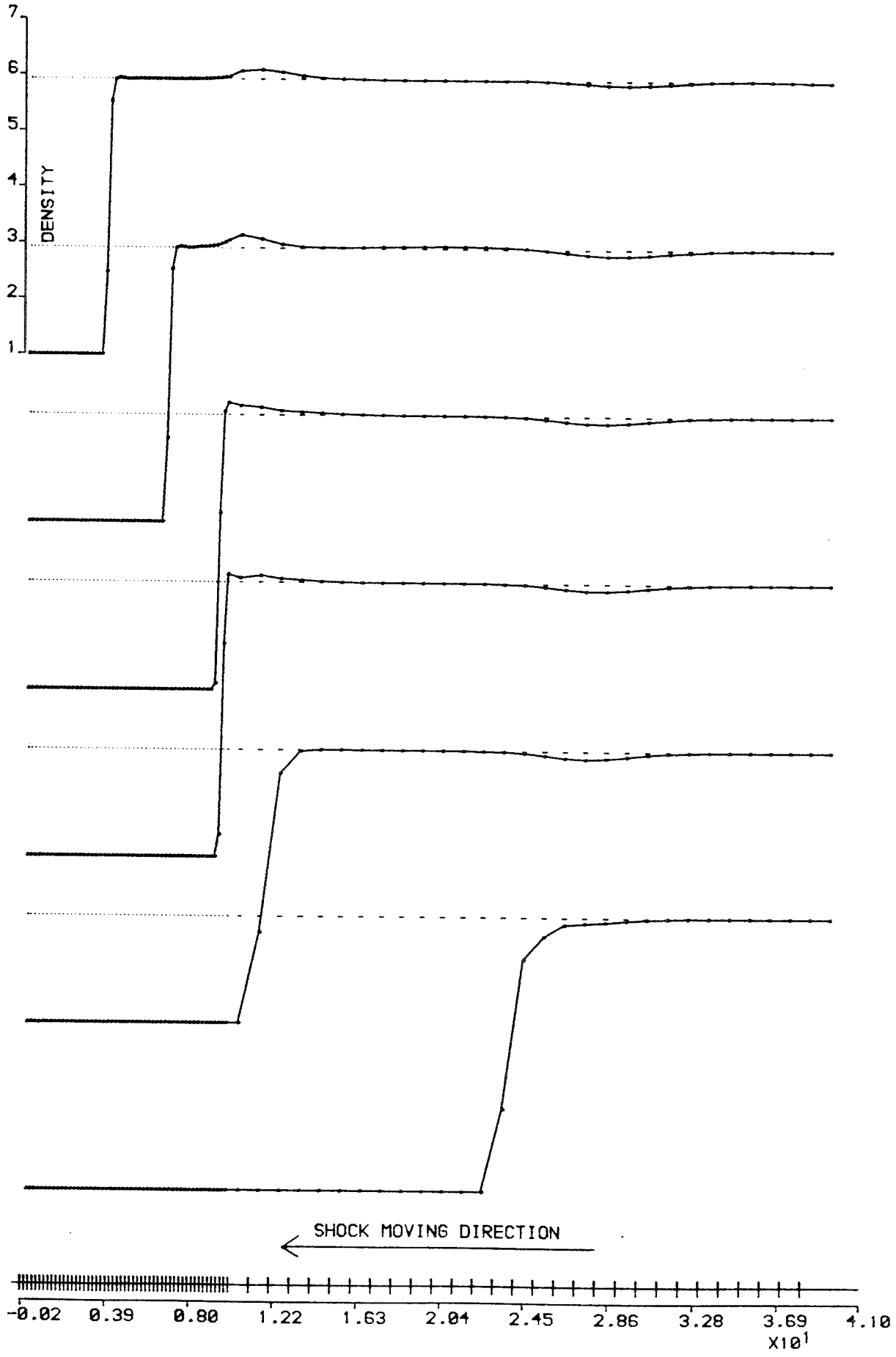

Fig. 24 : Osher's scheme M=20 SR=-0.28 Case D Mesh ratio 1:5

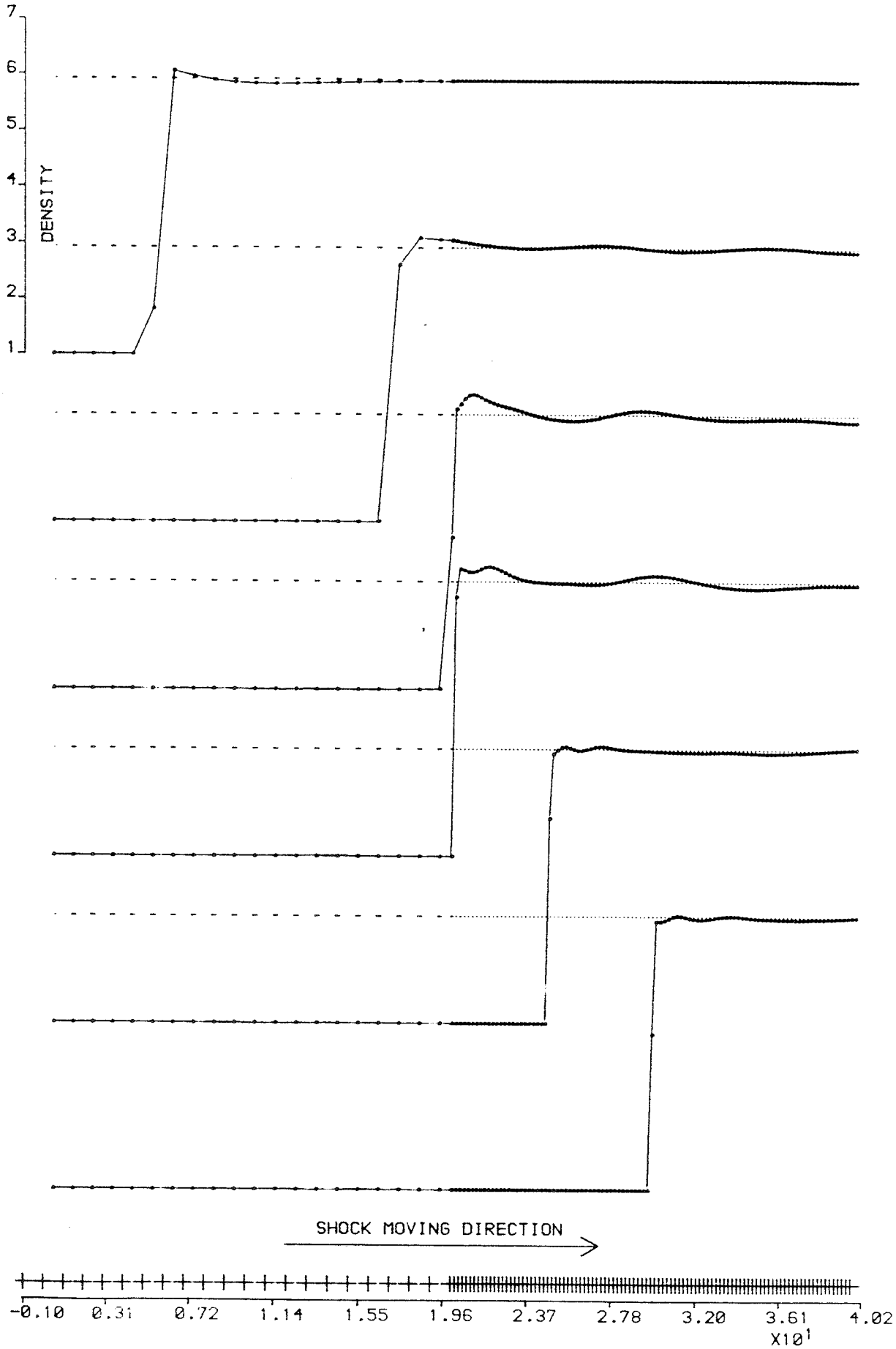

Fig. 25 : Roe's scheme M=20 SR=+0.035 Case A Mesh ratio 5:1

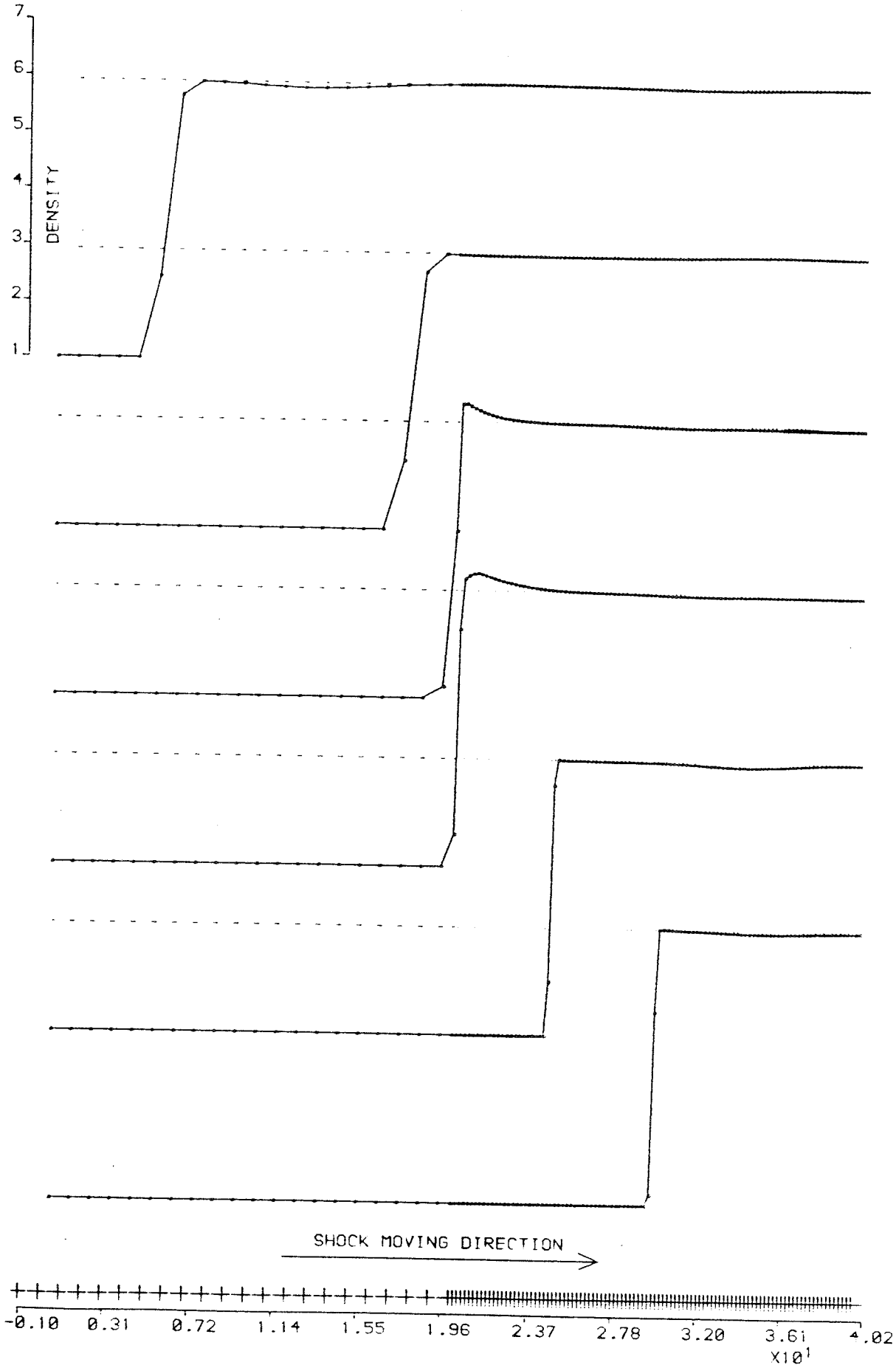

Fig. 26 : Roe's scheme with Harten's dissipation $\delta = 0.325$

M=20 SR=+0.035 Case A Mesh ratio 5:1

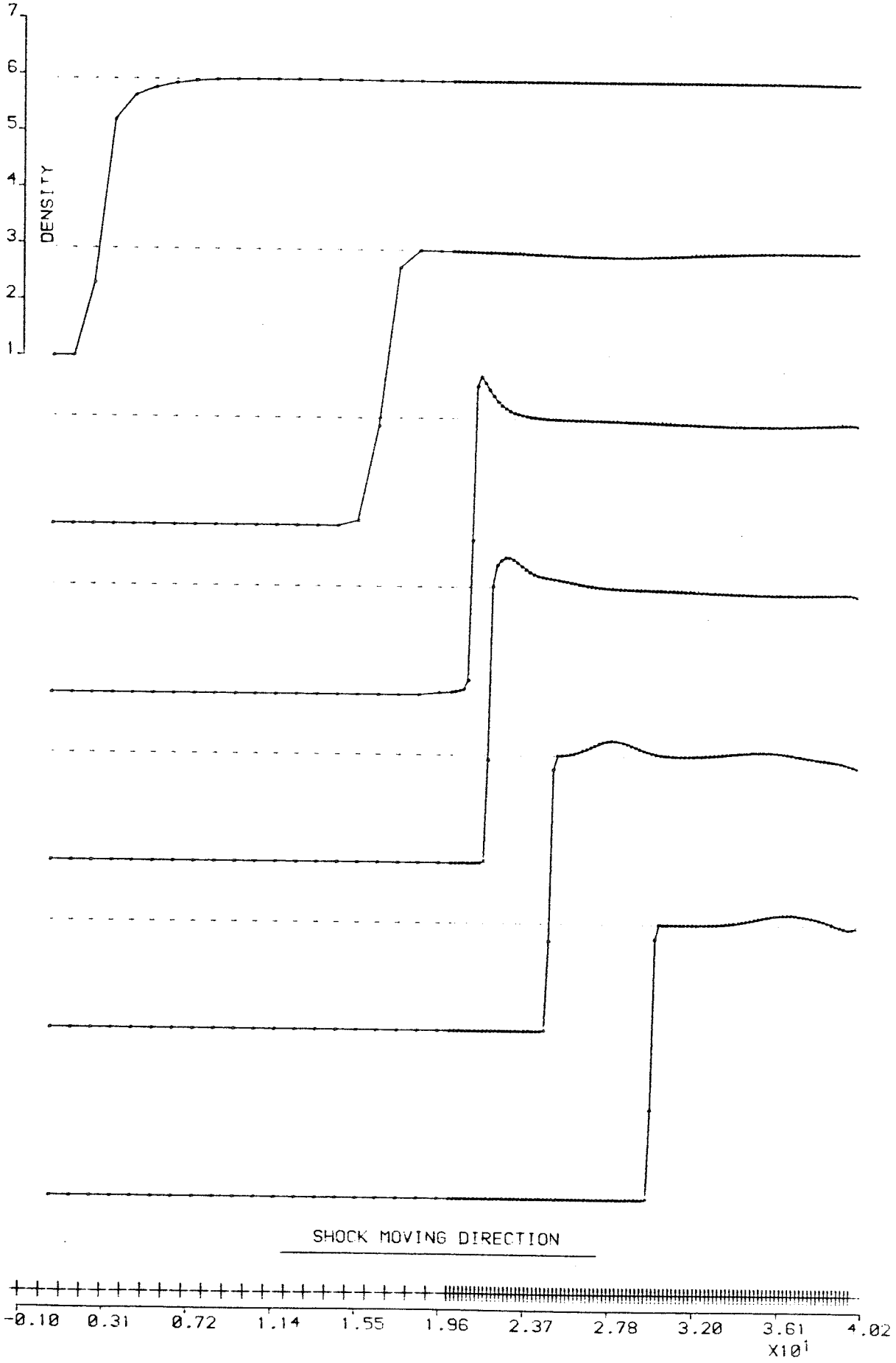

Fig. 27 : Roe's scheme M=20 SR=+0.28 Case A Mesh ratio 5:1

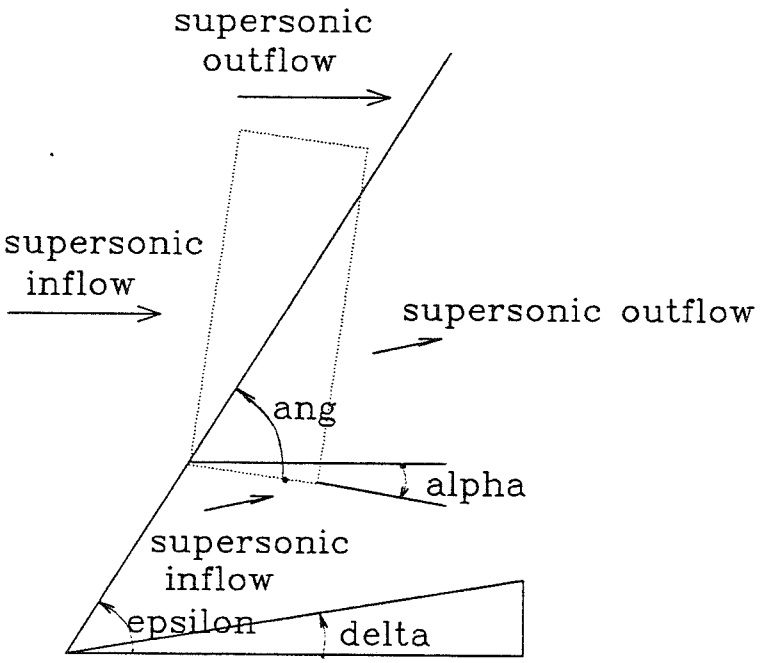

shock-grid angle (ang)=epsilon+alpha

Fig. 28 test case for an oblique shock

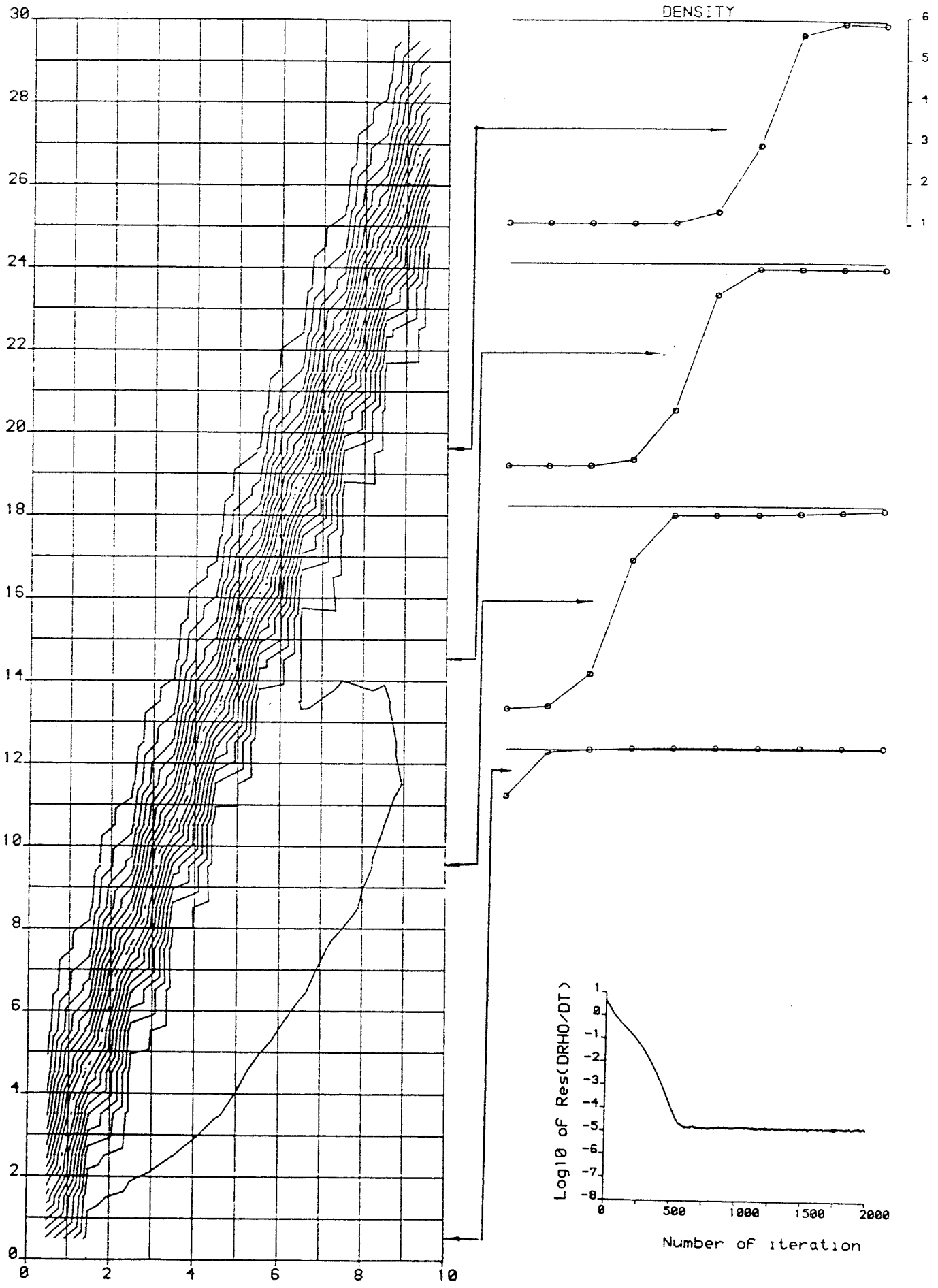

Fig. 29 1ST ORDER ROE SCHEME FOR 10X30WEDGE M=20 DELTA=43.6 ALPHA=10

ANG=70 ITER=2000 RES=1.3E-5 CFL=.9 DOTTED LINE DENSITY=3.5

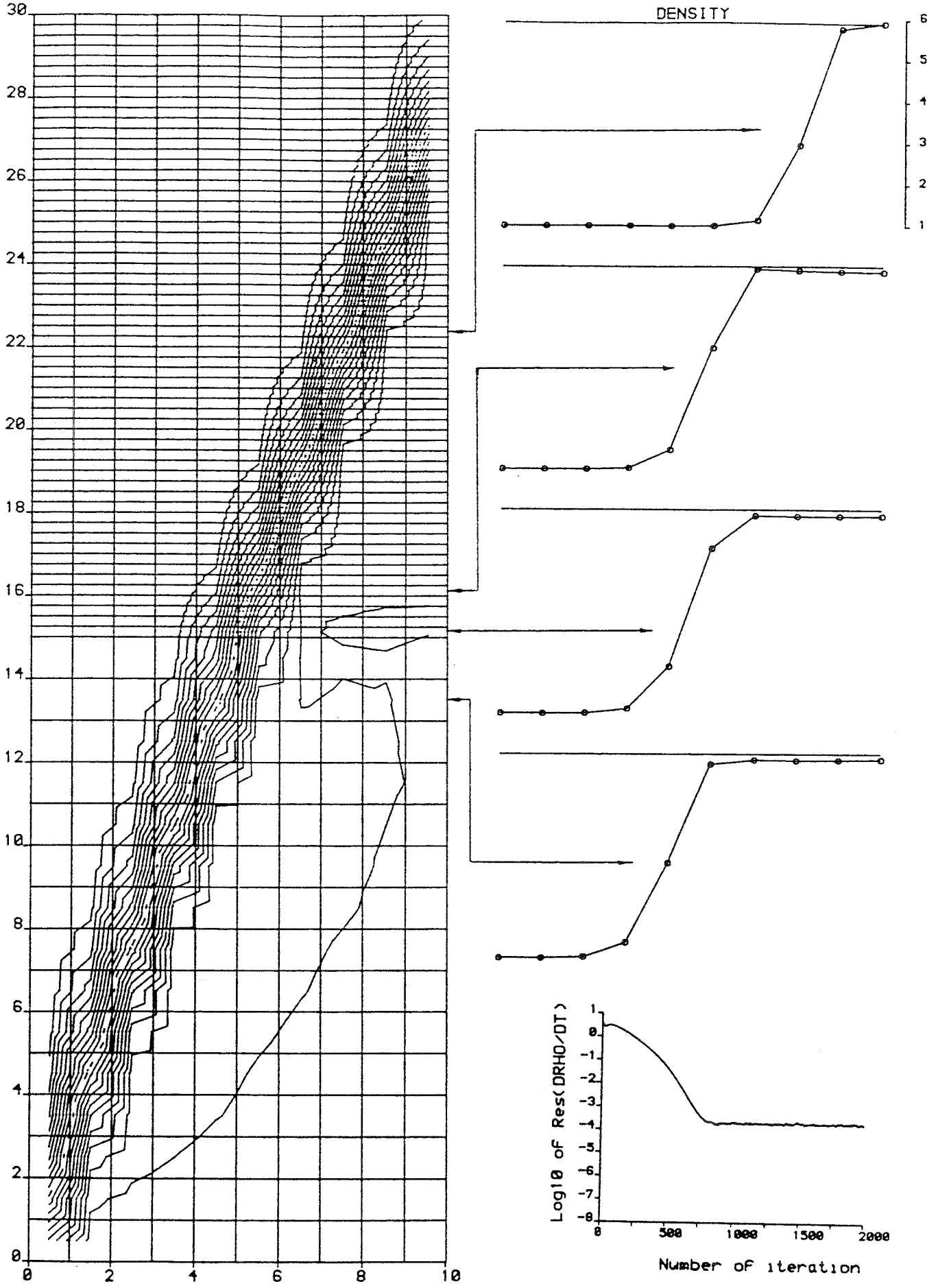

Fig. 30 1ST ORDER ROE SCHEME FOR 10X75WEDGE M=20 DELTA=43.6 ALPHA=10

ANG=70 ITER=2000 RES=1.7E-4 CFL=.9 DOTTED LINE DENSITY=3.5

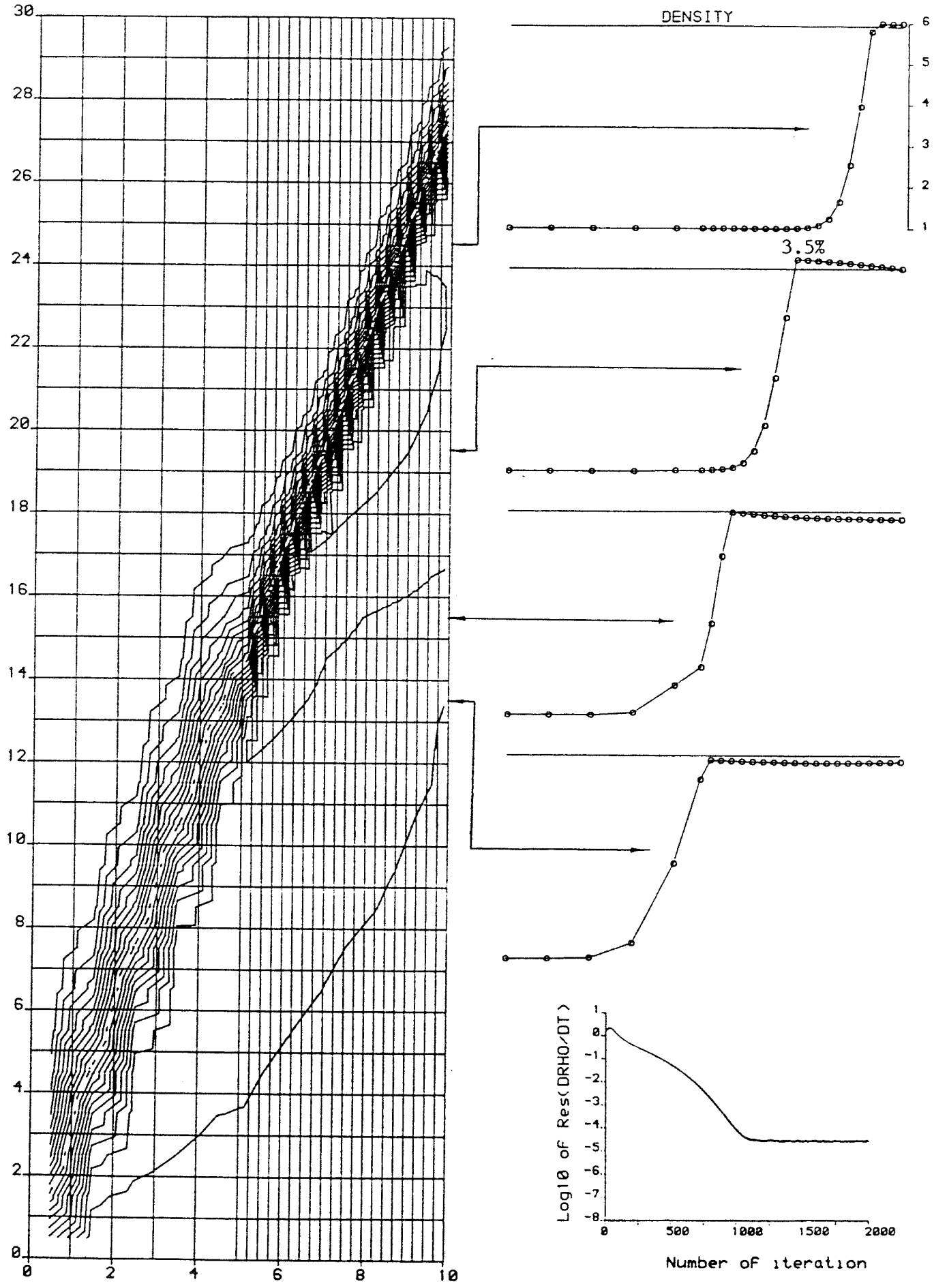

Fig. 31 1ST ORDER ROE SCHEME FOR 25X30WEDGE M=20 DELTA=43.6 ALPHA=10 ANG=70 ITER=2000 RES=2.7E-5 CFL=.9 DOTTED LINE DENSITY=3.5

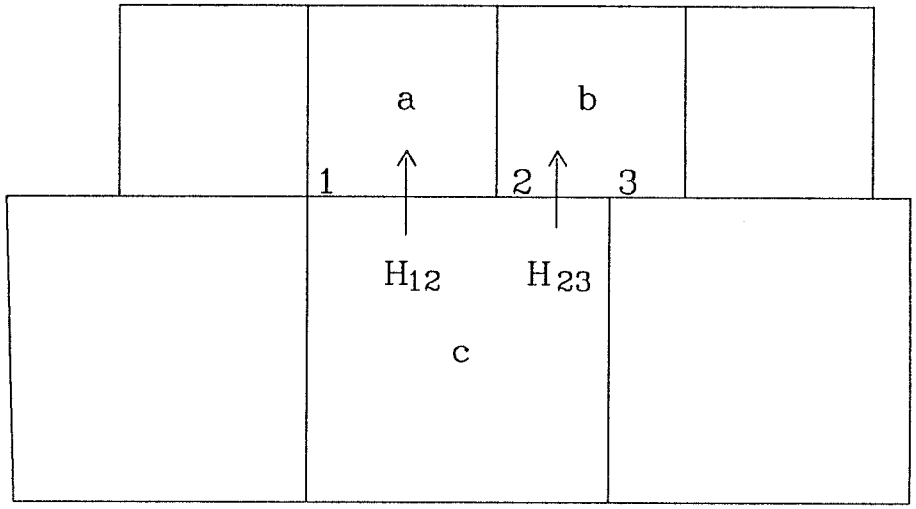

Fig. 32 interface treatment

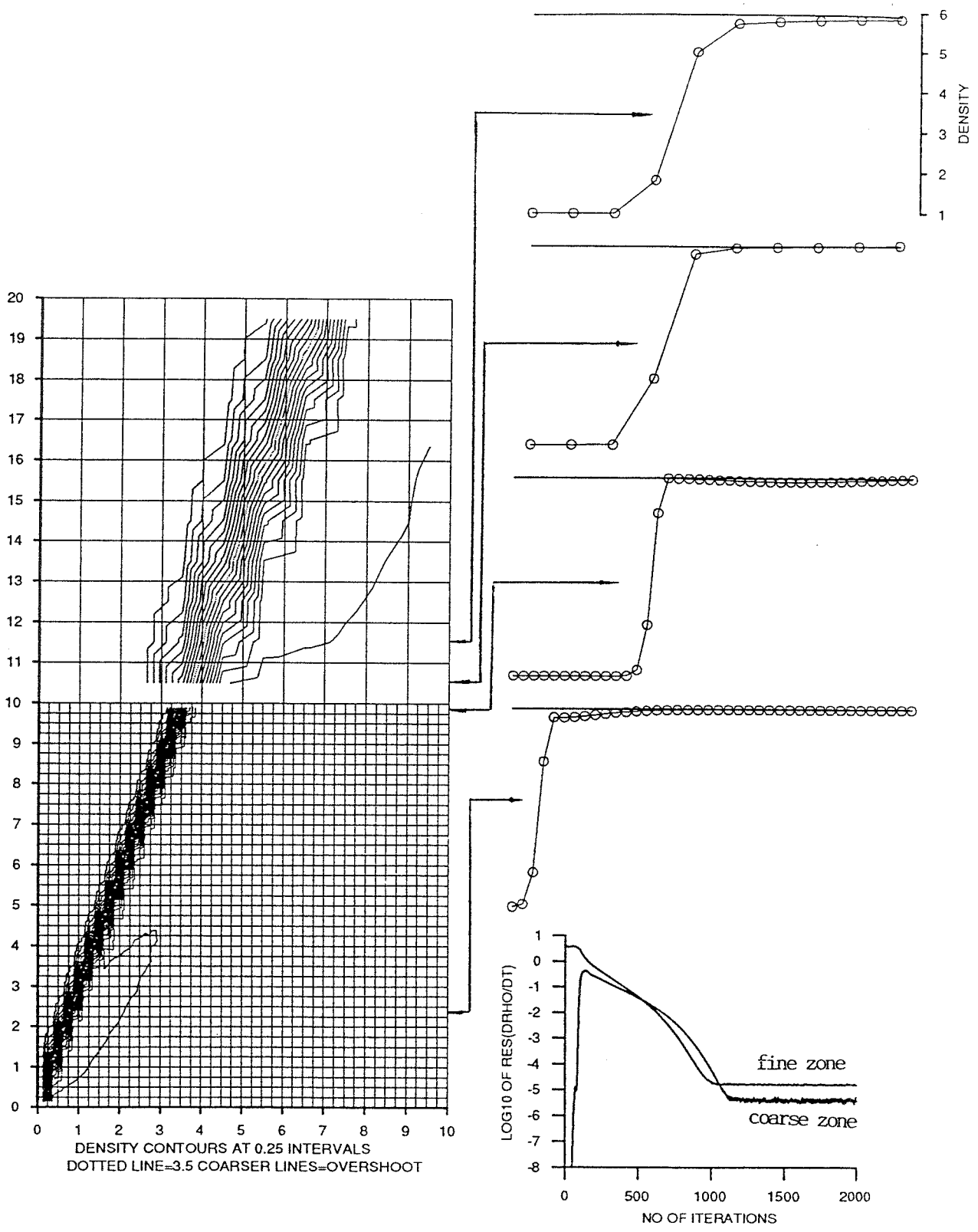

1ST ORDER ROE SCHEME FOR AN OBLIQUE SHOCK M=20 DELTA=43.64 EPSILON=60 ALPHA=10
LOCAL CFL=0.9 N=2000 PRE-SHOCK COND. AS INITIAL COND.

Fig. 33

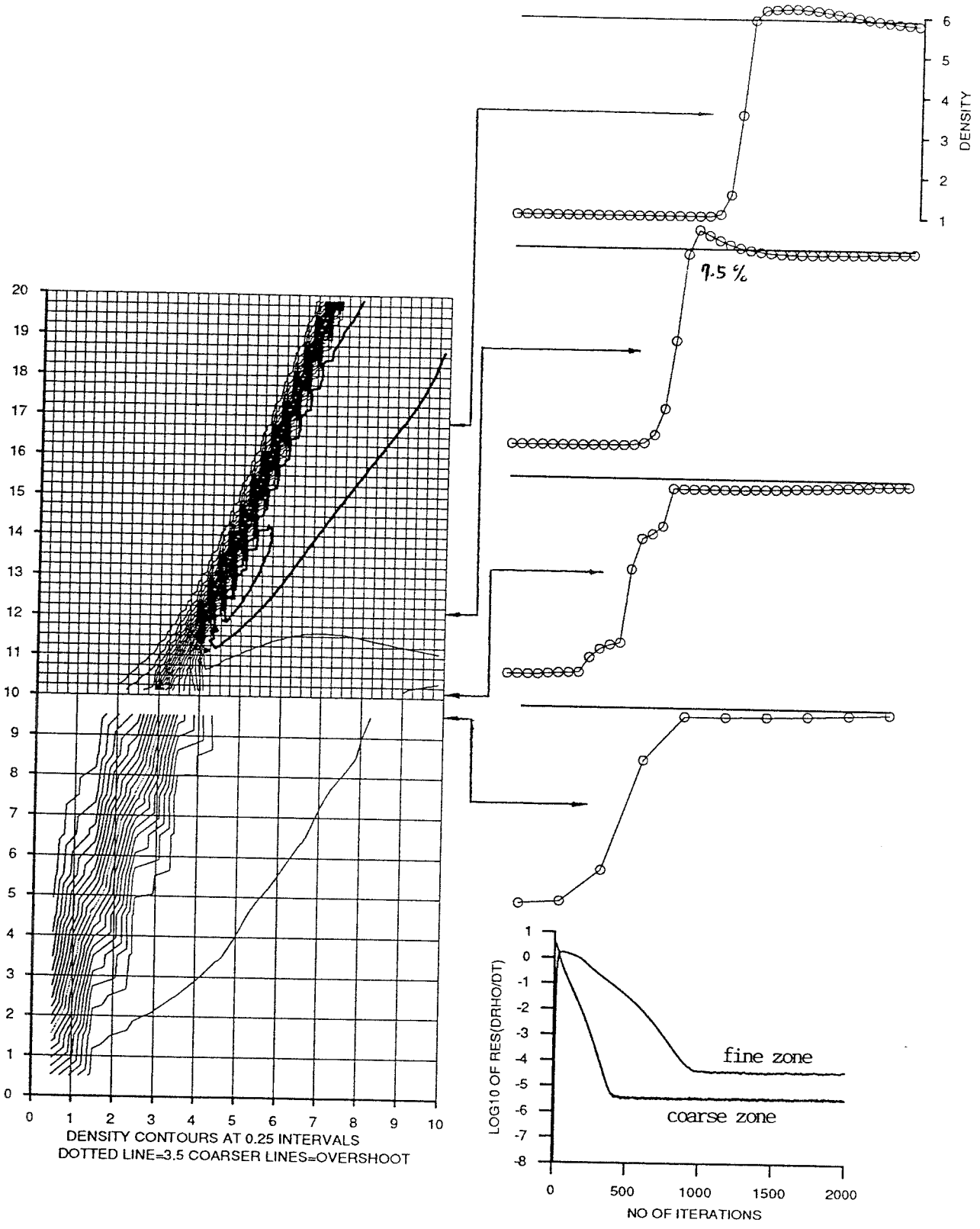

1ST ORDER ROE SCHEME FOR AN OBLIQUE SHOCK M=20 DELTA=43.64 EPSILON=60 ALPHA=10
LOCAL CFL=0.9 N=2000 PRE-SHOCK COND. AS INITIAL COND.

Fig. 34

MEHTOD 1

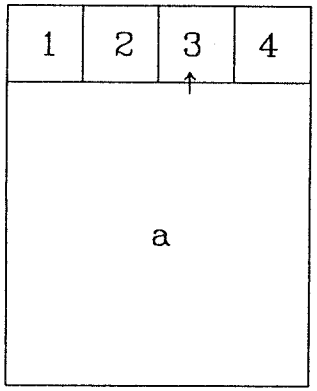

$$\text{Flux}=\text{R.S.}(W_a, W_3)$$

R.S.=Riemann Solver

MEHTOD 2

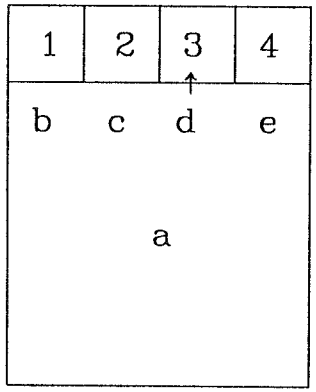

$$W_b = W_a - \frac{3}{6}(W_4 - W_1)$$
$$W_c = W_a - \frac{1}{6}(W_4 - W_1)$$
$$W_d = W_a + \frac{1}{6}(W_4 - W_1)$$
$$W_e = W_a + \frac{3}{6}(W_4 - W_1)$$

$$\text{Flux}=\text{R.S.}(W_d, W_3)$$

METHOD 3

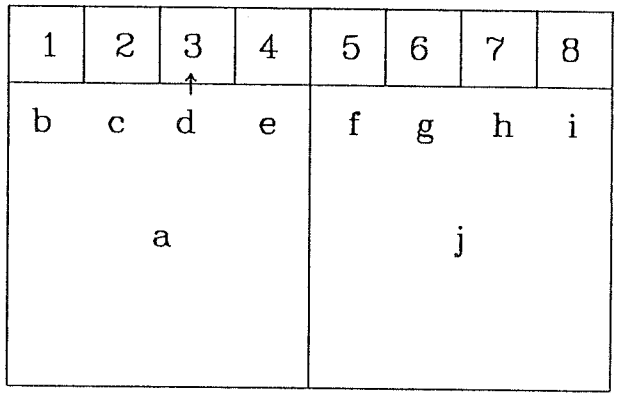

$$W_g = W_j - \frac{1}{8}(W_j - W_a)$$
$$W_f = W_j - \frac{3}{8}(W_j - W_a)$$
$$W_e = W_j - \frac{5}{8}(W_j - W_a)$$
$$W_d = W_j - \frac{7}{8}(W_j - W_a)$$

$$\text{Flux}=\text{R.S.}(W_d, W_3)$$

Fig. 35 various interpolations for flux calculation

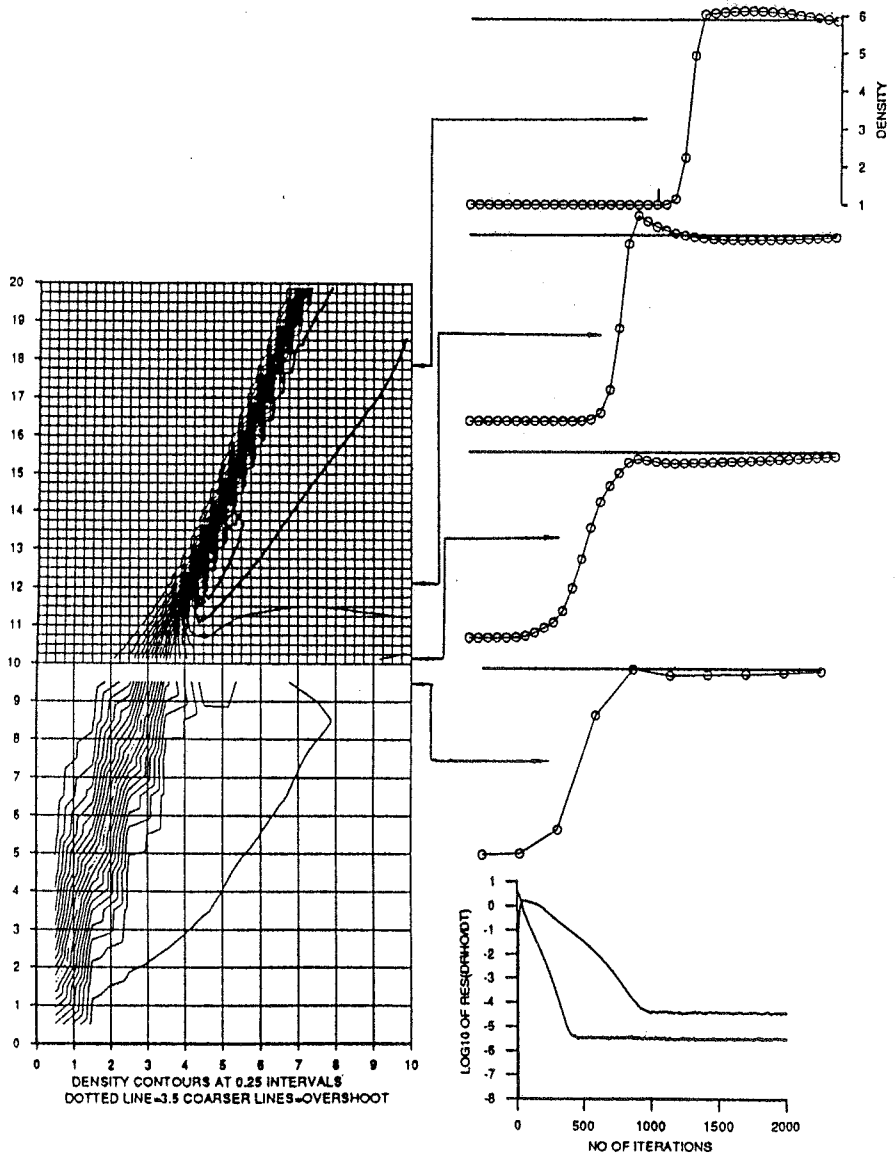

method 3

1ST ORDER ROE SCHEME FOR AN OBLIQUE SHOCK M=20 DELTA=43.64 EPSILON=60 ALPHA=10
LOCAL CFL=0.9 N= 2000 PRE-SHOCK COND. AS INITIAL COND. 'INTERP L'

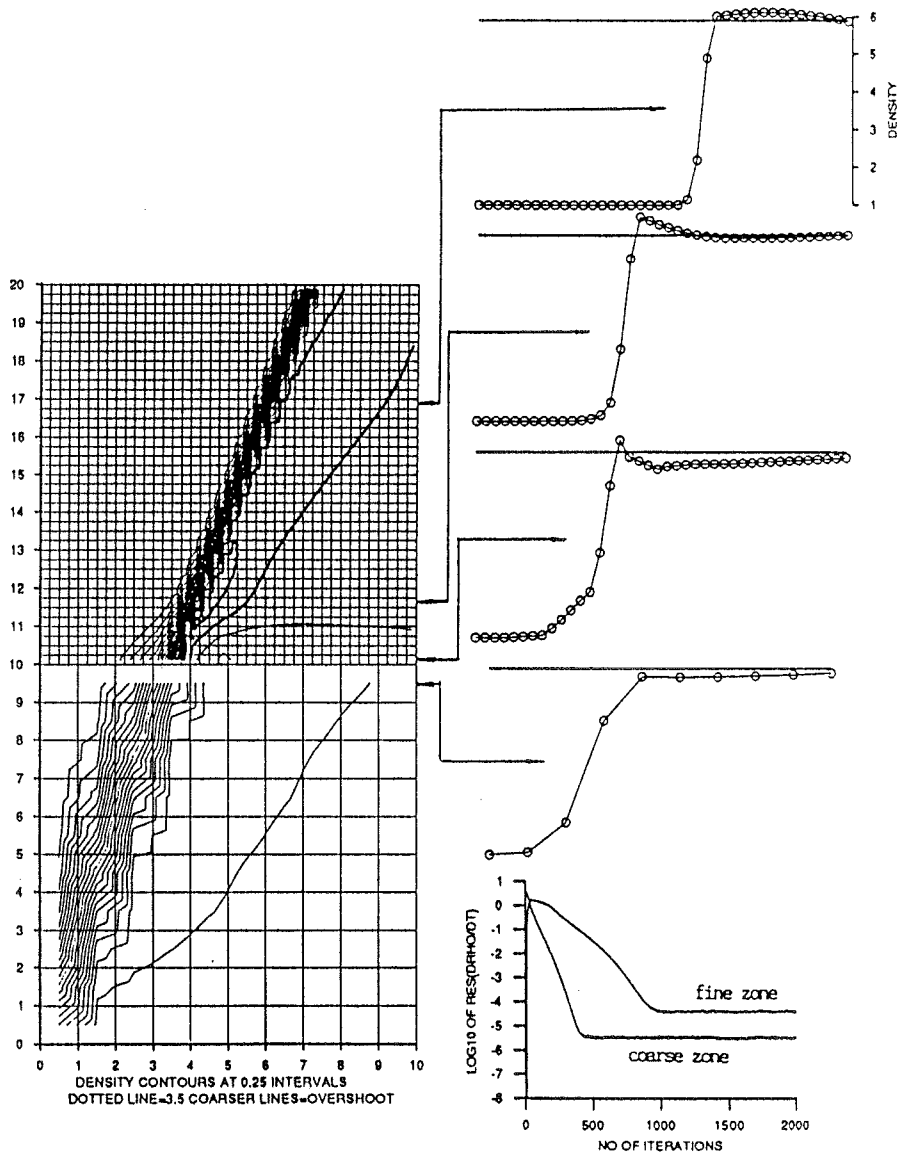

Method 2

1ST ORDER ROE SCHEME FOR AN OBLIQUE SHOCK M=20 DELTA=43.64 EPSILON=60 ALPHA=10
LOCAL CFL=0.9 N=2000 PRE-SHOCK COND. AS INITIAL COND.

Fig. 36 results from using interpolation method 2 and 3

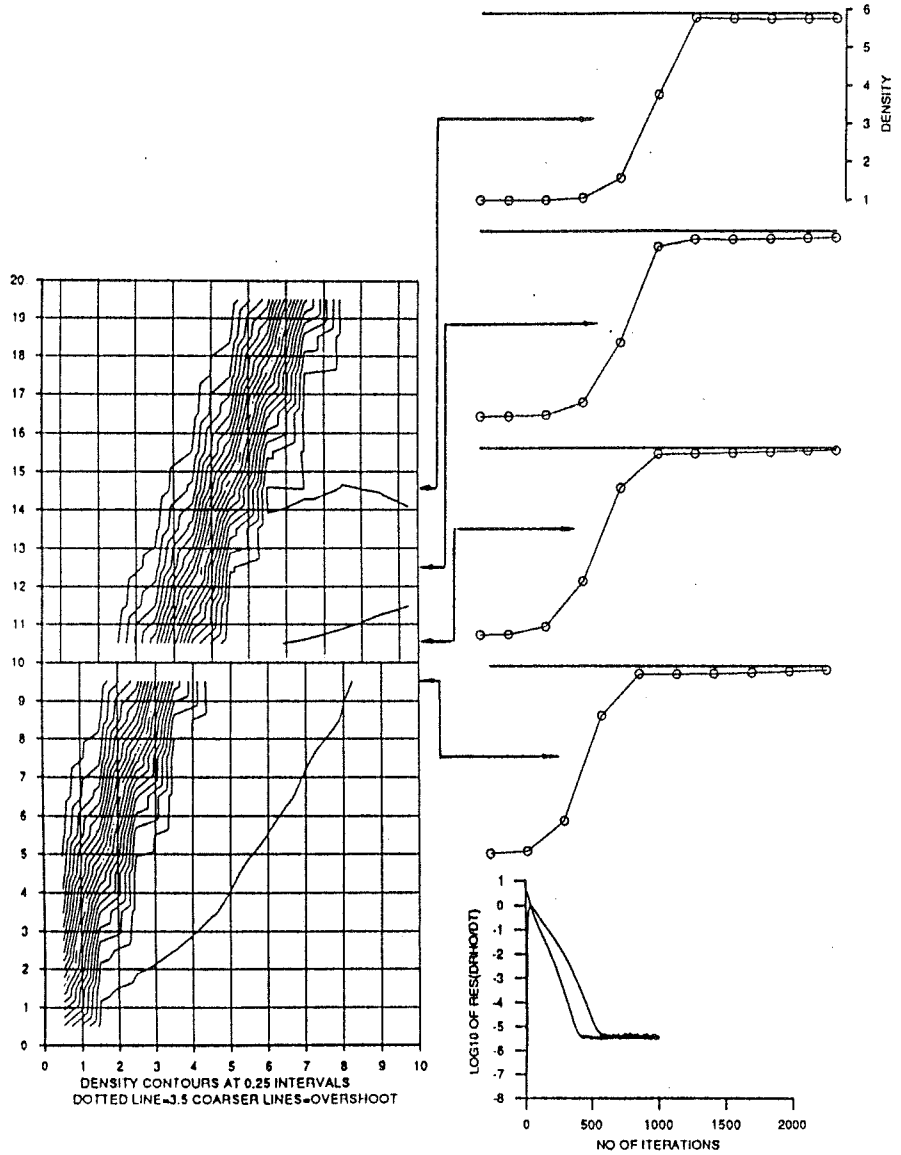

1ST ORDER ROE SCHEME FOR AN OBLIQUE SHOCK M=20 DELTA=43.64 EPSILON=60 ALPHA=10
LOCAL CFL=0.9 N=1000 PRE-SHOCK COND. AS INITIAL COND.

Fig. 37 result from equal spacing but discontinuous grid

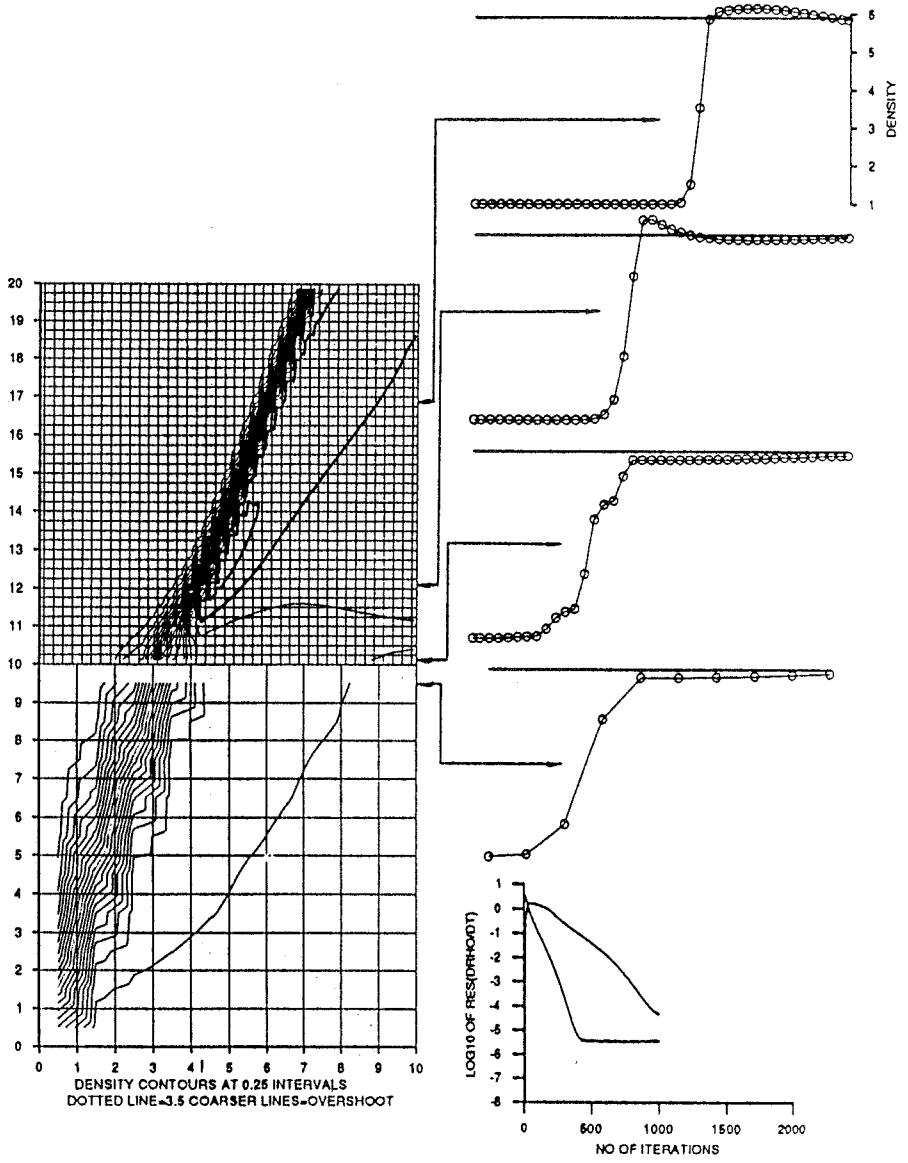

1ST ORDER ROE SCHEME FOR AN OBLIQUE SHOCK M=20 DELTA=43.64 EPSILON=60 ALPHA=10
LOCAL CFL=0.9 N=1000 PRE-SHOCK COND. AS INITIAL COND.

Fig. 38 result from noninteger grid spacing

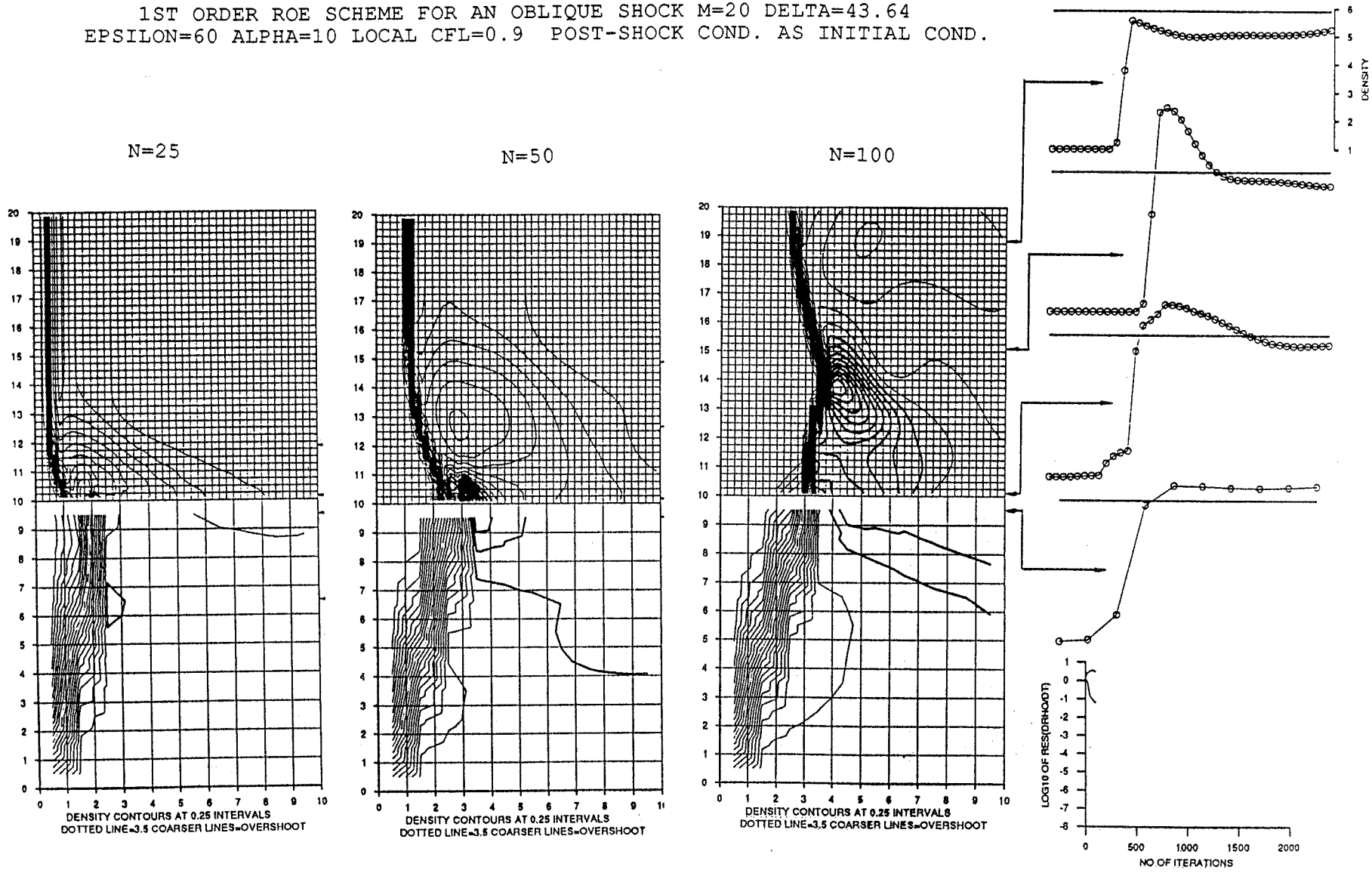

Fig. 39 shock evolution from local time stepping results

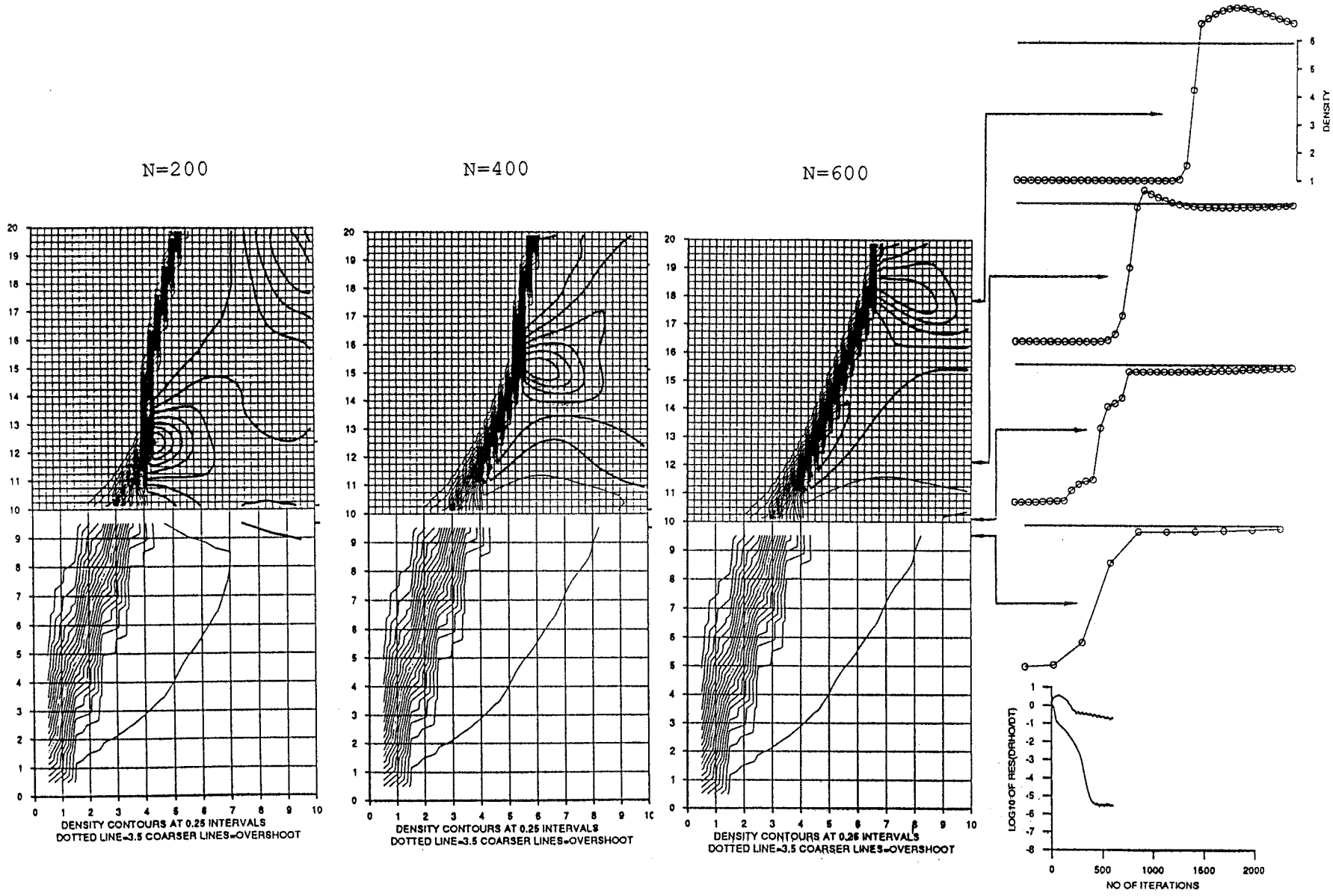

Fig. 40 shock evolution from local time stepping results (continued)

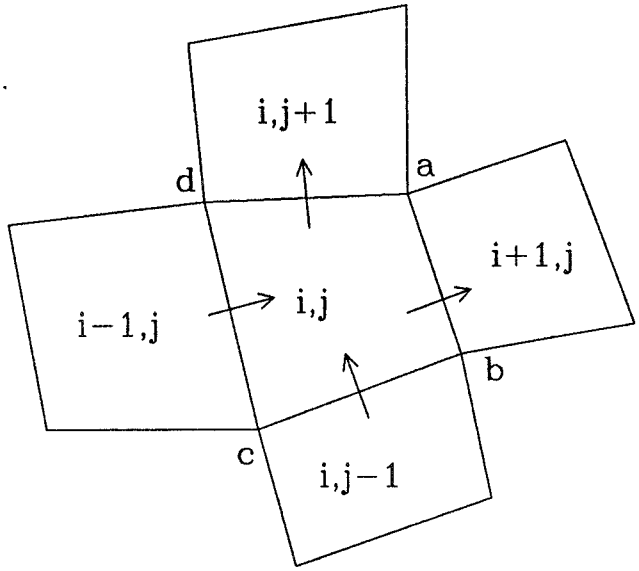

Fig. 41 GRID INDEX SYSTEM

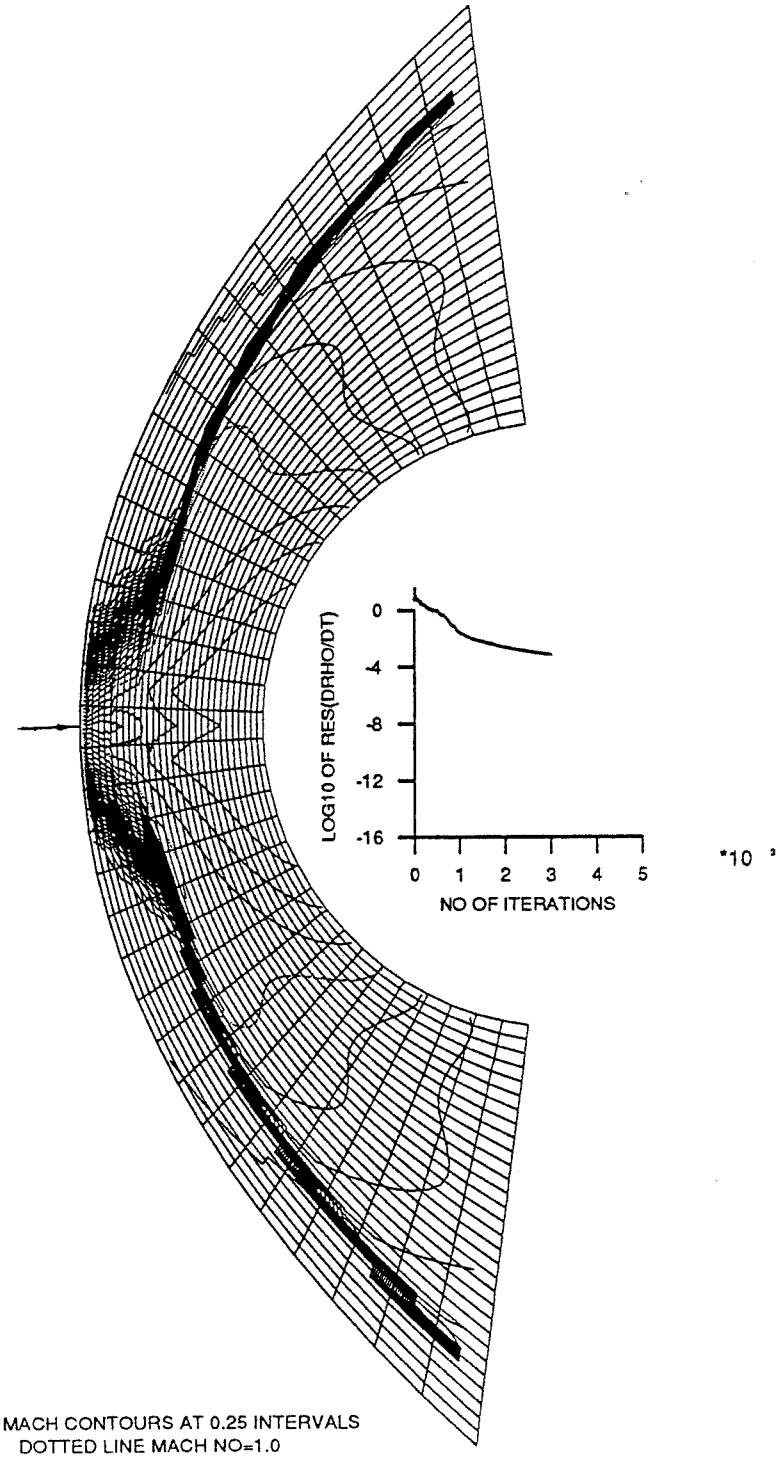

EXPLICIT 1ST ORDER SCHEME WITH ROE'S RIEMANN SOLVER
MACH NO.=8 LOCAL CFL=0.8

Fig. 42 BLUNT NOSE INSTABILITY

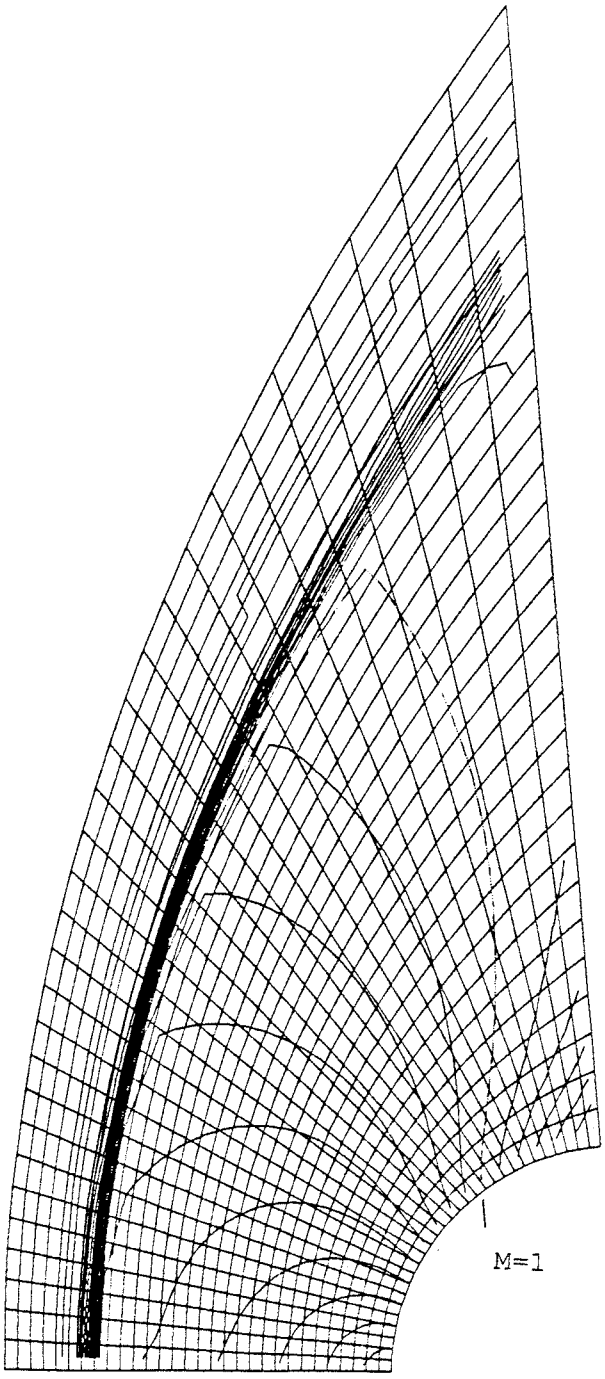

MACH CONTOURS AT 0.1 INTERVALS
DOTTED LINE MACH NO=1.0

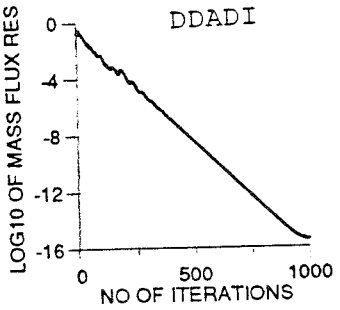

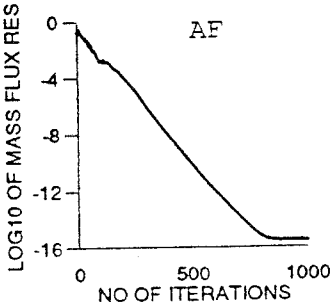

CONSERVATIVE IMPLICIT OPERATOR 30X30 CELLS
VAN ALBADA LIMITER MACH NO.=2. LOCAL CFL=20 $\tilde{\delta}_{1,4}=0.25$ $\tilde{\delta}_{2,3}=0.25$

Fig. 43 FLOW PAST CYLINDER

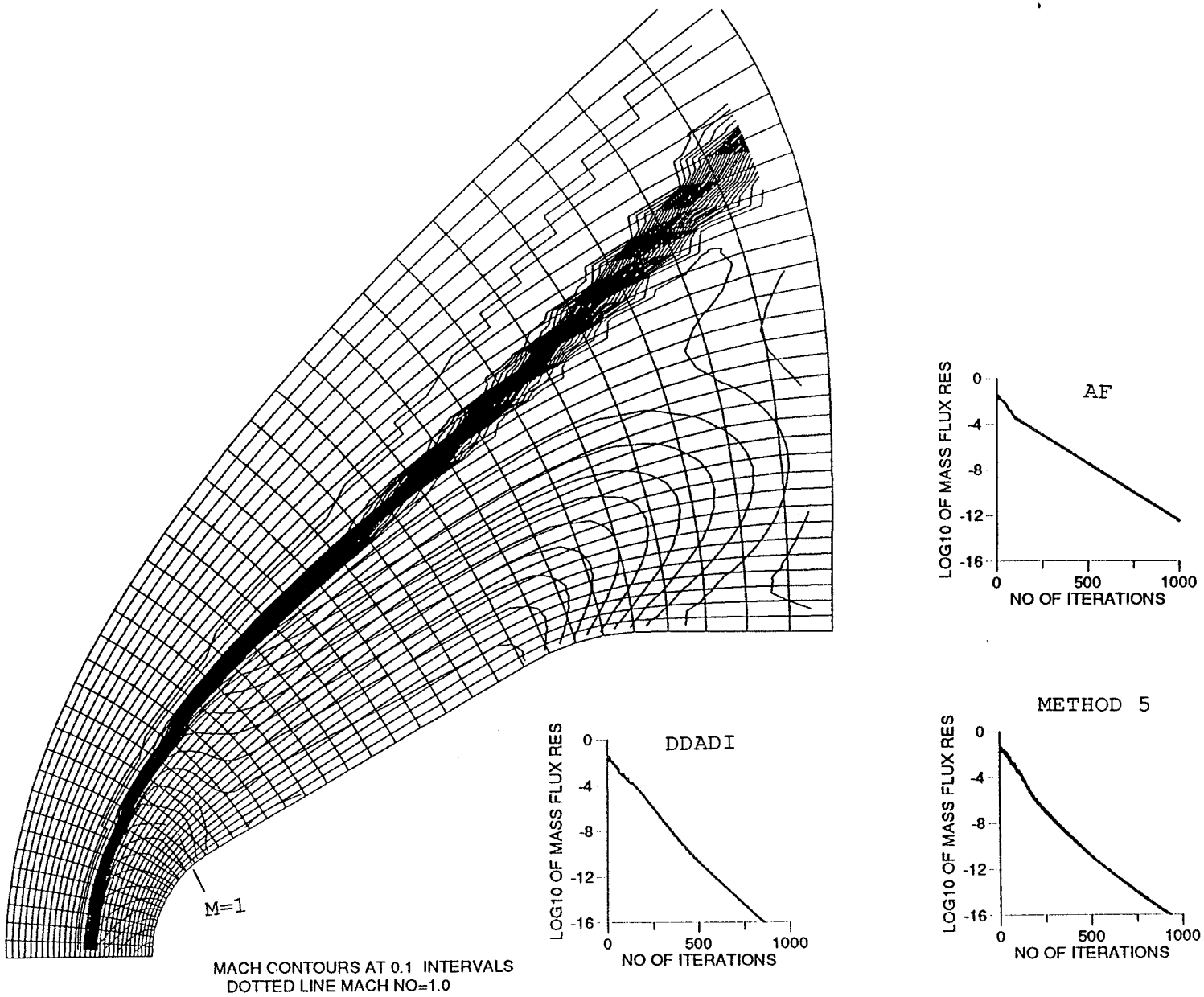

CONSERVATIVE IMPLICIT OPERATOR 30X35 CELLS
VAN ALBADA LIMITER MACH NO.=5. LOCAL CFL=10 $\tilde{\delta}_{1,4}=0.25$ $\tilde{\delta}_{2,3}=0.5$

Fig. 44 FLOW PAST REENTRY BODY

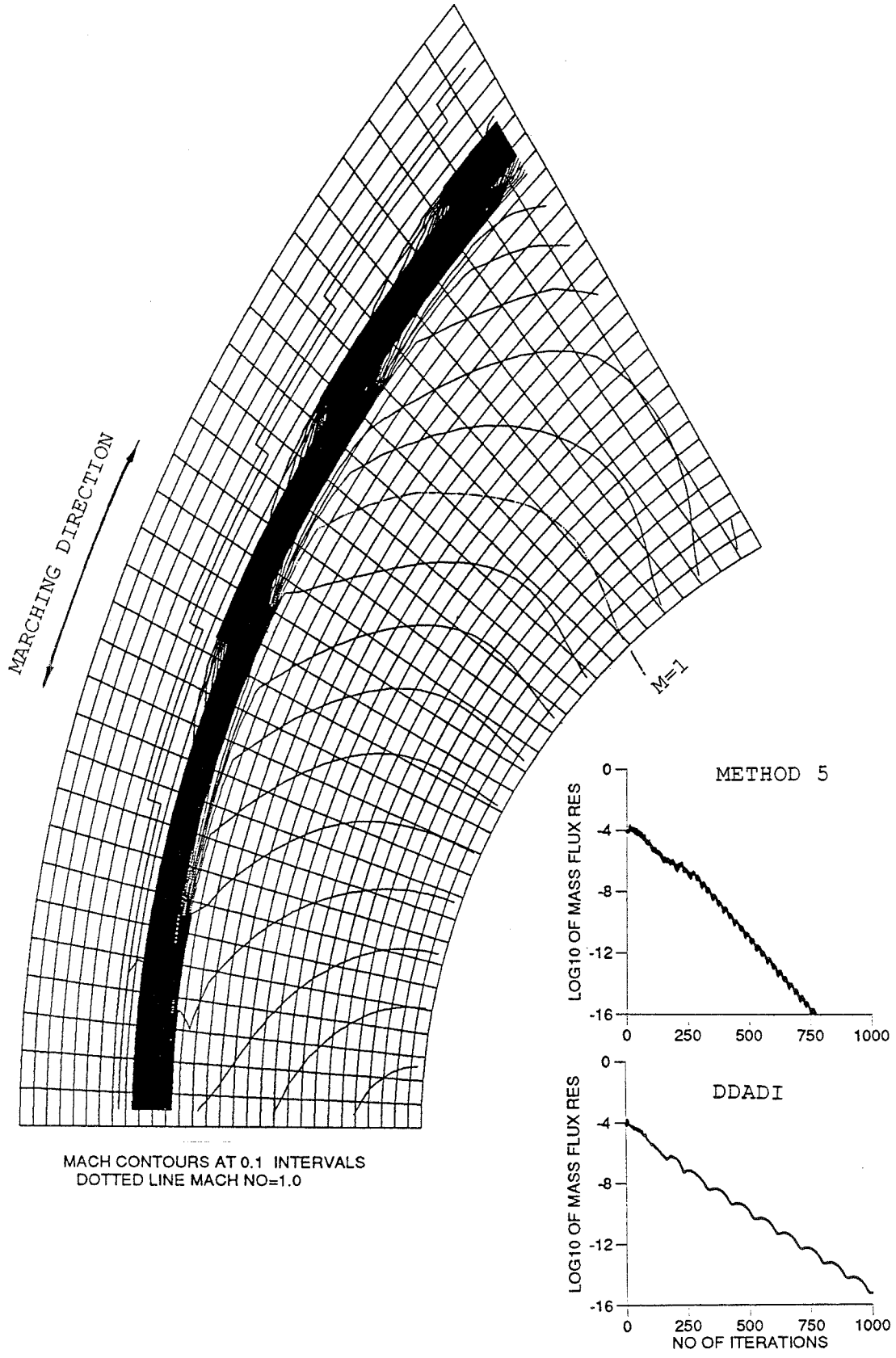

CONSERVATIVE IMPLICIT OPERATOR 30X30 CELLS
VAN ALBADA LIMITER MACH NO.=20. LOCAL CFL=10 $\tilde{\delta}_{1,4}=0.25$ $\tilde{\delta}_{2,3}=0.8$

Fig. 45 FLOW PAST CYLINDER

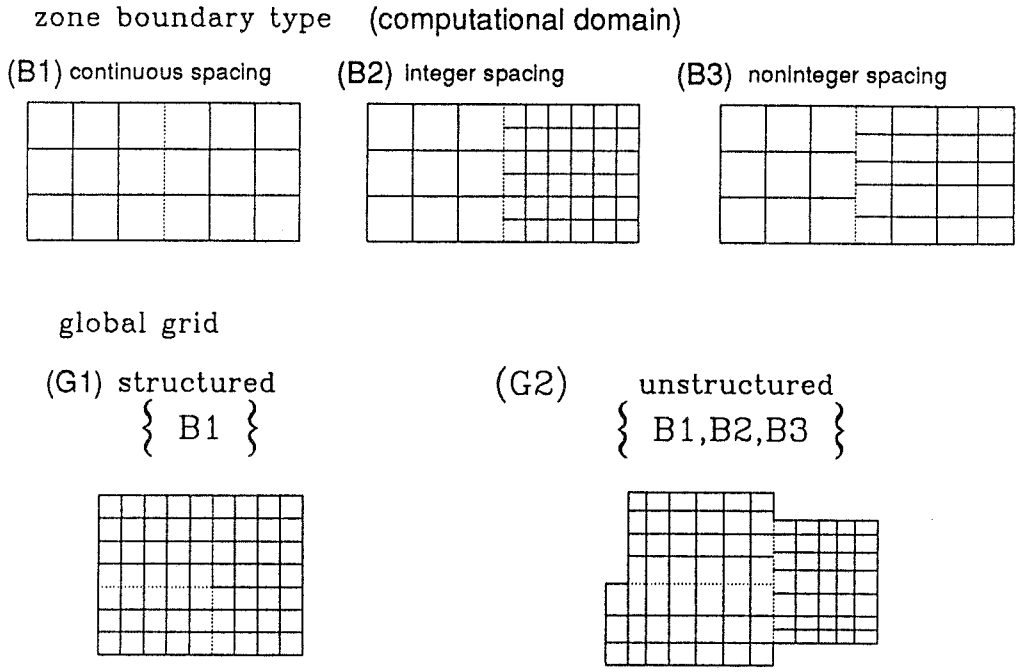

Fig. 46 VARIOUS GRID STRUCTURES

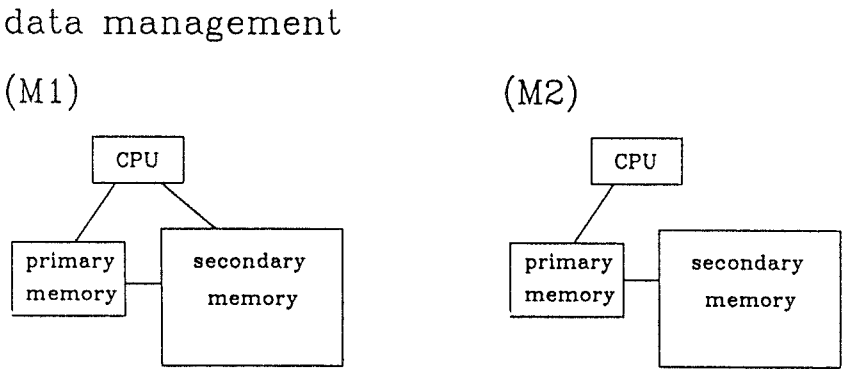

Fig. 47 DATA MANAGEMENT

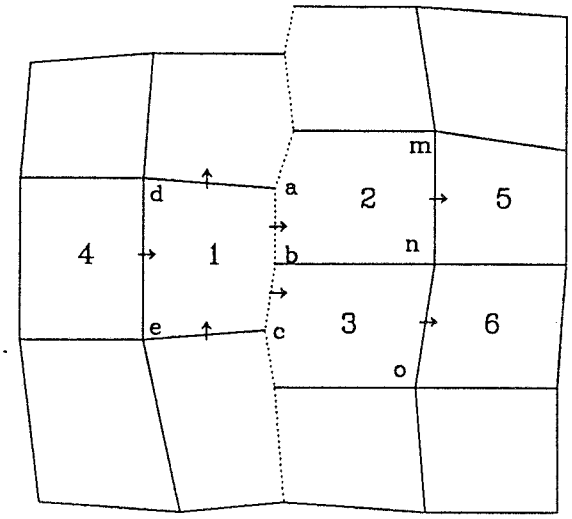

Fig. 48

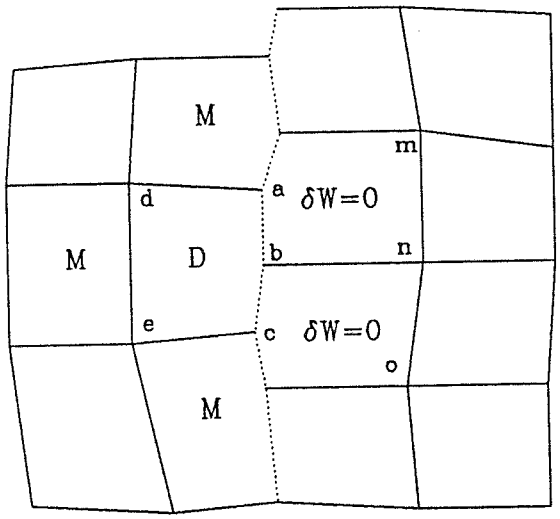

Fig. 49

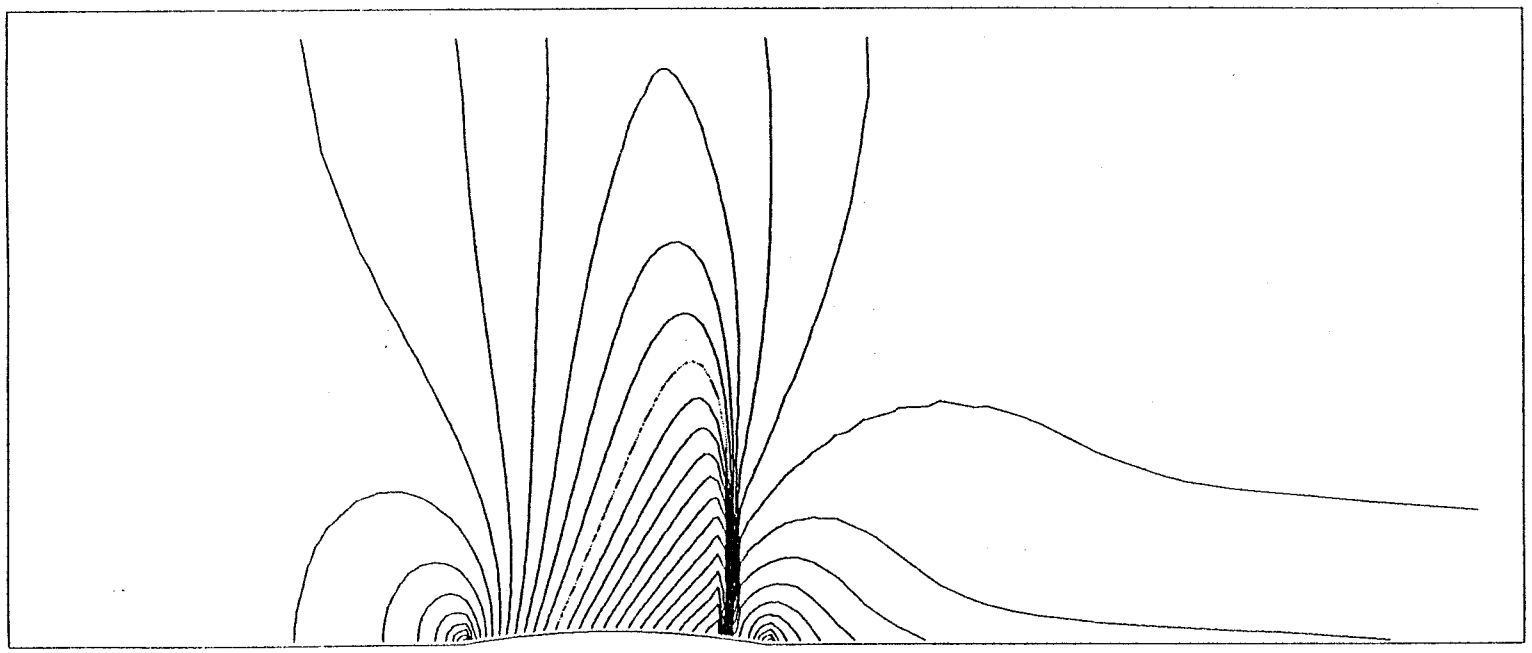

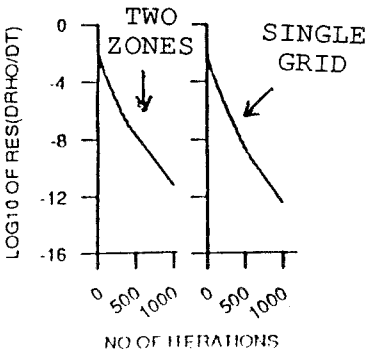

ZONAL BOUNDARY INSIDE THE SHOCK

MACH CONTOURS AT 0.025 INTERVALS
DOTTED LINE MACH NO=1.0

NONCONSERVATIVE IMPLICIT OPERATOR WITH DDADI+SYN 71X20 CELLS
VAN ALBADA LIMITER MACH NO.=0.85 LOCAL CFL=40

Fig. 50 GAMM GUMP

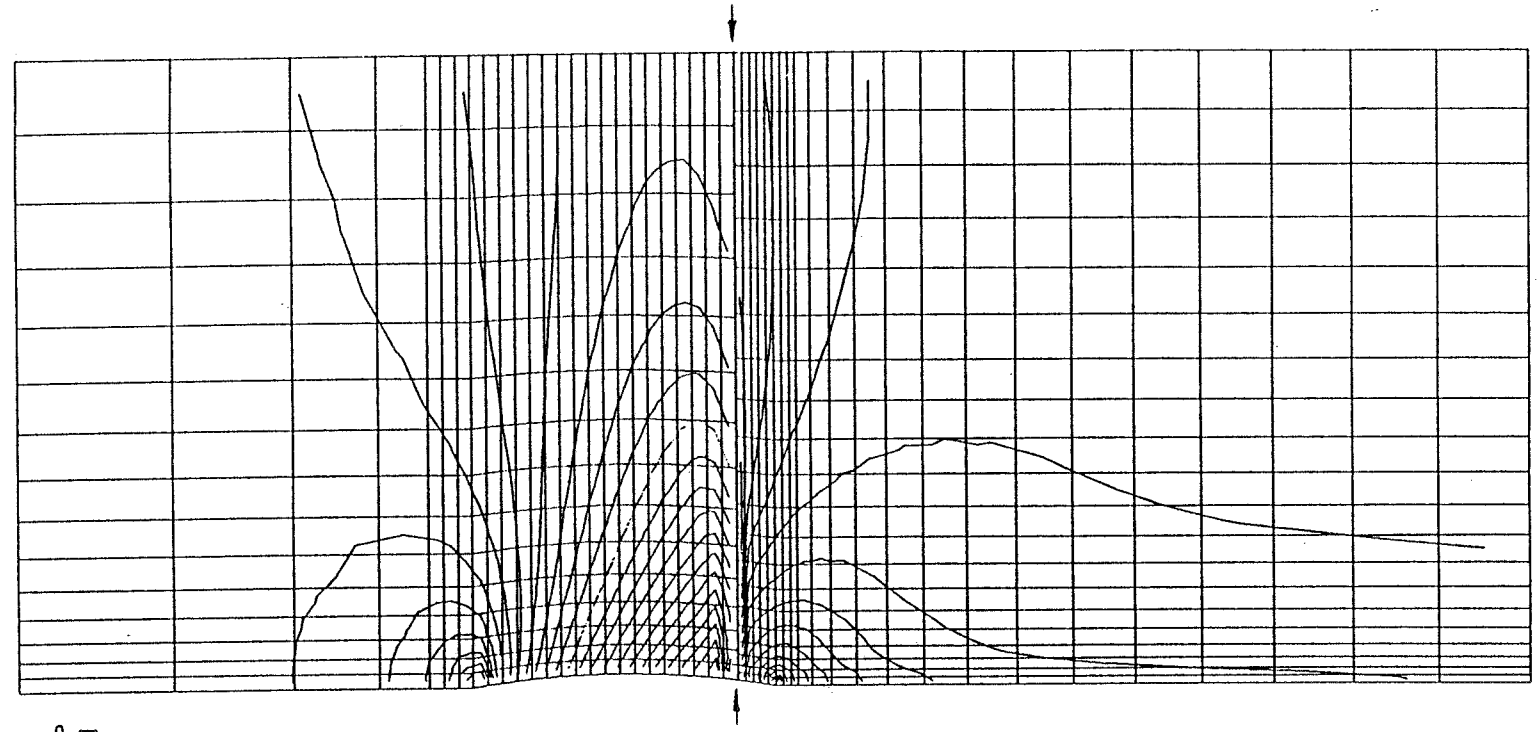

MACH CONTOURS AT 0.025 INTERVALS
DOTTED LINE MACH NO=1.0

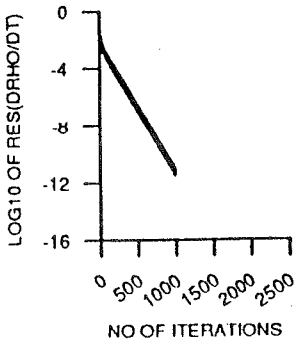

NONCONSERVATIVE IMPLICIT OPERATOR WITH DDADI+UNSYN 25X15+22X20 CELLS
VAN ALBADA LIMITER MACH NO.=0.85 LOCAL CFL=40

Fig. 51 GAMM BUMP

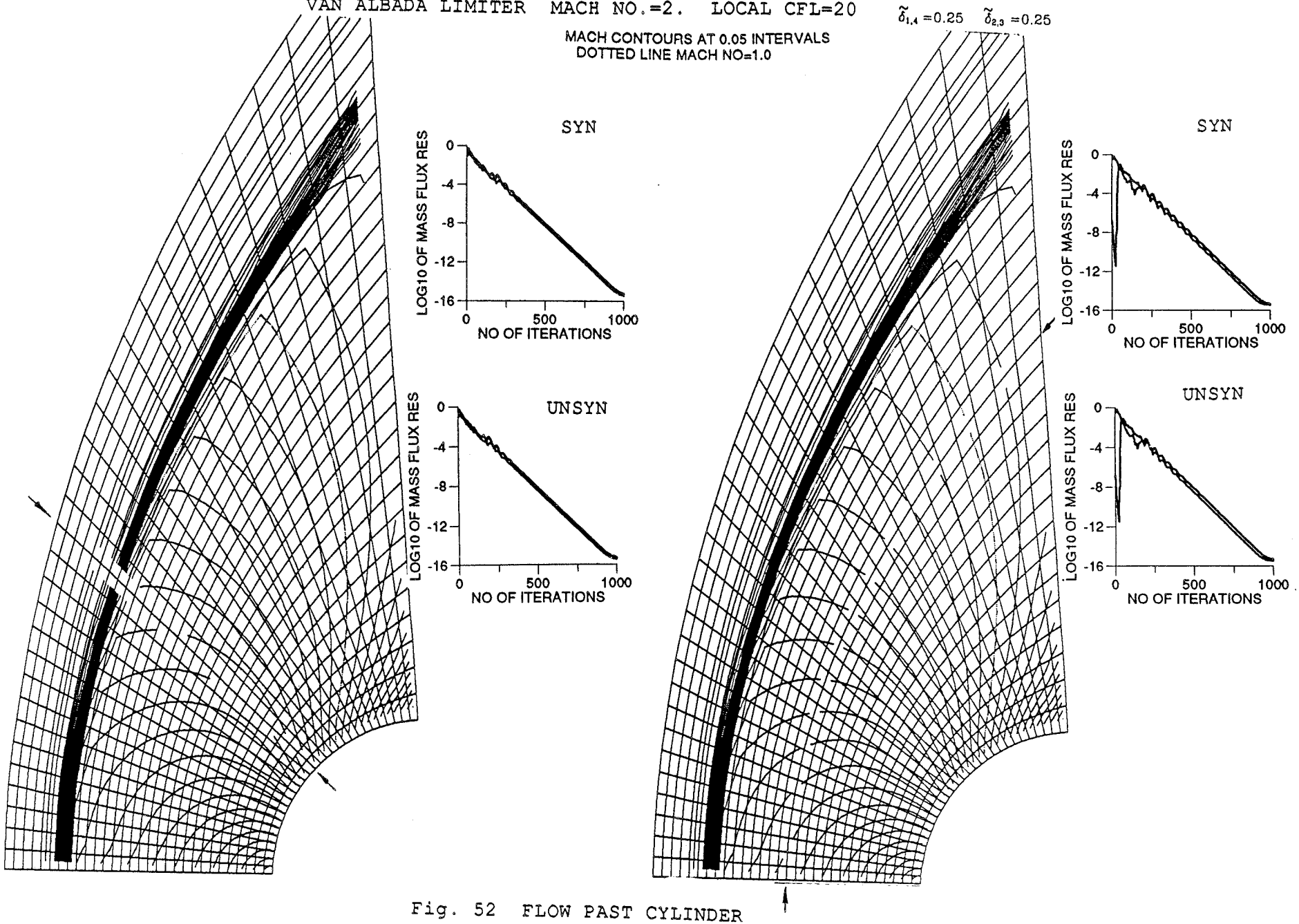

Fig. 52 FLOW PAST CYLINDER

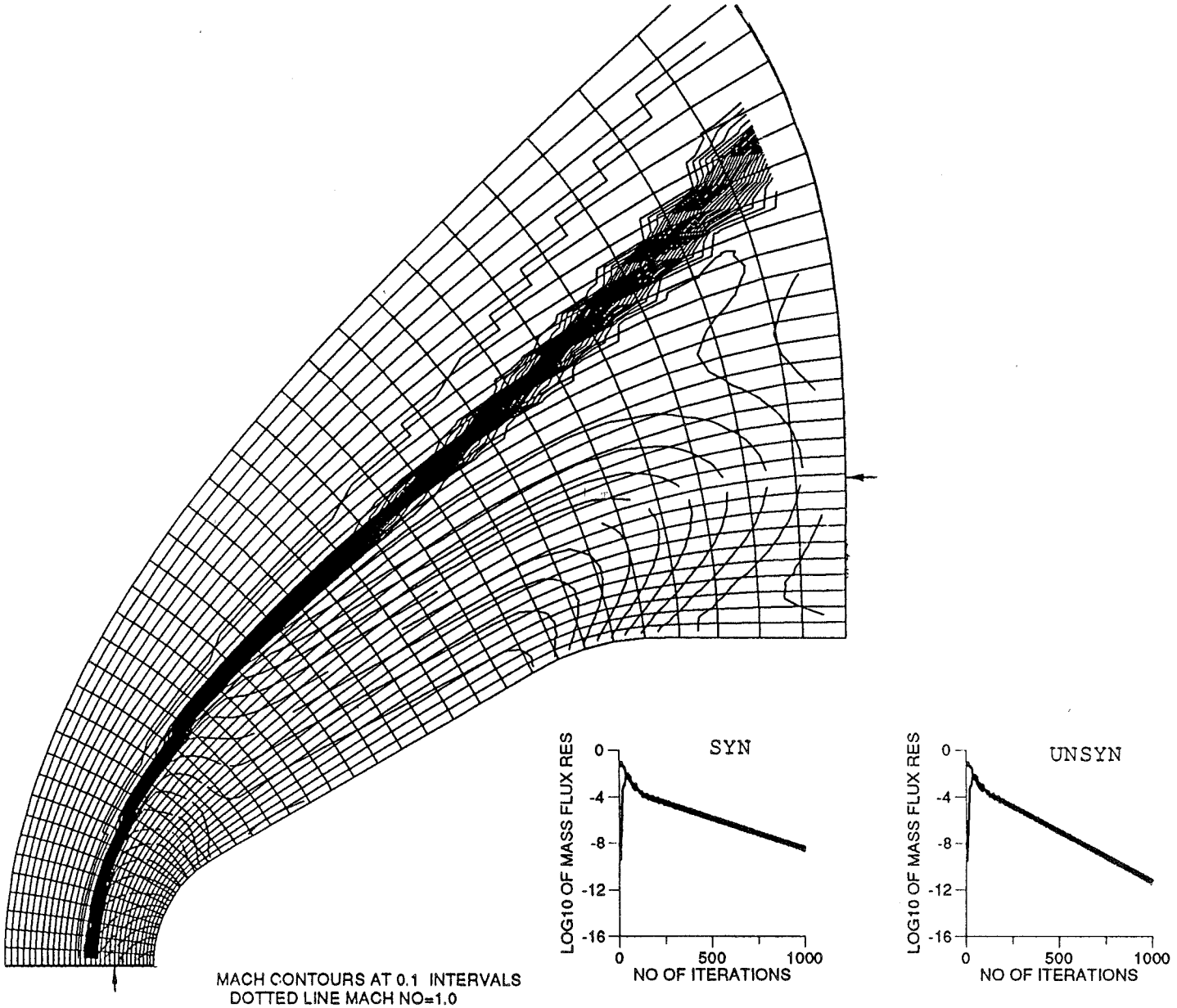

CONSERVATIVE IMPLICIT OPERATOR WITH DDADI 20X35+10X35 CELLS
VAN ALBADA LIMITER MACH NO.=5. LOCAL CFL=10

Fig. 53 FLOW PAST REENTRY BODY

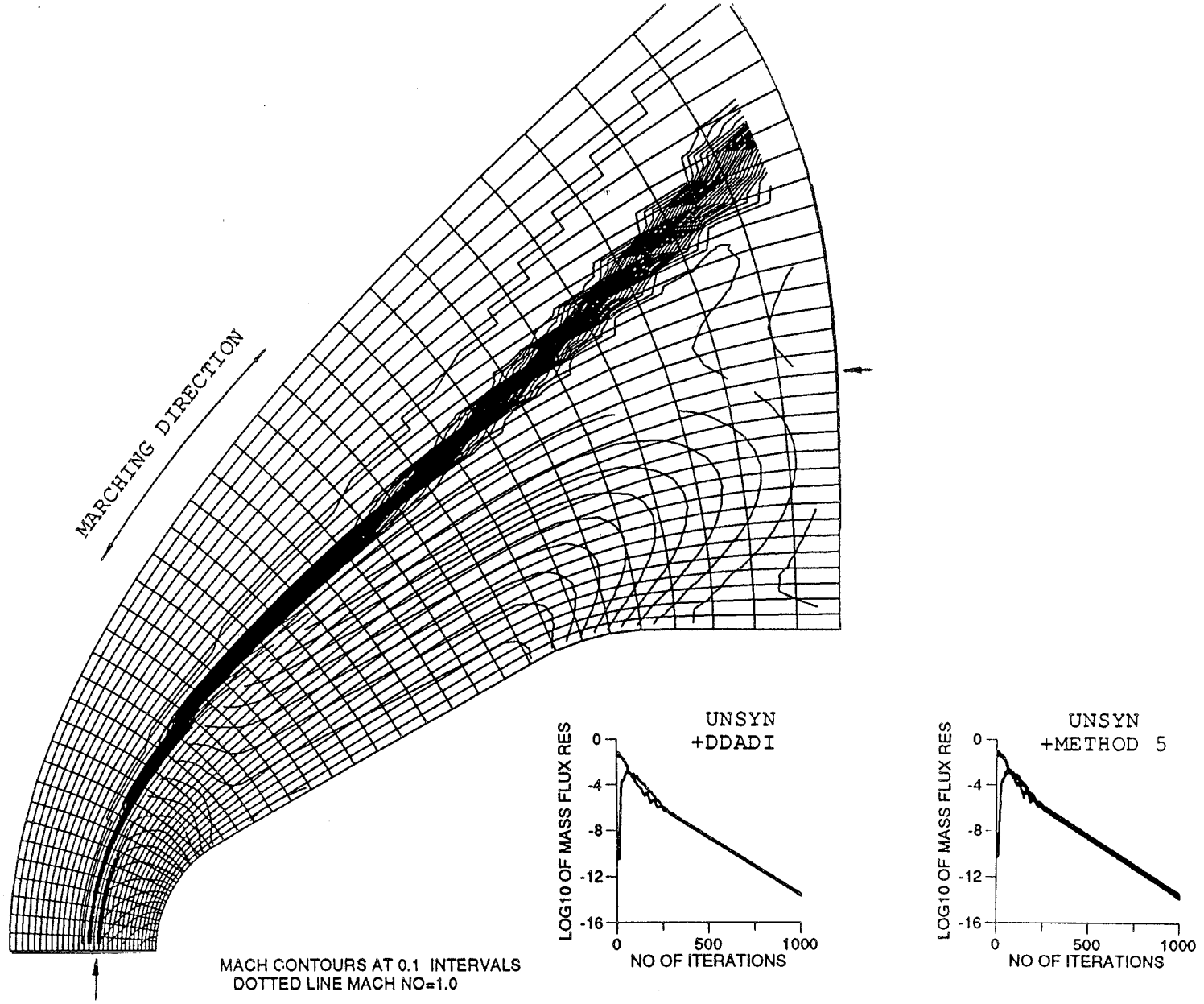

CONSERVATIVE IMPLICIT OPERATOR 15X35+15X35 CELLS
VAN ALBADA LIMITER MACH NO.=5. LOCAL CFL=10 $\tilde{\delta}_{1,4}=0.25$ $\tilde{\delta}_{2,3}=0.5$

Fig. 54 FLOW PAST REENTRY BODY

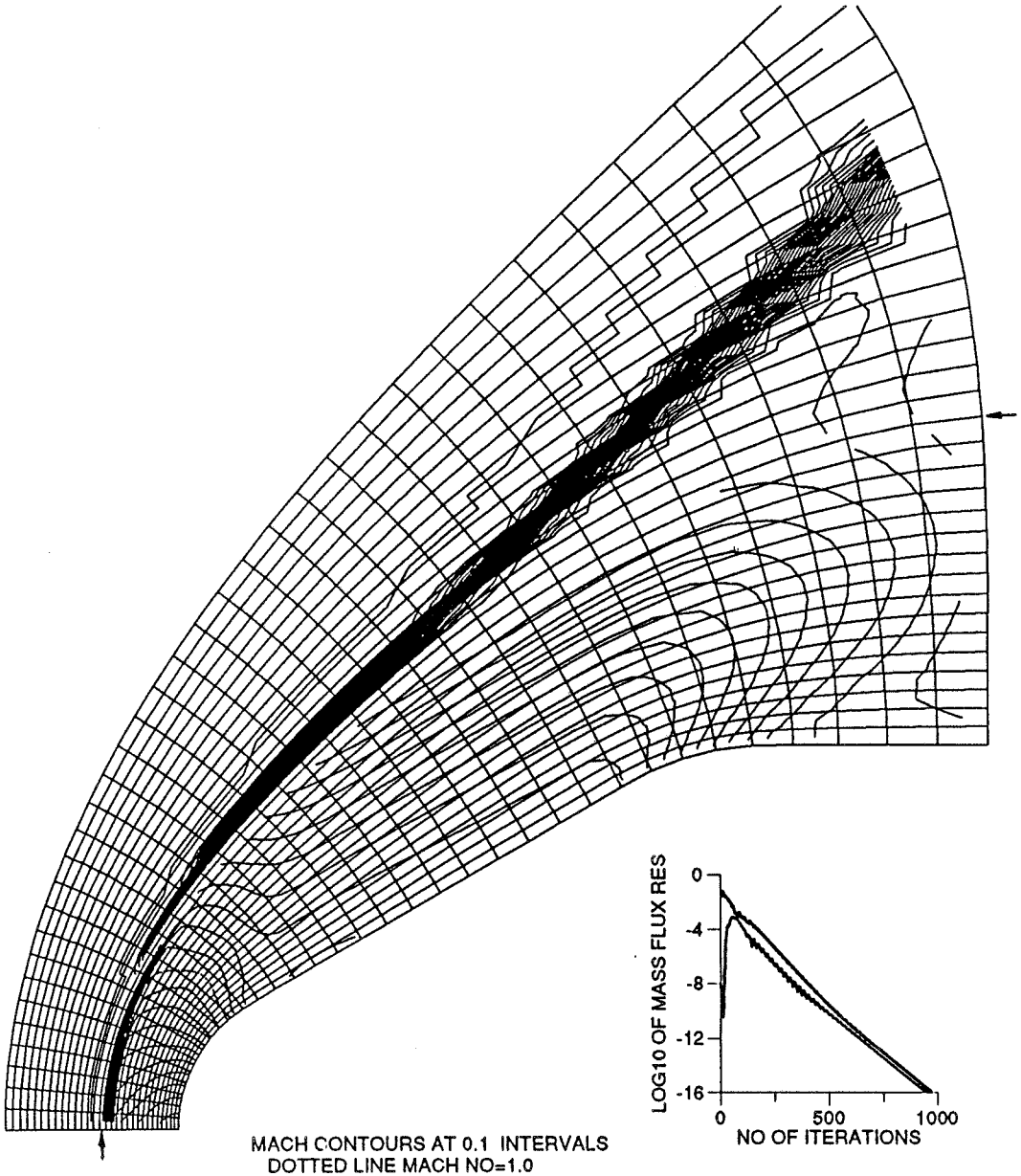

CONSERVATIVE IMPLICIT OPERATOR WITH DDADI+UNSYN 14X35+16X35 CELLS
VAN ALBADA LIMITER MACH NO.=5. LOCAL CFL=10 $\tilde{\delta}_{1,4}=0.25$ $\tilde{\delta}_{2,3}=0.5$

Fig. 55 FLOW PAST REENTRY BODY

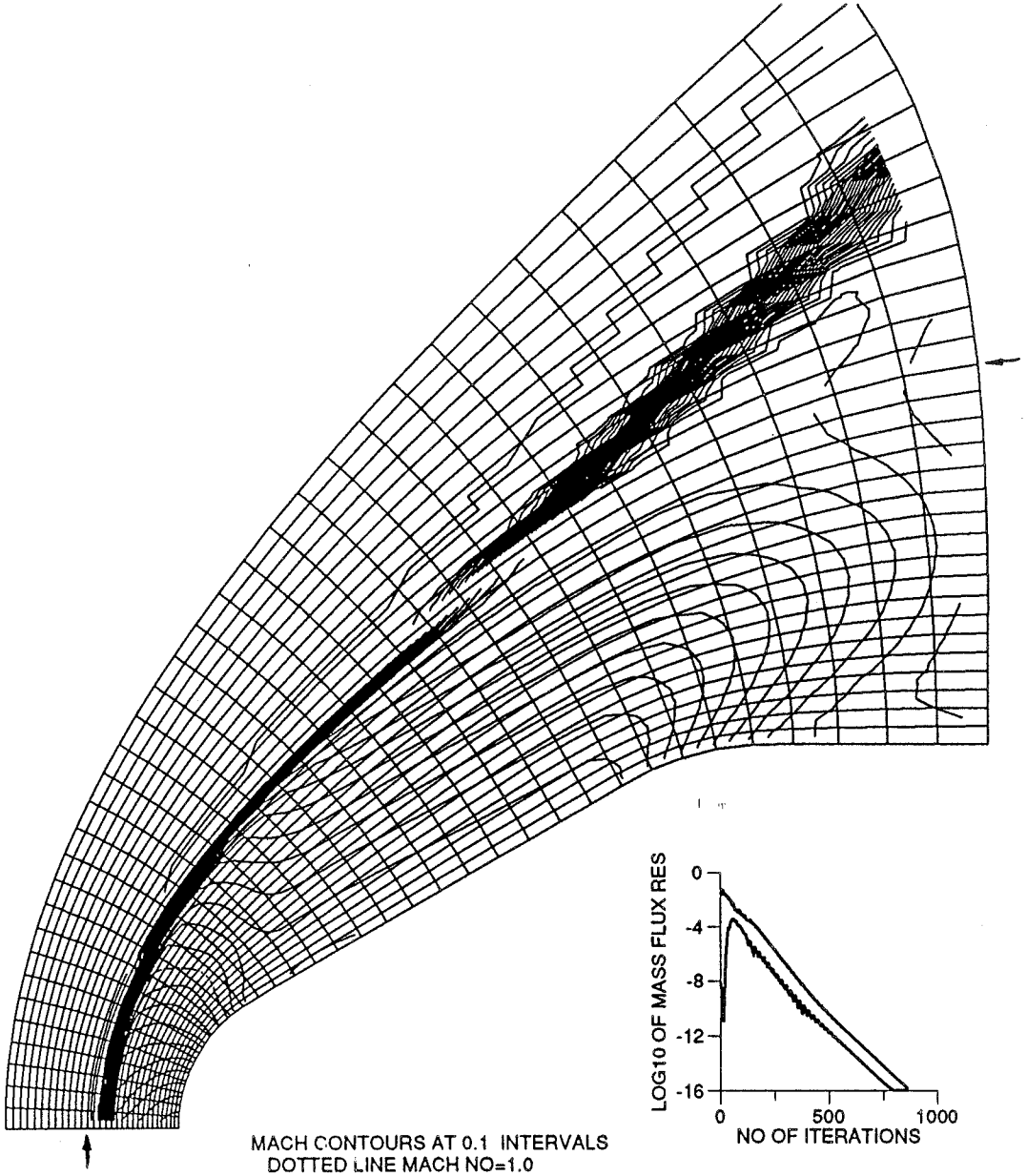

CONSERVATIVE IMPLICIT OPERATOR WITH DDADI+UNSYN 12X35+18X35 CELLS
VAN ALBADA LIMITER MACH NO.=5. LOCAL CFL=10 $\tilde{\delta}_{1,4}=0.25$ $\tilde{\delta}_{2,3}=0.5$

Fig. 56 FLOW PAST REENTRY BODY

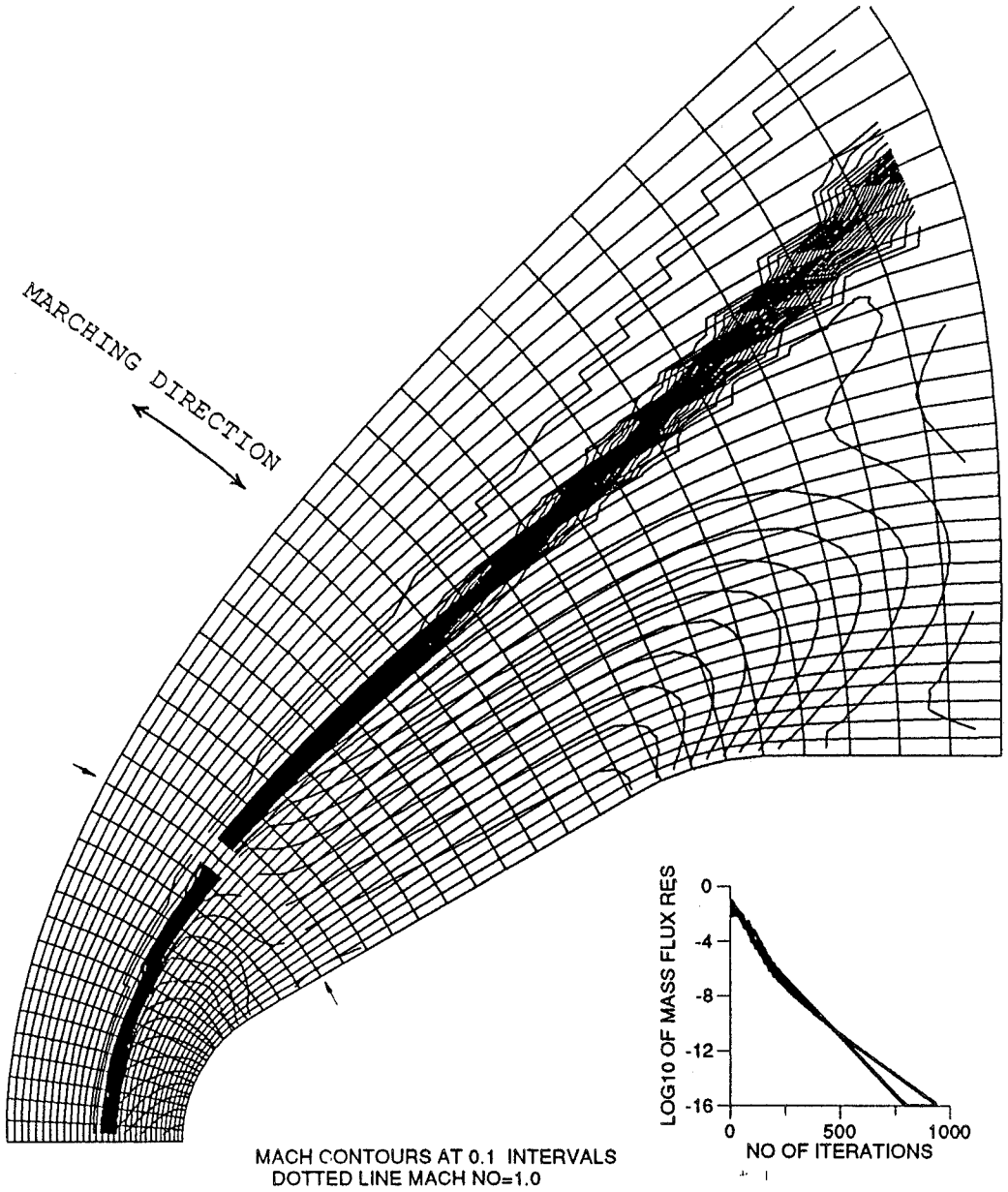

CONSERVATIVE IMPLICIT OPERATOR WITH METHOD 5+UNSYN 30X15+30X20 CELLS
VAN ALBADA LIMITER MACH NO.=5. LOCAL CFL=10 $\tilde{\delta}_{1,4}=0.25$ $\tilde{\delta}_{2,3}=0.5$

Fig. 57 FLOW PAST REENTRY BODY

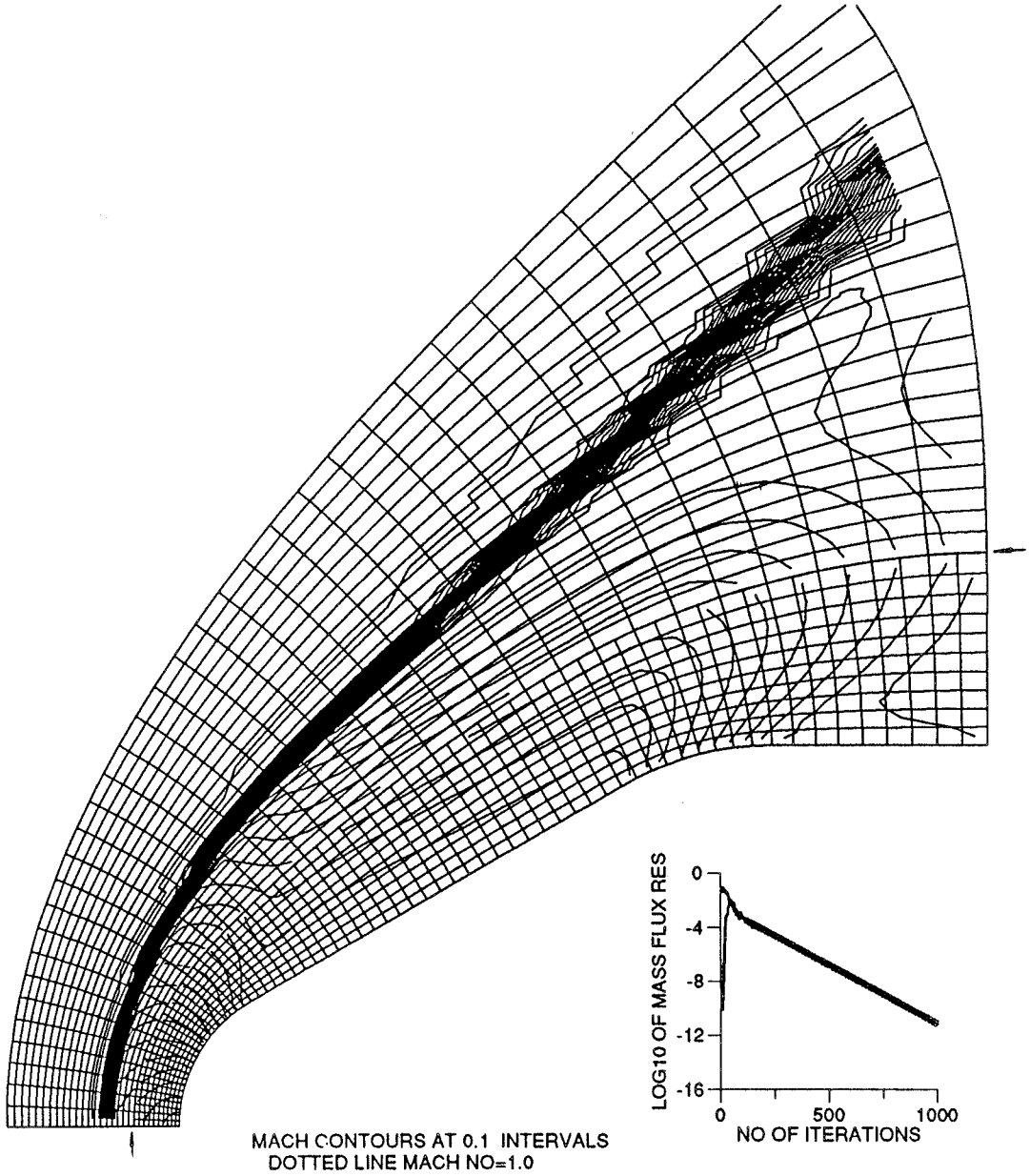

CONSERVATIVE IMPLICIT OPERATOR WITH DDADI+UNSYN 20X35+10X70 CELLS
VAN ALBADA LIMITER MACH NO.=5. LOCAL CFL=10 $\tilde{\delta}_{1,4}=0.25$ $\tilde{\delta}_{2,3}=0.5$

Fig. 58 FLOW PAST REENTRY BODY

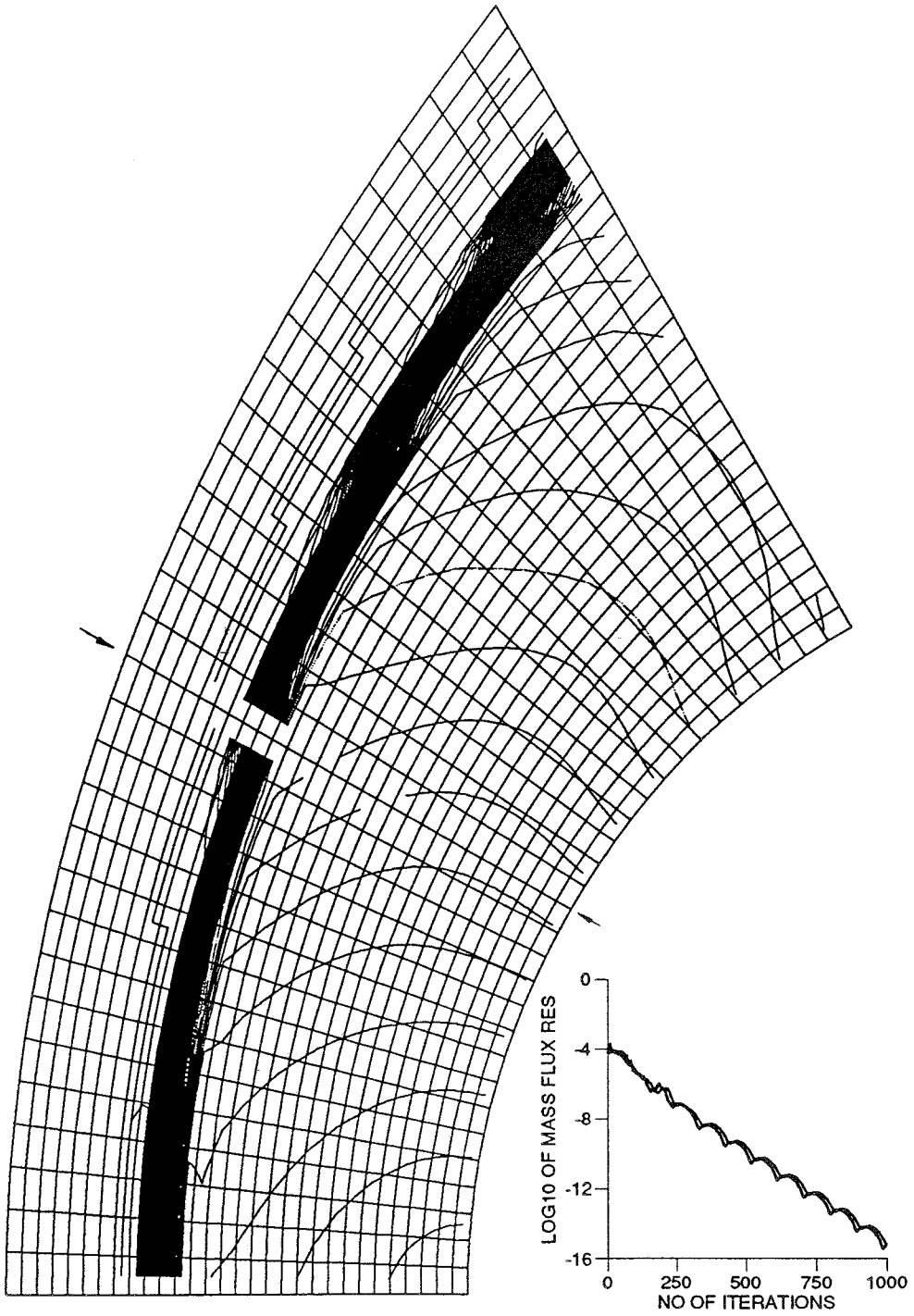

MACH CONTOURS AT 0.1 INTERVALS
DOTTED LINE MACH NO=1.0

CONSERVATIVE IMPLICIT OPERATOR WITH DDADI+UNSYN 30X15+30X15 CELLS
VAN ALBADA LIMITER MACH NO.=20. LOCAL CFL=10 $\tilde{\delta}_{1,4}=0.25$ $\tilde{\delta}_{2,3}=0.8$

Fig. 59 FLOW PAST CYLINDER

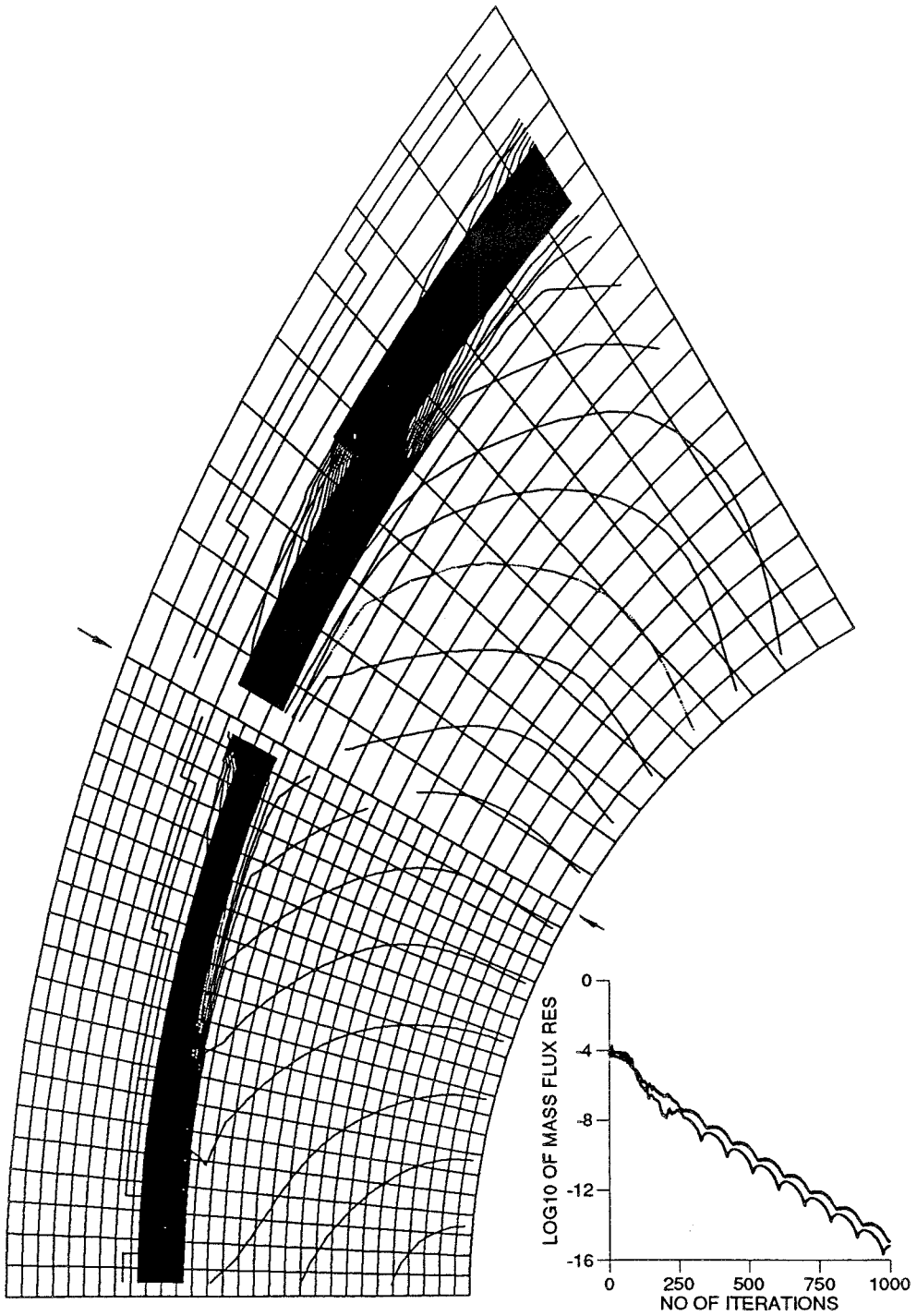

MACH CONTOURS AT 0.1 INTERVALS
DOTTED LINE MACH NO=1.0

CONSERVATIVE IMPLICIT OPERATOR WITH DDADI+UNSYN 30X20+20X10 CELLS
VAN ALBADA LIMITER MACH NO.=20. LOCAL CFL=10 $\tilde{\delta}_{1,4}=0.25$ $\tilde{\delta}_{2,3}=0.8$

Fig. 60 FLOW PAST CYLINDER

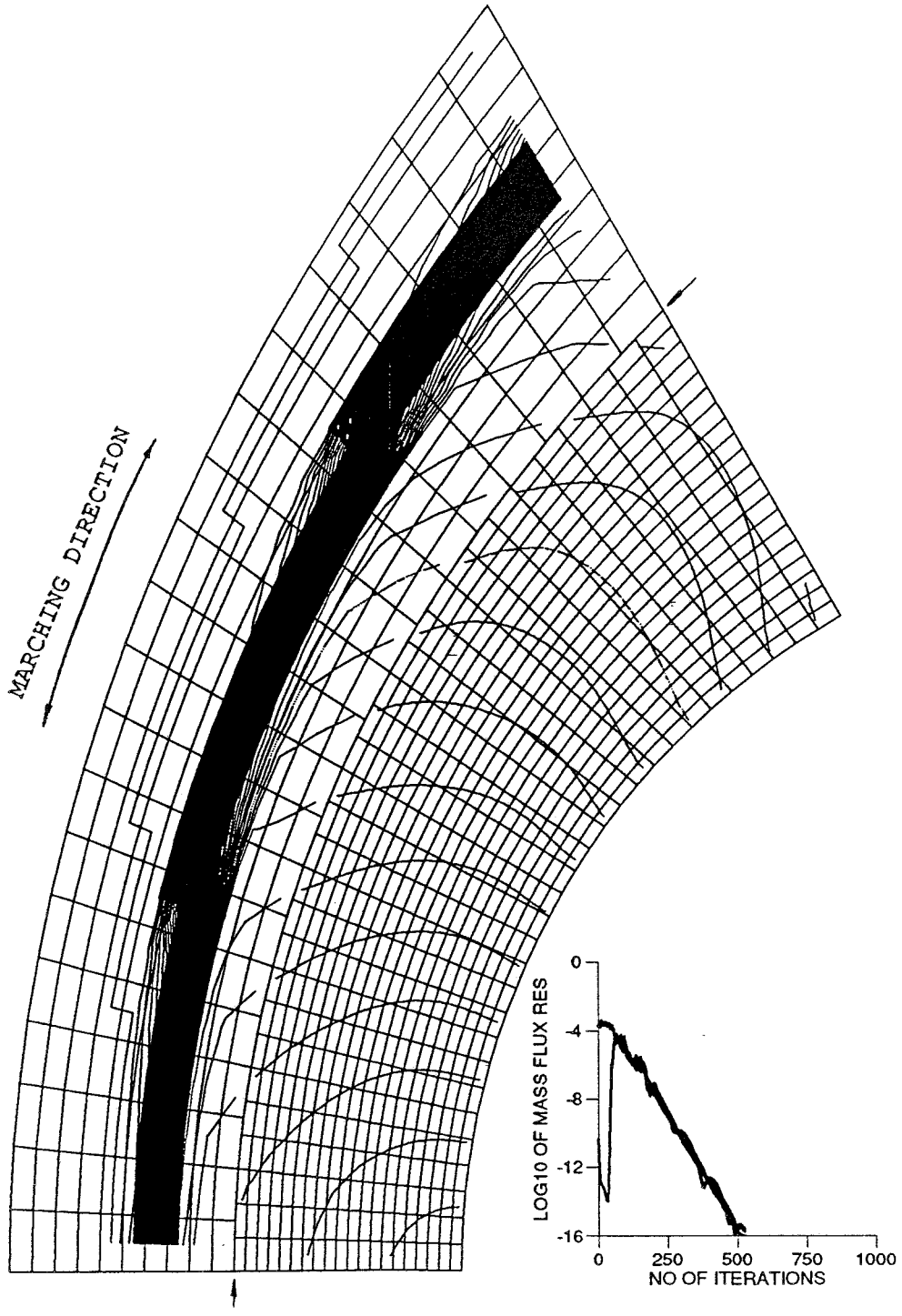

MACH CONTOURS AT 0.1 INTERVALS
DOTTED LINE MACH NO=1.0

CONSERVATIVE IMPLICIT OPERATOR WITH METHOD 5+UNSYN 10X20+20X30 CELLS
VAN ALBADA LIMITER MACH NO.=20. LOCAL CFL=10 $\tilde{\delta}_{1,4}=0.25$ $\tilde{\delta}_{2,3}=0.8$

Fig. 61 FLOW PAST CYLINDER

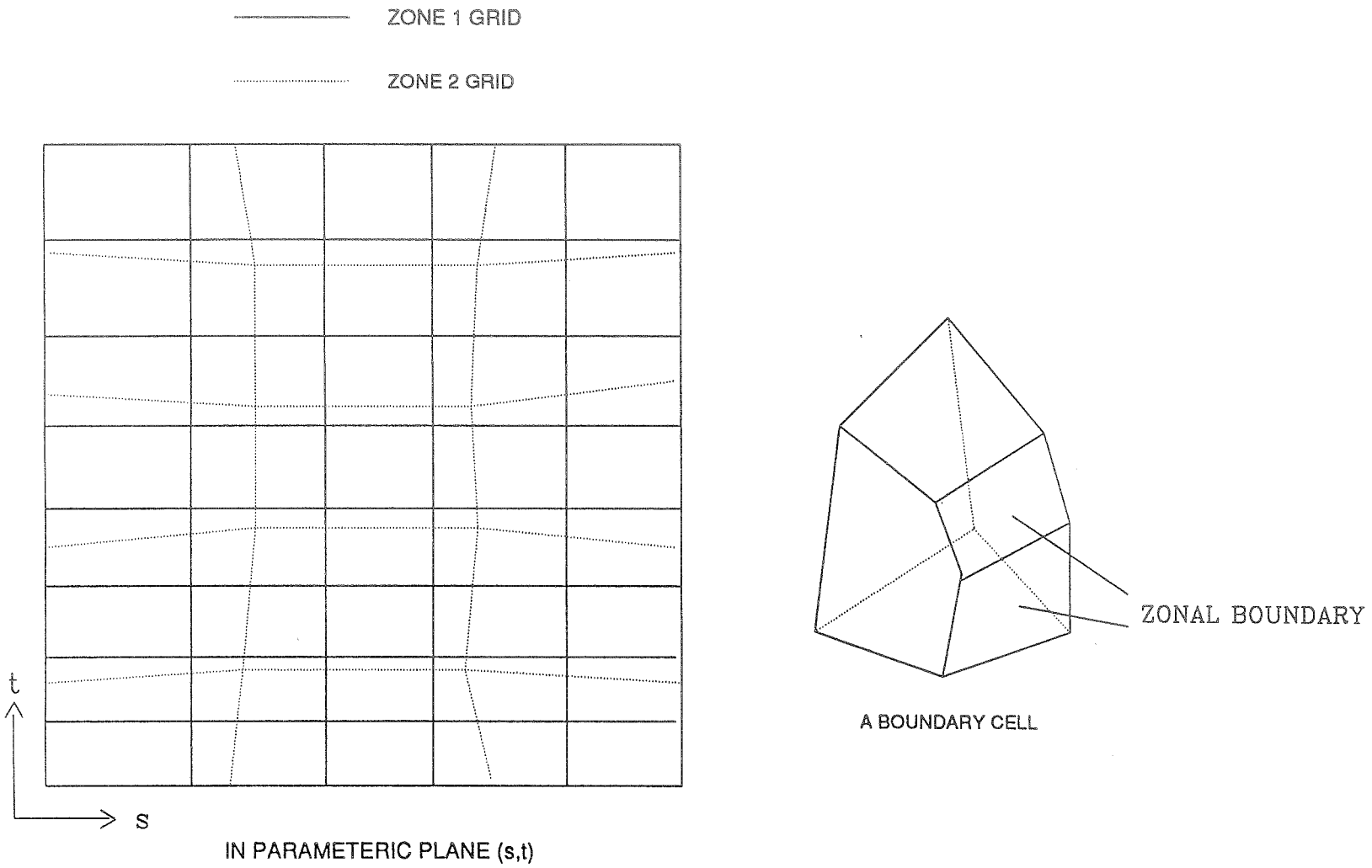

Fig. 62 THREE DIMENSIONAL ZONAL BOUNDARY